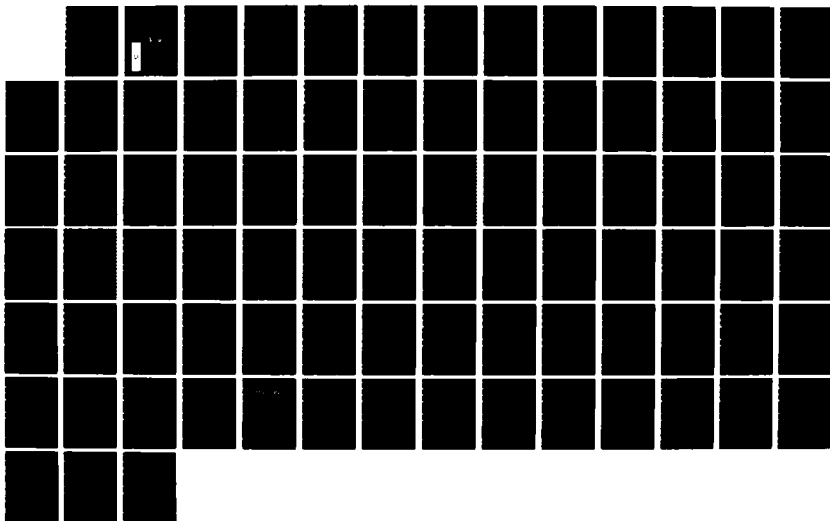REMOTE SENSING OF ATMOSPHERIC OPTICAL THICKNESS AND
SEA-WATER ATTENUATION. (U) SCRIPPS INSTITUTION OF
OCEANOGRAPHY LA JOLLA CA VISIBILITY LA

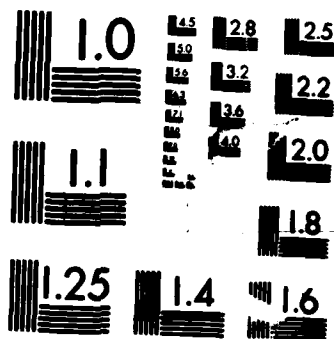UNCLASSIFIED   T J PETZOLD ET AL. JUL 87 SIO-REF-87-18   F/G 20/6   NL

MICROCOPY RESOLUTION TEST CHART
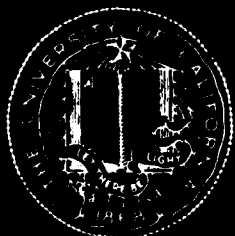NATIONAL BUREAU OF STANDARDS-1963-A

SIO Ref. 87-18

July 1987

AD-A187 609

Remote Sensing of Atmospheric Optical Thickness and Sea-Water Attenuation when Submerged: Wavelength Selection and Anticipated Errors

DTIC
ELECTE
NOV 1 0 1987
S   D
D

T.J. Petzold
R.W. Austin

UNIVERSITY
OF
CALIFORNIA
SAN DIEGO

SCRIPPS
INSTITUTION
OF
OCEANOGRAPHY

VISIBILITY LABORATORY   La Jolla, California 92093

87   10

AD-A187609

REPORT DOCUMENTATION PAGE

1a. REPORT SECURITY CLASSIFICATION Unclassified	1b. RESTRICTIVE MARKINGS None
2a. SECURITY CLASSIFICATION AUTHORITY	3. DISTRIBUTION/AVAILABILITY OF REPORT Approved for public release; distribution is unlimited
2b. DECLASSIFICATION/DOWNGRADING SCHEDULE	

4. PERFORMING ORGANIZATION REPORT NUMBER(S) SIO Ref 87-18	5. MONITORING ORGANIZATION REPORT NUMBER(S)

6a. NAME OF PERFORMING ORGANIZATION University of California, San Diego Visibility Laboratory	6b. OFFICE SYMBOL (If applicable)	7a. NAME OF MONITORING ORGANIZATION Office of Naval Research
6c. ADDRESS (City, State and ZIP Code) La Jolla, CA 92093-0703		7b. ADDRESS (City, State and ZIP Code) 800 N Quincy St. Arlington, VA 22217-5000

8a. NAME OF FUNDING/SPONSORING ORGANIZATION Office of Naval Research	8b. OFFICE SYMBOL (If applicable) N00014	9. PROCUREMENT INSTRUMENT IDENTIFICATION NUMBER N0014-78-C-0556

| 8c. ADDRESS (City, State and ZIP Code) Dept. of the Navy, Office of Naval Research 800 N Quincy St. Arlington, VA 22217-5000 | 10. SOURCE OF FUNDING NOS. | | | |

PROGRAM ELEMENT NO.	PROJECT NO.	TASK NO.	WORK UNIT NO.
2E20	62301E	3650	NR395-625

11. TITLE (Include Security Classification) Remote Sensing of Atmospheric Optical Thickness and Sea-Water Attenuation when submerged.

12. PERSONAL AUTHOR(S) T. J. Petzold and R. W. Austin

13a. TYPE OF REPORT Final	13b. TIME COVERED FROM 1 Jul 78 TO 30 Apr 86	14. DATE OF REPORT (Yr., Mo., Day) 1987, July 1	15. PAGE COUNT 84

16. SUPPLEMENTARY NOTATION

17. COSATI CODES			18. SUBJECT TERMS (Continue on reverse if necessary and identify by block number) Remote Sensing, atmospheric attenuation; sea-water attenuation
FIELD	GROUP	SUB. GR.	

19. ABSTRACT (Continue on reverse if necessary and identify by block number)

Prior analysis and experimentation has provided strong support for determining the attenuation of optical radiation for the atmosphere and the water column above a submerged platform by measuring the absolute downwelling irradiance at two wavelengths. The technique requires knowing the two irradiance values and in addition (1) the spectral irradiance of the sun outside the atmosphere; (2) the solar zenith angle and (3) the depth at which the irradiances are measured.

With this capability in hand, the questions considered in this report are which wavelengths to use and the effect of errors in the measurement of irradiance and other parameters.

20. DISTRIBUTION/AVAILABILITY OF ABSTRACT UNCLASSIFIED/UNLIMITED ☒ SAME AS RPT. ☐ DTIC USERS ☐	21. ABSTRACT SECURITY CLASSIFICATION Unclassified
22a. NAME OF RESPONSIBLE INDIVIDUAL Dr. Matthew B. White	22b. TELEPHONE NUMBER (Include Area Code) (617) 451-3172	22c. OFFICE SYMBOL N00014

DD FORM 1473, 83 APR   EDITION OF 1 JAN 73 IS OBSOLETE.

University of California, San Diego
Scripps Institution of Oceanography
Visibility Laboratory
La Jolla, California 92093

Remote Sensing of Atmospheric Optical Thickness and Sea-Water Attenuation when Submerged: Wavelength Selection and Anticipated Errors

T.J. Petzold and R.W. Austin

SIO Ref. 87-18

July 1987

Approved: Approved:

Roswell W. Austin, Director   Edward A. Frieman, Director
Visibility Laboratory   Scripps Institution of Oceanography

TABLE OF CONTENTS

LIST OF TABLES AND ILLUSTRATIONS

FOREWORD

The remote sensing technique which is discussed in this report represents a new capability which could potentially have several important applications. The use of the term "remote sensing" we believe is appropriate since a sensor unit, located at a known depth in the ocean is used (during daylight hours) to determine the optical attenuation properties of the water above the sensor and of the atmosphere above the water. Knowing the time, date, latitude, longitude, and the extra-terrestrial solar spectral irradiance, (all easily obtained) it is a straightforward matter to compute the total path transmittance at a single wavelength, i.e. a single value representing the combined water and atmospheric attenuation. The problem of determining the two component parts of the attenuation separately was the challenge.

Our approach was to make measurements at two or more wavelengths and use these measurements in a set of equations which can be solved for the separate attenuations. This required models describing how the attenuation coefficients of sea water and of the atmosphere varied with wavelength for various turbidities. Atmospheric models existed which had been used successfully by the Visibility Laboratory and others to infer and remove the effects of the atmosphere on the water-leaving radiances arriving at the Coastal Zone Color Scanner satelite sensor. Simplified versions of these atmospheric models worked satisfactorily. The problem was that there was no existing comparable analytic model for seawater. The often quoted and used water types of Jerlov are described by a table of attenuation values specified at 25nm intervals throughout the visible spectrum for 5 oceanic and 5 coastal water types. To devise a model around the Jerlov table would have required fitting analytic functions to his attenuation values, putting the model another step removed from the actual data set upon which the table was based. Furthermore we had available to us a large and high quality data base of spectral irradiance profiles which had been obtained by investigators at the Visibility Laboratory, in France at Prof. Morel's laboratory, and by Okami and his colleagues in Japan. These data, which were obtained in a wide variety of oceanic and coastal waters, were acquired at wavelength intervals of approximately 5 nm thus permitting a better representation of the shape of the spectral attenuation coefficient in the resulting model. That model, described in Austin and Petzold, 1984 (Ref. 2 and Appendix 2, attached), allows the complete specification of the diffuse attenuation coefficient at all wavelengths in the visible spectrum, given the value of the coefficient at any one wavelength in that spectral region.

The technique which was developed uses that analytic model for the spectral attenuation of the water and the results have been very promising indeed. This report describes the technique and examines the errors that might be expected due to errors in radiometric calibration, wavelength assignment, depth, solar zenith angle, and in solar and atmospheric constants. It also addresses the matter of optimum wavelength selection. A subsequent report will provide an evaluation of the technique using data sets obtained from various cruises on surface ships. Among the applications we see for this remote sensing technique are the following.

- The determination of the amount of attenuation above a submerged sensor from a set of measurements made at a single point in time and space. Separate determinations of the amount of attenuation due to the water and due to the atmosphere are provided.

- A rather precise assessment of the mean diffuse attenuation coefficient, K, from the ocean surface to the depth of the sensor can be obtained on a continuous basis.

- The technique is particularly useful for applications involving installations on towed sensor systems and on unattended buoys or bottom mounted sensor systems.

For the genesis of this technique we must credit Dr. Matthew B. White of the Office of Naval Research. It was he who asked the critical question: "Isn't there some way you can determine, using a submerged sensor, the separate losses due to the water and to the atmosphere without moving the sensor vertically? Perhaps use more than one wavelength." or words to that effect. With that challenge we have proceeded to develop the Submerged Remote Sensing (SRS) technique together with the required water attenuation model, both of which potentially have important future applications.

R.W. Austin

REMOTE SENSING OF ATMOSPHERIC OPTICAL
THICKNESS AND SEA-WATER ATTENUATION WHEN SUBMERGED:
WAVELENGTH SELECTION AND ANTICIPATED ERRORS

T.J. Petzold and R.W. Austin

ABSTRACT

Prior analysis and experimentation has provided strong support for determining the attenuation of optical radiation for the atmosphere and the water column above a submerged platform by measuring the absolute downwelling irradiance at two wavelengths. The technique requires knowing the two irradiance values and in addition (1) the spectral irradiance of the sun outside the atmosphere, (2) the solar zenith angle and (3) the depth at which the irradiances are measured.

With this capability in hand the questions considered in this report are which wavelengths to use and the effect of errors in the measurement of irradiance and other parameters.

1.0 INTRODUCTION

The concept and theory for the determination of the optical properties of the atmosphere above the ocean's surface from spectral measurements of the natural light made below the surface was presented in detail in Ref.1[*].

One requirement to achieve a solution is that there be a known spectral relationship between the diffuse attenuation coefficient, $K(\lambda)$ for at least two wavelengths which is valid for the various "types" of natural waters found in open oceans. Preferably, a way of relating $K(\lambda)$ for all wavelengths over the range of interest would allow flexibility in the choice of wavelengths at which to make the measurement. From the results, the $K(\lambda)$ at any other wavelength, within the range covered, could be determined. A study of a large body of spectral $K(\lambda)$ data obtained by several investigators has yielded a model which can be used for these purposes. The model and it's basis are presented in Ref. 2.

The scheduling of a field experiment prompted asking the question of what wavelengths to select. Five photometers were available for this experiment and as a result five wavelengths were selected. Unfortunately, there is not a straightforward answer that is "best" for all situations. The "type" of water is critical to the selection of wavelengths and since this is unknown the selection must be based on predictions of the type of water expected. The effect of errors, particularly photometric, has played a large role in the wavelength selection. If the photometric measurements could be made without error, then the criteria for wavelength selections could be, by and large, those that would allow useable results to be acquired at maximum depth. Perversely, the use of wavelengths which would allow the system to perform at greater depths tend to make the system very sensitive to photometric error. As we gain more field experience and develop more precise and stable radiometers for this application, we can expect to obtain greater depth capability.

---

[*]Copies of Ref. 1, and 2 are appended to this report

2.0 METHOD

Using our knowledge of the optical characteristics of the atmosphere and seawater it is possible to compute, for a given wavelength, λ, the transmission of light downward through the atmosphere, the air-water interface, and through the water to some depth, z, for a given set of conditions. Using known values for the spectral irradiance from the sun outside the atmosphere, $E_o(\lambda)$, we can obtain an estimated value for the downwelling irradiance at depth z, $E_z(\lambda)$, for any wavelength for the given set of conditions. This is done at two wavelengths to produce a pair of irradiance values $E_z(\lambda_1)$, $E_z(\lambda_2)$. Then, using only these values, the procedure given in Refs. 1 & 2 is used to perform the inverse computation to calculate the diffuse attenuation of the water, $K(\lambda)$, and the optical depth of (or transmission through) the atmosphere at either of the wavelengths. These computed attenuation values are then compared with the original given or "true values" to get an estimate of the magnitude of error. This is the error which exists for a perfect system and results from assuming for the inverse computation that the optical properties of the aerosols in the atmosphere are not wavelength dependent. This assumption is necessary to enable the solution from measurements at two wavelengths.

Other sources of error will be present in a real system due to such causes as radiometric accuracy, errors in the values used for the solar input, solar zenith angle, depth measurement, etc. Offsets commensurate with those types of errors have been inserted into the calculations to find the sensitivity of the system to each of those sources of error.

Note: In the figures which follow the "true" values are indicated by a straight solid line, the computed values for a perfect two wavelength system are shown with a diamond ($\Diamond$) symbol, and the results of applying an error to some particular parameter are plotted using (+).

2.1 The Forward Calculation

The two values for $E_z(\lambda_1)$ and $E_z(\lambda_2)$ are determined as follows:

For values of $\tau_a(\lambda) \leq 1$ the transmittance for irradiance through the atmosphere is taken to be

$$T_A(\lambda) = \exp - \left[.48\tau_R(\lambda) + \tau_o(\lambda) + 0.5(1\text{-}g)\tau_a(\lambda) \right]/\mu_o \qquad \text{* (1)}$$

where

λ	indicates wavelength
$T_A(\lambda)$	is the total path transmission through the atmosphere
μ_o	is the cosine of the sun's zenith angle
$\tau_R(\lambda), \tau_o(\lambda), \tau_a(\lambda)$	are the optical depths for unit air mass due to: air molecules (Rayleigh scattering), ozone absorption, and aerosols respectively
g	is an asymmetry factor for aerosol particles and is approximately equal to 2/3.

The transmittance for irradiance through the water column is

$$T_W(\lambda) = e^{-K(\lambda)z} \qquad (2)$$

where

$K(\lambda)$	is the diffuse attenuation, and
z	is depth of water over sensor.

---

* See Ref. 5

A value of 0.98 is used for the irradinace transmittance through the air-water interface for all wavelengths. While this is not strictly true, any variation from this value will not be large and would have a very small effect upon the final results.

The irradiance at depth z is then:

$$E_z(\lambda) = 0.98 \cdot T_A(\lambda) \cdot T_w(\lambda) \cdot E_0(\lambda) \ . \tag{3}$$

where

$E_0(\lambda)$ is the solar irradiance outside
the atmosphere at a nominal wavelength λ
and over the band width of the sensor.

In this simulation two wavelengths are selected and a spectral bandwidth is chosen for the radiometric measurements. The radiometric response is taken to be uniform within this band width. In a real system the spectral response of the radiometers will have to be carefully determined and the mean, or effective wavelengths calculated. Also it will be necessary to calculate the proper effective values for the spectrally dependent parameters used such as $E_0(\lambda)$.

The value for $E_0(\lambda)$ was obtained from the work of Neckel and Labs Ref. 4. Figure 1 is a plot of these data. The data fluctuate markedly with wavelength and can not be represented by simple curve fitting procedures. Therefore, $E_0(\lambda)$ is calculated by interpolation at one nanometer increments over the passband and the average value used.

The Rayleigh (molecular) optical depth, $\tau_R(\lambda)$, for diffuse propagation of light through the atmosphere varies very nearly with the inverse fourth power of wavelength and is calculated using

$$\tau_R(\lambda) = 0.044(\lambda/670)^{-4} \ .$$

The effective value, $\overline{\tau_R(\lambda)}$, over the pass band λ_1 to λ_2 is:

$$\overline{\tau_R(\lambda)} = 0.044(\lambda_2 - \lambda_1)^{-1} \cdot \int_{\lambda_1}^{\lambda_2} (\lambda/670)^{-4} \cdot d\lambda = 2.956 \cdot 10^9 \, (\lambda_2 - \lambda_1)^{-1} \cdot (\lambda_1^{-3} - \lambda_2^{-3}) \tag{4}$$

The work of Klenk et al, Ref. 3, is used to find the spectral absorption coefficicent for ozone as a function of latitude and season. Figure 2 shows the spectral data (+) and a function curve which adequately describes the absorption per unit atmosphere - centimeter, (a/atm-cm). The total spectral absorption coefficient may be found by multiplying these values by "total ozone" which is a function of latitude and season. A value of 0.300 atm-cm was used as representative for mid-latitudes. The optical depth $\tau_0(\lambda)$ is taken to be equal to the total absorption coefficient and may be calculated from:

$$\tau_0(\lambda) = 0.300 \cdot 0.13879 \cdot e^{-A(\lambda)} \tag{5}$$

$$A = 0.0014717 \cdot (|\lambda - 589.75|)^{1.5301}. \tag{6}$$

Where the effective value, τ_0, over the pass band λ_1 to λ_2 is

$$\overline{\tau_0(\lambda)} = (\lambda_2 - \lambda_1)^{-1} \cdot \int_{\lambda_1}^{\lambda_2} \tau_0(\lambda) \cdot d\lambda \ . \tag{7}$$

The summation is done at one nanometer increments over the bandwidth and the average value used for $\tau_o(\lambda)$.

The optical depth for the aerosol, $\tau_a(\lambda)$ has a spectral dependency which appears to follow the power law

$$\tau_a(\lambda_1) = (\lambda_1/\lambda_2)^{-\alpha} \cdot \tau_a(\lambda_2) \ . \tag{8}$$

The exponent, α, known as the Angstrom exponent, is dependent upon the amount and quality of the aerosol. It falls in the range of 1.1 to 1.4 for clear atmospheres and, approaches zero for very large aerosols (fog, overcast).

Two types of atmosphere are used for illustration purposes, as follows:

Number Designation	Type Designation	$\tau_a(490)$	α
1	Haze	0.10	1.0
2	Heavy Overcast	10-20	0

For the "Heavy Overcast" case, the term $0.5 (1-g) \tau_a(\lambda)$ in Eq. (1) for transmittance (see Section 2.1) does not hold true. The transmittance of diffuse light is nearly spectrally independant for a heavy overcast consisting of fog or complete cloud cover. For this case the transmittance of diffuse light through the aerosol is taken to be 10% and the constant 2.3 *i.e.* -ln 0.1, is substituted for the term involving $\tau_a(\lambda)$.

In some of the figures the number(s) appearing on the right side are the number designation for the type of aerosol for which the information displayed applies.

The calculations used to obtain the irradiance values at the two wavelengths at depth z, viz. $E_z(\lambda_1)$ and $E_z(\lambda_2)$ and then using only these two values to estimate the atmosphere and water properties, require that a relationship exist between the diffuse attenuation coefficients, $K(\lambda)$, of the water at these two wavelengths. For the forward calculation, *i.e.*, propagating the light downward, a "type" of water must be selected. The value of $K(490)$ is used to specify the water type and from this, values for $K(\lambda_1)$ and $K(\lambda_2)$ may be calculated using the model and procedure presented in Ref. 2.

2.2 The Inverse Calculation

The model from Ref. 2 is also used to obtain the function relating $K(\lambda_1)$ and $K(\lambda_2)$ required for the inverse solution to the problem, given only $E_z(\lambda_1)$ and $E_z(\lambda_2)$.

Neither of the wavelengths λ_1 or λ_2 at which the two irradiance measurements are made needs to be at the wavelength for which we would like to know the atmospheric and water optical properties. To estimate the diffuse transmission of light through the atmosphere at some other wavelength, λ_3, we may use the same approximate assumption used to enable the inverse solution of the problem which is that the optical depth of the aerosol, $\tau_a(\lambda)$, is independent of wavelength, hence, $\tau_a(\lambda_1) \approx \tau_a(\lambda_2) \approx \tau_a(\lambda_3)$. In effect the calculated $\tau_a(\lambda)$ applies equally well at any wavelength. The error caused by this assumption is not large enough to preclude the usefulness of the procedure. Using Eq. (4) and (5) we can calculate $\tau_R(\lambda_3)$ and $\tau_o(\lambda_3)$. From Eq. (1) for diffuse atmospheric transmittance and using the approximation that the aerosol term is constant we can derive:

$$T_A(\lambda_3) = T_A(\lambda_1) \cdot \exp - \{ .48[\tau_R(\lambda_3) - \tau_R(\lambda_1)] + \tau_o(\lambda_3) - \tau_o(\lambda) \} \tag{9}$$

Thus we can obtain an estimate for the vertical diffuse transmittance through the total atmosphere at wavelengths other than the measurement wavelengths. For the water we can find $K(\lambda_3)$ from $K(\lambda_1)$ or $K(\lambda_2)$ using the model for $K(\lambda)$.

3.0 CONSIDERATIONS IN THE SELECTION OF WAVELENGTHS

Two criteria were considered in making the wavelength selection. The first and most obvious was to achieve maximum depth at which the radiometric measurements can be made. The second was to minimize the sensitivity to system error. The best

pair of wavelengths to use is highly dependent on the type of water for both of these criteria. The wavelengths which might be chosen for use in clear waters would not be a good choice for more turbid waters. Also these two criteria are not compatible. Using wavelengths to achieve maximum depth capability can result in the system being very sensitive to radiometic error, particularly those induced by wavelength calibration, and using wavelengths which minimize sensitivity to system error will lessen the depth at which the radiometric measurement can be made.

It is felt, at this time, that the second criteria should be dominant in the wavelength selection, *i.e*, do the best we can to enhance the probability of acheiving good results. After it has been demonstrated that the radiometric measurements can be made with the precision required to obtain satisfactory results over the long path lengths and high attenuations involved, then we can work toward greater depth capability.

To illustrate the effect of wavelength selection on sensitivity to radiometric error, water with a diffuse attenuation coefficient of K(490) = 0.067 (Jerlov Type II) will be used. If we are trying for greatest depth capability we should choose wavelengths in the region where light penetration is the greatest. Figure 3 shows typical values of $K(\lambda)$ plotted as a function of wavelength, λ, for seven Jerlov water types. Figure 4 shows the "optimum" wavelength, *i.e.*, the wavelength at which the minimum $K(\lambda)$ occurs, for water types in the region from pure sea water, K(490) = 0.022, to K(490) = 0.250. Considering only the water transmission properties we find that for water with a K(490) = 0.067 the "optimum" wavelength is in the region of 489nm and we would select two wavelengths on either side of this value. Figure 5 gives, as a function of wavelength, the depth at which the downwelling irradiance is $0.0002\mu W \cdot cm^{-2} \cdot nm^{-1}$[*].

This somewhat arbitrary number allows depth limit computations which are useful in wavelength selection. Ideally, in a "balanced" system both photometers would run out of adequate signal at the same depth. Figure 5 helps in the selection of two wavelengths in an attempt to acheive this, for water with a K(490) = 0.067. The solar input outside the atmosphere, $E_o(\lambda)$, and the diffuse transmittance through the atmosphere are included in the computations used for Fig. 5. The spectral solar irradiance, $E_o(\lambda)$, and the effective spectral diffuse optical depths, $\tau_R(\lambda)$ (Rayleigh), τ_o(ozone), and τ_a(aerosol) are all, in this case, computed over a 10nm pass band. Also a clear air case has been used with $\tau_a(490)$ being set to be 0.01 and the sun is at the zenith.

If the separation between the wavelengths selected is not large enough, the system will be insensitive to the spectral properties of the diffuse attenuation coefficient, $K(\lambda)$, of the water and poor results will be obtained. For a separation of 20nm Fig. 5 indicates that 480 and 500nm are nearly "balanced" wavelengths for K(490) = 0.067 type water. The sensitivity of measurement at these two wavelengths to change in water type, K (490), is demonstrated in Fig. 6. The value "Q" is a "figure of merit" where:

$$Q = 2.3026 \cdot [\log R_2 - \log R_1]/[K(490)_2 - K(490)_1] \cdot z \qquad (10)$$

and

$$R = E_z(\lambda_2) / E_z(\lambda_1) . \qquad (11)$$

The statement "if $\Delta K(490)$ =.001 then ΔR = 1.019" in Fig. 6, indicates that a change in K(490) of .001 will result in a change in the ratio of the irradiances, $R = E_z(500)/E_z(480)$, at depth z (100 meters in this case) of 1.9%. It can also be inferred from this that an error in the determination of the ratio, R, of 1.9% will cause, approximately, an error or .001 in the computation of $K(\lambda)$. In a similar manner but using wavelength separations of 50 nm and 100 nm, the results shown in Figs. 7 & 8 are obtained. It is seen that increasing the separation markedly improves the sensitivity to change in the water quality. This improved performance comes at the cost of depth capability. Again using Fig. 5 we can estimate the depth limitation; *i.e.*, the depth at which the irradiance, $E_z(\lambda)$, arriving at one or both photometers is $0.0002\mu W \cdot cm^{-2} \cdot nm^{-1}$. To summarize:

For Water Type K(490) = 0.067

λ_1(nm)	λ_2(nm)	Sensitivity change in DR with 0.001 change in $K_{(490)}$	Approximate Depth Limitation (meters)
480	500	1.019	200
460	510	1.049	180
440	540	1.092	160

---

[*] This is the level at which a photometer employing a high quality photomultiplier tube having an irradiance collector with a 3/4 inch diameter, a band pass of 10nm, and a transmission through the optical path of 1%, might be expected to have a signal to noise ratio in excess of ten.

The above selection process could be used to obtain maximum depth capability for any one water type. Using 460 and 510nm, Fig. 9 explores how the $E_z(460)$ and $E_z(510)$ values and their ratio would change with depth in K(490) = 0.067 type water. Since K(460) = 0.0759 and K(510) = 0.0739 are not greatly different, the ratio does not change much with depth. Figures 10 and 11 are similar, using the same two wavelengths, but in water types K(490) = 0.038 (Jerlov Type IB) and K(490) = 0.115 (Jerlov Type III). Note that the arbitrary irradiance limit of $0.0002\mu w \cdot cm^2 \cdot nm^{-1}$ is reached at a depth of about 100 meters at $\lambda=460nm$ when K(490) = 0.115 and has not been reached at 200 meters when K(490)=0.038.

The selection of wavelength based on the second criteria, minimum sensitivity to system error (primarily wavelength), leads to a different set of wavelengths and some loss in depth capability. By wavelength error is meant the difference between the wavelength at which we think the radiometer is making the measurement, (the assigned wavelength used in the computations), and the actual effective or mean wavelength to which the radiometer responds. For instance if the radiometer's effective response was at 492nm and we used 490nm in the calculations the wavelength error would be -2nm.

To acheive minimum sensitivity to wavelength error we must find a wavelength where $K(\lambda)$ (and to a much lesser extent $E_o(\lambda)$, $\tau_R(\lambda)$, $\tau_o(\lambda)$ and $\tau_a(\lambda)$) is not changing rapidly with wavelength over the channel band width. We also need to do this at two wavelengths which are far enough apart and in regions which will give good responsivity to the quality of the water. Observation of the $K(\lambda)$ vs λ curves, Fig. 4, is helpful in the selection for this criteria and also shows the difficulty in such a selection. Certainly the selection of the "optimum" pair of wavelengths is highly dependent upon water type.

To illustrate the difference in sensitivity to wavelength error between wavelengths selected with this in mind as opposed to wavelengths selected to obtain maximum depth capability, the use of wavelengths 420 and 490nm will be compared with 460 and 510nm when the water type is again K(490)=0.067. In the figures starting with Fig. 12, the solid lines are the "true" values; the points indicated by diamonds (◊), are values which would be calculated if the system were perfect, *i.e.* had no errors including the values used for $E_o(\lambda)$, $\tau_R(\lambda)$ and $\tau_o(\lambda)$; and crosses (+), are values which would be calculated if the error shown in the heading under "error factors" is introduced. The small error of the "perfect" system is due to the assumption, made to allow the inverse problem to be solved, that the diffuse transmission properties of the aerosol, $\tau_a(\lambda)$ are spectrally independent, *i.e.* $\tau_a(\lambda)$ is the same at all wavelengths. Two "types" of aerosol are used: (1) haze, $\tau_a(490)=0.10$ and $\alpha=1.00$, and (2) overcast, $\tau_a(490)=10\text{-}20$ and $\alpha=0.00$. The type of aerosol is indicated on the graphs by the numbers 1,& 2 on the right hand side. In all cases 30° is used for the solar zenith angle and 10nm for the radiometric bandpass. Frequently we would like to know the atmospheric and water attenuations at a wavelength other than either of the two at which the measurement is made. In these figures two wavelengths have been used for the measurement wavelengths, the problem solved at one of these wavelengths, both with and without the applied error, and then the results transferred to a third "wavelength of interest" λ_c, via the model(s). The figures have three graphs: (1) transmission through the total atmosphere. This is the vertical transmission, *i.e.* for unit air mass. It is shown for both atmospheric types. (2) Logarithm of the transmission through the total path. This is the vertical transmission through the atmosphere, the air-water interface and the water column. It is shown for both atmospheric types. (3) The ratio of the calculated transmission to the true transmission for the total vertical path. It is shown for one atmospheric type*. All of these values are plotted as a function of depth, and are the results obtained for the third wavelength, the "wavelength of interest".

In Fig. 12 the photometric measurement wavelengths are 420 and 490nm and the wavelength of interest is 459nm. A wavelength error of +2nm has been applied to the photometric measurement at $\lambda_2(490nm)$. The problem is solved to obtain the results at 490nm and the values for $\lambda=459nm$ calculated. To calculate the effect of the applied error, values indicated by crosses (+), the problem is solved using 492nm, the erroneous wavelength, in place of 490nm, the true wavelength. Figure 13 is a repeat of Fig. 12 except that the error applied to λ_2 is -2nm. Figures 14 and 15 show the effect of the same wavelength error offsets when 460nm and 510nm, the wavelengths arrived at previously to obtain greater depth capability, are used for the measurement wavelengths.

Comparison of Fig. 12 & 13 with Fig. 14 & 15 demonstrates that the sensitivity to wavelength error is highly dependent on wavelength selection. The penalty for lower wavelength sensitivity is loss of depth capability. In this case the depth limit, (K (490)=0.067 type water and again using $0.0002\mu W \cdot cm^{-2} \cdot nm^{-1}$ for the photometer's limit of sensitivity), is about 140 meters at 420nm when 420nm and 490nm are used and about 180 meters when 460nm and 510nm are used. This sensitivity to wavelength error becomes even more drastic in more turbid waters. Figures 16 through 19 is another case with the same magnitude of wavelength error applied for water type K(490)=0.248 (Jerlov Type 2). For maximum depth, 527nm and 577nm would be used (Fig. 18 & 19) and the depth limit would be about 64 meters. For the other wavelengths used, 420 &

---

*The results presented this way are nearly identical for all atmospheric types.

550nm, the depth limit is about 33 meters (see Figs. 16 & 17).

4.0 OTHER SOURCES OF ERROR

4.1 RADIOMETRIC ERROR (other than wavelength)

Two measurements of the absolute downwelling irradiance at some depth, z , are required. An error in these measurements produces a corresponding error in the determination of the atmospheric and water diffuse attenuation properties. The radiometric error is the sum of the error in calibration, drift in sensitivity with time, and change in sensitivity with temperature. The effect of this error is a function of the two wavelengths used and in general is lessened by increasing the separation between the wavelengths. This is illustrated in Fig. 20 where $\lambda_1=420$nm and $\lambda_2=470$nm, the water is pure seawater, K(490)=0.022, and an error of -5% is applied to the irradiance measurement at λ_1; and in Fig. 21 where the same error is applied but the wavelengths used are 420nm and 530nm. Figures 22 & 23 are similar to Figs. 20 & 21 but for water type K(490)=0.125. The effect of this type of error is independent of depth and essentially independent of water type.

4.2 DEPTH ERROR

A one meter offset in the depth value used in the computations will cause the errors shown in Figs. 24 & 25 for water types K(490)=0.038 and 0.250 respectively. The errors caused by a 1% non-linearity in depth are shown in Fig. 26 & 27 for the same water types. In all cases 420nm and 530nm were used for the two photometric wavelengths. An offset produces errors in T_A, total atmospheric transmisssion, and T, total transmission atmosphere and water, which quickly reach an asymptote and become essentially independent of depth. A non-linearity, of course, produces an error which is proportional to depth.

4.3 SOLAR ZENITH ANGLE ERROR

The error caused by using an incorrect zenith angle, θ_s, for the sun is a function of the cosine of the zenith angle. It is small for high suns, (small zenith angle) and large for low suns, (large zenith angle). Two examples are given in Figs. 28 & 29 for $\theta_s=30°$ and $\theta_s=60°$ both with an applied error of +5°. This error is independent of depth and water type.

4.4 ERROR INTRODUCED BY THE MODEL USED
FOR SEA WATER OPTICAL PROPERTIES

To use this system it is necessary to use a relationship which allows the determination of the diffuse attenuation coefficient of the water at a second wavelength, $K(\lambda_2)$, from knowledge of the value at some other wavelength, $K(\lambda_1)$ (Ref. 1 & 2). For flexibility it is most desirable that this can be done between any two wavelengths within a span of practical values. The model used for this purpose is presented in detail in Ref. 2. To obtain good results over the long water path lengths desired, it is necessary to determine accurately the $K(\lambda)$ values involved. The prospect of doing this depends to a large extent on how well this model matches the spectral character of the water in which the system is being used. The data on which the model is based is not very precise. It is subject to usual experimental errors and adversely affected by difficult, at sea, environmental operating conditions. It can be hoped that the fairly large data base used in forming the model, resulted in statistically significant smoothing of the data base and that the model is satisfactory for this application.

The correctness of the model and the uniformity of fairly clear deep oceanic water such that the model will match all such waters can only be determined by future experimentation and testing. The model remains a potential source of error, the magnitude of which, at this time, is unknown.

4.5 SOLAR AND ATMOSPHERIC CONSTANTS

The sun is used as a known source of irradiance outside of the atmosphere. The absolute spectral level of this irradiance, $E_o(\lambda)$, is a primary input for this system. Much effort has been put into determing the correct values for this spectral solar irradiance. It is believed the values of Neckel and Labs (1981) are correct within approximately one percent. However, this

must be considered a potential source of error. Figures 30 & 31 show the results of a +5% error in $E_o(\lambda)$ at 420nm using 420nm and 470nm for the measurement wavelengths. Figure 30 is for pure sea water, K(490)=0.022 and for Fig. 31 K(490)=0.125. Figures 32 & 33 are for the same water types and error offset but 420nm and 530nm are the wavelengths used. This type of error is independent of depth and water type and has less effect, at least on the atmospheric transmission calculated, when the wavelengths used are farther apart.

5.0 DIFFUSE ATTENUATION COEFFICIENT OF THE WATER

The ability to determine the effective diffuse attenuation coefficient, $K(\lambda)$, of the water at any wavelength of practical interest from the measurement of downwelling irradiance at two wavelengths is a significant secondary objective of this type of system. Examples are given, all using 420nm and 530nm for the measurement wavelengths and the results shown for the computed $K(\Lambda)$ at 459nm. The computed $K(\lambda)$ vs depth for water type K(490)=0.067 with an applied error of +2nm at λ_1(420nm) is shown for two types of atmosphere in Fig. 34. Figure 35 has the same error applied at 420nm but for water types K(490)=0.038 and K(490)=0.152 with atmosphere No. 2 (overcast). Figures 36 through 41 all show examples using these same two water types. In Fig. 36, the error applied makes the irradiance measurement at 420nm low by 5%. Figure 37 has a depth offset error of +1 meter at all depths and Fig. 38 has a depth non-linearity of +5%. The effect of a +5° error in the solar zenith angle is shown in Fig's. 39 & 40; with the "true" zenith angle 30° in Fig. 39 and 60° in Fig. 40. Figure 41 has an error of -5% in the assumed solar irradiance at 420nm.

When a fairly long path length is used (2-4 attenuation lengths; transmission about 2 to 10%), the theoretical computations produce, even with these applied errors, values which are closer to the real value than can be expected from the usual *in-situ* methods normally employed to get this type of data. How well this works in the real world needs to be determined. The accuracy of the $K(\lambda)$ calculated is subject to degradation by all the errors discussed in previous sections. It is largely the error involved in determining $K(\lambda)$ which will cause an error in the calculated atmosphere and water path transmissions.

6.0 SUMMARY AND COMMENTS

Wavelength Selection - There are two considerations in selecting the two wavelengths: (1) maximum depth at which the photometers will have adequate signal and (2) sensitivity of the system to radiometric and other error sources. These two criteria do not lead to the same wavelengths. Selection of "optimum wavelengths" to satisfy one has an adverse effect on the other and both are highly dependent on the type of water. There is no one "best choice". The choice is a matter of compromise, judgement and pratical considerations. Large separation between the wavelengths in most cases will improve system performance.

Radiometry - If adequate system performance is to be achieved, good radiometric calibrations and stability are required. The absolute responsivity, linearity and "effective mean wavelength" for both radiometers must be known. The radiometers need to be stable with respect to time, environment, and temperature. The spectral filters may degrade with time and the sensitivity of the radiometer may change. This suggests that periodic "re-calibration" should be done. The sensor, particularly if a photomultiplier tube, may suffer a change in spectral response with changes in temperature. Some method may be required to stablize or correct for such changes in sensitivity. A stable internal reference light source could be used to correct the readings for changes in sensitivity.

Errors - The system can be very sensitive to wavelength and the wavelength at which the measurements are made must be closely known to avoid possible large errors. Absolute radiometric error has less significance if both radiometers are in error in the same direction. The inherent error of the two wavelength system is small relative to the probable error caused by other sources such as radiometric measurement accuracy, the values used for the other inputs, and the fidelity of the $K(\lambda)$ model used.

Water Properties - The system can be a useful tool for the determination of the spectral diffuse attenuation properties of natural oceanic waters.

Atmosphere - It appears that an estimate of the optical depth of the atmosphere can be obtained which is adequate for assessing the total atmospheric transmittance loss.

<u>Total Transmission</u> - When the total spectral diffuse transmission, *i.e.*, the transmission through the total atmosphere, the air-water interface and the water path, is examined, it becomes apparent that for any appreciable water path (*i.e.*, depth) the attenuation through the water is predominate over the loss in the atmosphere. In estimating the total attenuation it appears that this type of system may produce very satisfactory results.

<u>Final Comment</u> - The inherent error in the computations which results from the assumption that the portion of the atmospheric attenuation caused by the aerosol is constant at all wavelengths is very small. For atmospheres which are not cloudy, heavily overcast, or foggy ($\tau_a < 1$), the term for the aerosol in Eq. (1) for the atmospheric transmittance given in section 2.1, i.e. $1/2(1-g)\tau_a(\lambda)$ is approximately $1/6 \cdot \tau_a(\lambda)$ and has a minor effect on the results. For aerosols of greater densities α is very small and the aerosol attenuation though large is essentially independent of wavelength.

All that has been presented in this report assumes perfection, other than for the errors intentionally introduced. In a real system the final results will be the summation of all sources of error. The goodness of the match between the $K(\lambda)$ water model and the actual waters is a source of error the magnitude of which is yet to be determined.

7.0 RECOMMENDED WAVELENGTHS

For a field test, five photometers were available allowing the choice of five different wavelengths. Two of those photometers had a linear response with auto-ranging. The remaining three had a pseudo-logarithmic response.

Using the approach presented in this report, five wavelengths were selected: 420, 470, 490, 530, and 550nm with 420nm and 530nm assigned to the linear photometers. Table A gives the selected combinations and lists the water types for which it is recommended these wavelengths be used. The first choice for wavelength pair is 420 and 530nm. Table B gives an estimate of certain errors that might be anticipated for a 2nm wavelength calibration offset, when using these two wavelengths in five different types of water. Table C gives the second choice of wavelength pairs which could be used to increase depth capability. Again the same estimates of error are given for the five types of water. The error values in Table C can be directly compared with the values in Table B where $\lambda_c = 459$. Tables B and C also give the depth limits which can be anticipated for the various pairs of wavelengths.

A photometric error of 5% in the measurement of the irradiance, $E_z(\lambda)$, can cause the resultant errors shown in Table D for the various recommended wavelength combinations. Similarly the effect of a 1 meter offset in depth is shown in Table E. Table F gives the errors which can result from a +5% offset in solar zenith angle. This error can be severe for large zenith angles (low sun). The errors indicated in Table G can result from a 5% error in the value used for $E_0(\lambda)$, the extra-terrestrial solar irradiance arriving outside the atmosphere.

Table H is a listing of the solar irradiance, $E_0(\mu W \cdot cm^{-2} \cdot nm^{-1})$, outside the atmosphere and the optical depths $\tau_R(\lambda)$ (Rayleigh), $\tau_0(\lambda)$ (ozone) and $\tau_0(\lambda)$ (aerosol); calculated as discussed in this report. A 10nm bandpass, uniform response from λ-5nm to λ+5nm and a value of $\tau_a(490)=0.01$ (clear atmosphere) was used.

8.0 REFERENCES

1. Petzold, T.J. (1983), *VisLab Tech Memo EN-001-83t*, University of California, San Diego, Scripps Institution of Oceanography, Visibility Laboratory.

2. Austin, R.W. and T.J. Petzold (1984), "Spectral dependence of the diffuse attenuation coefficient of light in ocean water", Proc. of the SPIE, *Ocean Optics VII*, Vol. 489, pp. 168-178, Monterey, California.

3. Klenk, K.F., P.I. Bhartia, E. Hilsenrath and A.J. Fleig, "Standard ozone profiles from balloon and satellite data sets", Journal of Climate & Applied Meteorology, December, 1983, Vol. 22, #12, pp. 2012-2022.

4. Neckel, H. and D. Labs, "Improved data of solar spectral irradiance from 0.33 to 1.25μ", Solar Physics, Vol. 74 (1981), pp. 231-249.

5. Tanre, D., M. Herman, P.Y. Deschamps and A. de Leffe, "Atmospheric modeling for space measurements of ground reflectances, including bidirectional properties", Appl. Opt., Vol. 18, #21 (Nov. 1979), pp. 3587-3594.

Table A. Recommended wavelengths.

λ_1 (nm)	λ_l (nm)	Water Type, K(490), Range (m⁻¹)	Depth Range(m)
420	530	.022 — .250	260 — 33
420	490	.022 — .046	620 — 229
470	530	.046 — .125	197 — 97
490	550	.125 — .250	109 — 55

NOTES: The combination λ_1=420 and λ_2=530 is the first reccommended choice. The other combinations should be used only if necessary to obtain adequate signal.

The depth range given is for the corresponding water type range and is the depth at which the irradiance, $E_z(\lambda)$, at either λ_1 or λ_2 first reaches $0.0002\mu W \cdot cm^{-2} \cdot nm^{-1}$ with a clear atmosphere and the sun at the zenith.

Table B. Wavelength error, λ_1=420, λ_2=530nm. Maximum error caused by a ± 2nm offset in wavelength calibration.

K(490) m⁻¹	Max Depth m ①	%ERROR IN T'_A AT ②				%ERROR IN T' AT ③				Transfered To λ_c(nm)	From Computations At λ_c(nm)	Error Applied At λ_c(nm) ④
		25m	50m	100m	200m	25m	50m	100m	200m			
.022	260	4	8	17	37	-0.5	-0.5	-0.5	-0.5	420 & 530	420 & 530	530(+2)
		4	8	17	37	0.5	1	3	7	459	420	530(+2)
.046	200	2	5	11	24	-0.5	-0.5	-0.5	-0.5	420 & 530	420 & 530	530(+2)
		2	5	11	24	0.5	1	2	5	459	420	530(+2)
.077	120	1	3	7	—	1	1	1	1	420 & 530	420 & 530	420(+2)
		1	3	7	—	1	2	2	—	459	420	
.125	70	3	6	—	—	1	1	—	—	420 & 530	420 & 530	420(+2)
		3	6	—	—	1	2	—	—	459	420	
.250	33	9	—	—	—	2	—	—	—	420 & 530	420 & 530	530(-2)
		9	—	—	—	2	—	—	—	459	420	

Notes: (1) Depth at which $E_z(\lambda)$=0.0002 $\mu W \cdot cm^{-2} \cdot nm^{-1}$ (clear atmosphere, sun at the zenith).
(2) Transmittance through atmosphere at wavelength λ_c
(3) Transmittance through total path (atmosphere + water) at wavelength λ_c
(4) Wavelength and direction (±) at which 2nm offset causes maximum error

Table C. Wavelength error for λ_1 and λ_2 in table.

Maximum error caused by a 2nm offset in wavelength calibration using λ_1 and λ_2 to obtain greater depth capability.

K(490) m⁻¹	λ₁ (nm)	λ₂ (nm)	① Max Depth (m)	② %ERROR IN T'_A AT 25m	50m	100m	200m	③ %ERROR IN T' AT 25m	50m	100m	200m	④ Error Applied λ(nm)
.022	400	490	620	2	8	20	48	-3	-4	-8	14	490(+2)
.046	420	490	229	-0.5	2	8	20	-2	-3	-4	-8	490(+2)
.046	470	530	197	3	7	16	35	-1	-1	-2	-3	530(+2)
.077	470	530	151	4	8	16	—	-1	-1	-2	—	470(+2)
.125	470	530	97	8	16	34	—	-1	-2	-3	—	470(+2)
.125	490	550	109	6	10	18	—	-4	-5	-8	—	490(+2)
.250	490	550	55	16	31	—	—	-7	-10	—	—	490(+2)

Notes:
(1) Depth at which $E_t(\lambda)=0.0002\ \mu W \cdot cm^{-2} \cdot nm^{-1}$ (clear atmosphere, sun at the zenith).
(2) Transmittance through atmosphere at $\lambda_c=459nm$.
(3) Transmittance through total path (atmosphere + water) at $\lambda_c=459nm$.
(4) Wavelength and direction (±) at which 2nm offset causes maximum error.

Table D. Maximum error caused by a 5% offset in the measured irradiance, $E_t(\lambda)$, at λ_1 or λ_2.

Calculated at $\lambda_c=459nm$

① λ₁ (nm)	② λ₂ (nm)	Water Type, K(490) from to	② Maximum Error in T'_A (%)	③ Maximum Error in T' (%)
420	530	.022 — .250	9	4
420	490	.022 — .046	13	3
470	530	.046 — .125	13	7
490	550	.125 — .250	13	9

Notes:
(1) λ_1, λ_2 are the two wavelengths at which the irradiance, $E_t(\lambda)$, measurements are made. (The errors are calculated for results transferred to $\lambda_c=459nm$).
(2) Transmittance through atmosphere at $\lambda_c=459nm$.
(3) Transmittance through total path (atmosphere + water) at $\lambda_c=459nm$.
(2), (3) Error is independent of depth.

Table E. Error caused by a 1 meter offset in depth. Calculated at $\lambda_c=459nm$.

λ_1 (nm) [1]	λ_2 (nm)	Water Type K(490) m^{-1}	Error in T'_A (%) [2]	Error in T' (%) [3]
420	530	.022	8	3
420	530	.046	8	7
420	530	.077	8	11
420	530	.125	8	18
420	530	.250	8	39
420	490	.022	3	2
420	490	.046	3	5
470	530	.046	11	–
470	530	.125	11	16
490	550	.125	13	13
490	550	.250	13	33

Notes: (1) λ_1, λ_2 are the two wavelengths at which the irradiance, $E_s(\lambda)$, are measured. (The errors are calculated for results transferred to $\lambda_c=459nm$).

(2) Transmittance through atmosphere at $\lambda_c=459nm$.

(3) Transmittance through total path (atmosphere + water) at $\lambda_c=459nm$.

(2), (3) Error is independent of depth.

Table F. Error caused by a +5% offset in solar zenith angle, θ_s

θ_s (deg.)	ERROR IN T'_A(%)		ERROR IN T'(%)	
	Haze	Overcast	Haze	Overcast
25	3	10	3	10
30	5	19	5	19
45	7	32	8	33
60	9	55	11	59
75	10	133	25	170

Notes: (1) Error is independent of depth.

(2) The wavelength at which the computations are made, λ_c, has negligible effect on the error ($\approx \pm 0.2\%$).

(3) The measurement wavelengths, λ_1 λ_2, used have a small effect on the resultant error ($\approx \pm 0.4\%$).

(4) The error is independent of type of water.

(5) T'_A = transmittance through the atmosphere.

(6) T' = transmittance through the total path (atmosphere + water).

-13-

Table G. Error caused by a ±5% offset in the solar irradiance, $E_o(\lambda)$.
Calculated at $\lambda_c = 459$nm.

λ_1 (nm)	λ_2 (nm) ①	Error in T'_A(%) ②	Error in T'(%) ③
420	530	9	3
420	490	14	3
470	530	13	7
490	550	14	10

Notes: (1) λ_1, λ_2 are the two wavelengths at which the irradiance, $E_z(\lambda)$, are measured. (The errors are calculated for results transferred to $\lambda_c = 459$nm).

(2) Transmittance through atmosphere at $\lambda_c = 459$nm.

(3) Transmittance through total path (atmosphere + water) at $\lambda_c = 459$nm.

(2), (3) Errors in T'_A and T' are independent of depth.

(3) Errors in T' can be larger or smaller if another "wavelength of interest", λ_c, is used.
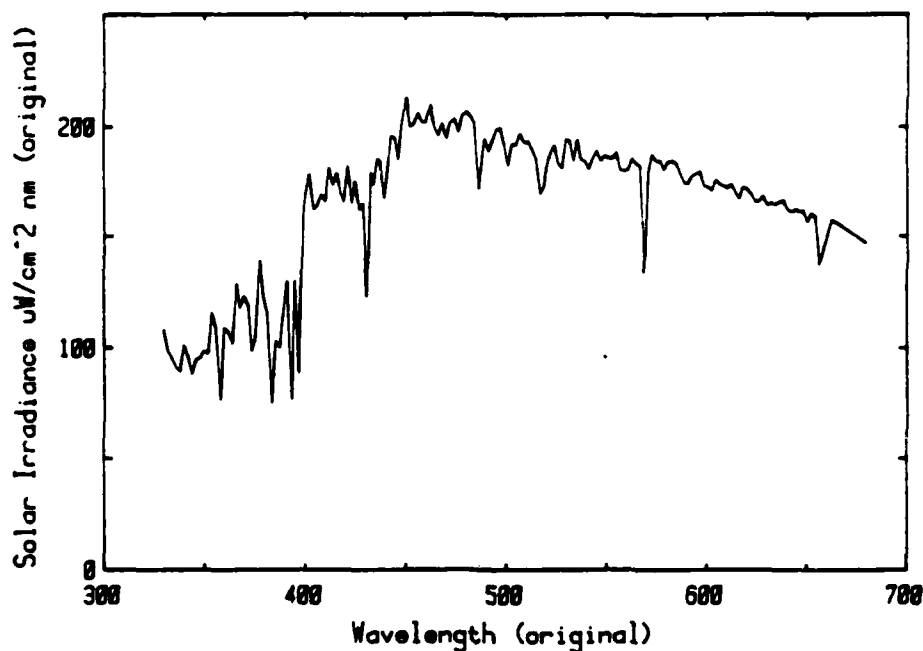
Fig. 1a. Extra terrestrial Solar Irradiance. Neckel and Labs Ref. 4.

```
MODEL  MLC761625

BANDPASS  10 nm

τ(490) = 0.010   σ = 1.298
```

λ(nm)	Eo	τRa	τOz	τa
410	170.99	0.1534	0.0022	0.0126
415	173.29	0.1509	0.0026	0.0124
420	172.62	0.1438	0.0031	0.0122
425	165.80	0.1372	0.0037	0.0120
430	162.49	0.1309	0.0044	0.0118
435	168.47	0.1250	0.0052	0.0117
440	183.93	0.1194	0.0061	0.0115
445	192.73	0.1141	0.0071	0.0113
450	200.19	0.1091	0.0083	0.0112
455	203.80	0.1044	0.0097	0.0110
460	203.37	0.0999	0.0112	0.0109
465	200.82	0.0957	0.0130	0.0107
470	199.14	0.0917	0.0150	0.0106
475	201.19	0.0879	0.0173	0.0104
480	201.86	0.0843	0.0198	0.0103
485	194.04	0.0809	0.0227	0.0101
490	189.03	0.0776	0.0258	0.0100
495	193.68	0.0745	0.0293	0.0099
500	192.48	0.0716	0.0332	0.0097
505	191.29	0.0688	0.0374	0.0096
510	191.48	0.0661	0.0421	0.0095
515	132.72	0.0636	0.0471	0.0094
520	131.62	0.0612	0.0525	0.0093
525	136.56	0.0589	0.0583	0.0091
530	187.38	0.0567	0.0644	0.0090
535	133.43	0.0546	0.0709	0.0089
540	185.90	0.0526	0.0777	0.0088
545	185.16	0.0507	0.0847	0.0087
550	186.29	0.0489	0.0919	0.0086
555	133.68	0.0472	0.0992	0.0085
560	182.38	0.0455	0.1065	0.0084
565	173.42	0.0439	0.1136	0.0083
570	174.13	0.0424	0.1204	0.0082
575	181.79	0.0409	0.1266	0.0081
580	133.24	0.0395	0.1321	0.0080

Fig. 1b. Table showing the effective extra-terrestrial solar irradiance in a 10nm band centered at the wavelength in column 1, and the optical depths $\tau_R(\lambda)$ (Rayleigh or molecular component), $\tau_O(\lambda)$ (ozone), and $\tau_a(\lambda)$ (aerosol). Uniform sensor response over the pass band and @ $\tau_a(490) = 0.01$ were assumed.
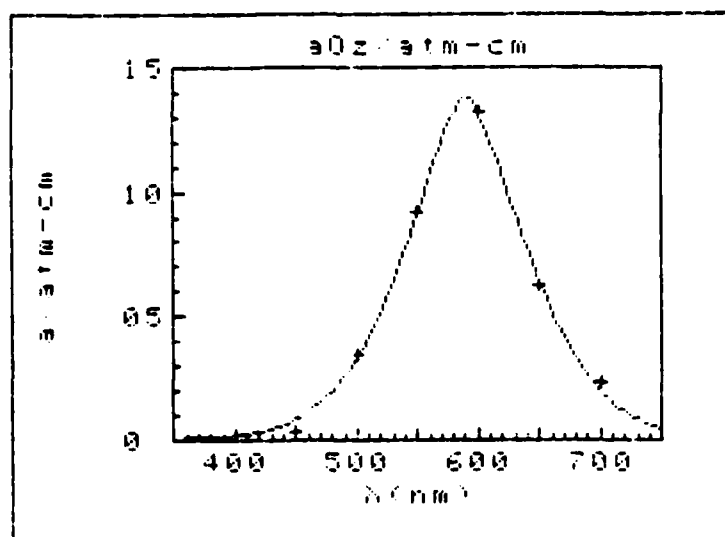
aOz/atm-cm

5370 G=P(1)*EXP(-(P(2)*ABS(H-P(3
))^P(4)))

```
P1 =  1.3879E-001
P2 =  1.4717E-003
P3 =  5.8973E+002
P4 =  1.5301E+000
```

a/atm-cm

NO LIMIT

λ	DATA	CURVE	DIFF
400	0.0000	0.0015	0.0015
450	0.0035	0.0083	0.0048
500	0.0345	0.0331	-.0014
550	0.0920	0.0919	-.0001
600	0.1320	0.1318	-.0002
650	0.0620	0.0637	0.0017
700	0.0230	0.0195	-.0035

NO. POINTS: 7

	DIFF
MEAN	.0004
SDEV	.0026

Fig. 2. Ozone spectral absorption. Data and model.

MODEL MLC761625

JERLOV -

TYPE	K(490)
I	0.023
IA	0.029
IB	0.038
II	0.067
III	0.115
1	0.152
2	0.248
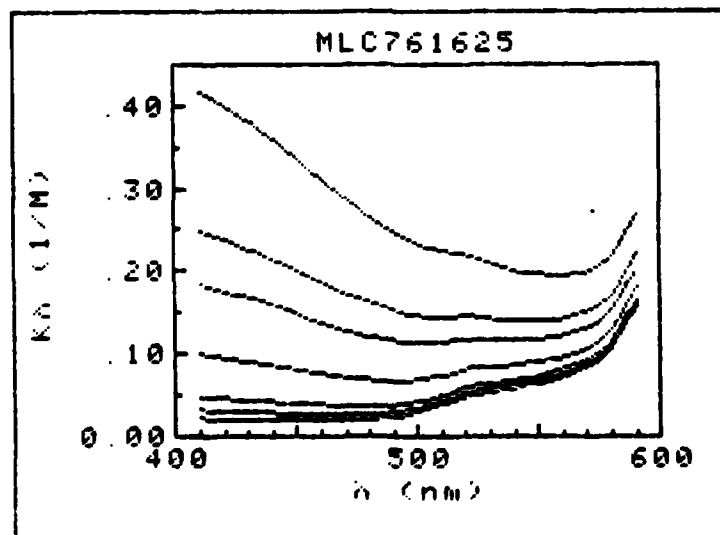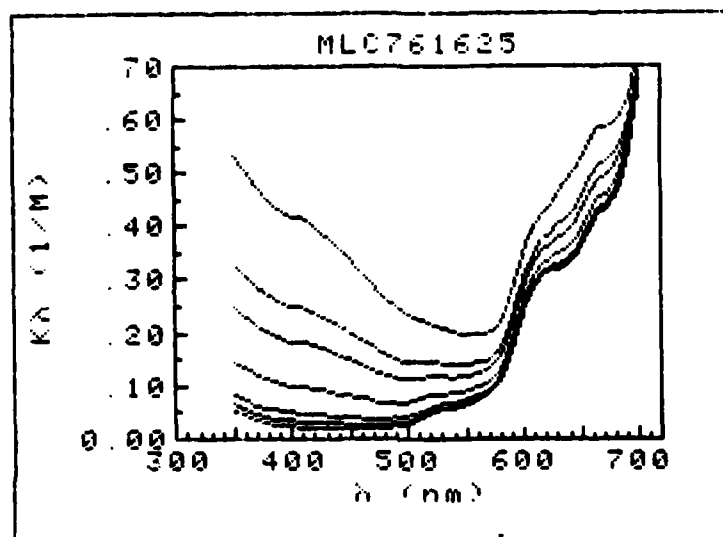
Fig. 3. Values of K(λ) for Jerlov water types I-III and 1 & 2. See Ref. 2.

MODEL MLC761625

OPTIMUM WAVELENGTH

K(490)	λ(nm)	F
0.022	453	0.018
0.030	470	0.027
0.040	478	0.039
0.050	483	0.049
0.060	487	0.060
0.070	490	0.070
0.080	494	0.080
0.090	496	0.089
0.100	499	0.099
0.110	501	0.108
0.120	503	0.117
0.130	505	0.126
0.140	543	0.132
0.150	545	0.133
0.160	547	0.145
0.170	548	0.150
0.180	550	0.156
0.190	551	0.162
0.200	552	0.168
0.210	553	0.174
0.220	554	0.179
0.230	555	0.185
0.240	556	0.191
0.250	557	0.196
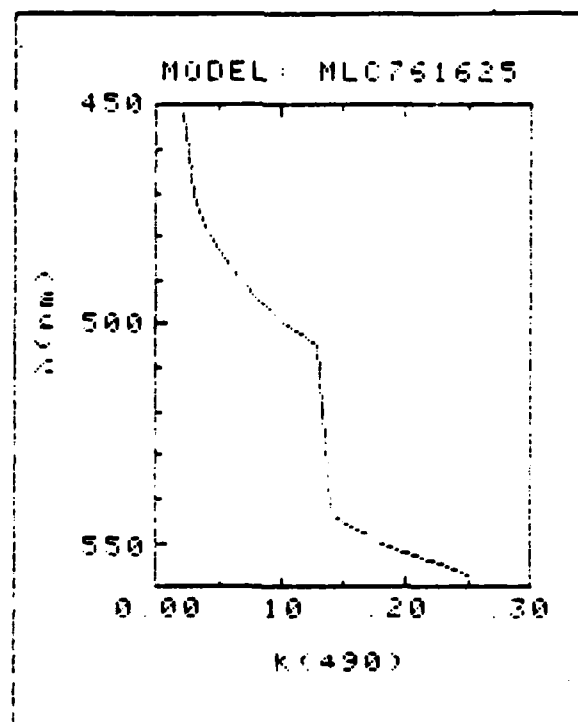
Fig. 4. Optimum wavelengths for maximum depth vs K (490).

```
MODEL  MLC761625
BANDPASS  10 nm
K(490) = .067  τs(490) = .01
DEPTH AT WHICH IRRADIANCE IS:
   Ez =  .002 uW cm²
   Ez =  .0002 uW cm²nm
```

λ(nm)	K(1/m)	DEPTH(m)
420	0.0946	147
425	0.0923	146
430	0.0900	149
435	0.0877	154
440	0.0854	159
445	0.0830	164
450	0.0807	170
455	0.0783	175
460	0.0759	181
465	0.0735	186
470	0.0714	192
475	0.0695	197
480	0.0682	201
485	0.0673	203
490	0.0670	204
495	0.0674	203
500	0.0687	199
505	0.0708	193
510	0.0739	185
515	0.0781	174
520	0.0836	163
525	0.0827	165
530	0.0835	163
535	0.0846	161
540	0.0860	158
545	0.0879	155
550	0.0902	151
555	0.0930	146
560	0.0966	140
565	0.1012	133
570	0.1073	126
575	0.1155	117
580	0.1285	105

Fig. 5. Depth limit (for $0.2\mu w \cdot cm^{-2} \cdot nm^{-1}$) vs wavelength when $K(490)=0.067 m^{-1}$.

MODEL MLC761625

Z = 100 METERS

Ez(500)/Ez(490)
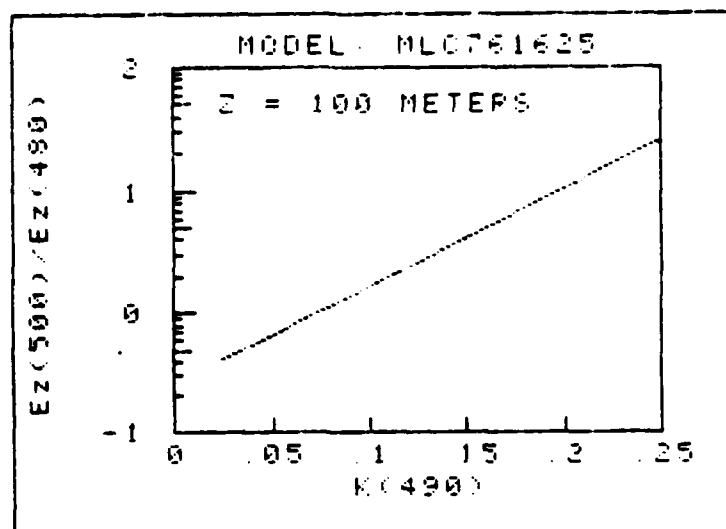
K(490)

MODEL MLC761625

WAVELENGTHS 480 AND 500 nm.

DEPTH (Z) = 100 METERS

BANDPASS 10 nm Ta(490) = .01

Q = 184

IF ΔK(490) = .001 THEN ΔR=1.013

K(490)	K(480)	K(500)
0.0234	0.0197	0.0280
0.0400	0.0386	0.0440
0.0600	0.0605	0.0623
0.0800	0.0824	0.0805
0.1000	0.1043	0.0987
0.1200	0.1262	0.1170
0.1400	0.1481	0.1352
0.1600	0.1700	0.1535
0.1800	0.1920	0.1717
0.2000	0.2139	0.1899
0.2200	0.2358	0.2082
0.2400	0.2577	0.2264
0.2600	0.2796	0.2446

K(490)	Ez(490)	Ez(500)
0.0234	2.60E+001	1.04E+001
0.0400	3.77E+000	2.08E+000
0.0600	4.23E-001	3.36E-001
0.0800	4.73E-002	5.42E-002
0.1000	5.27E-003	8.76E-003
0.1200	5.90E-004	1.41E-003
0.1400	6.59E-005	2.28E-004
0.1600	7.37E-006	3.69E-005
0.1800	8.24E-007	5.95E-006
0.2000	9.21E-008	9.61E-007
0.2200	1.03E-008	1.55E-007
0.2400	1.15E-009	2.50E-008
0.2600	1.29E-010	4.04E-009

Fig. 6. Sensitivity of proposed method to changes in water type (K(490)) when wavelengths are $\lambda_1=480$ and $\lambda_2=500$nm. Depth in example is 100m. For definition of Q see text.
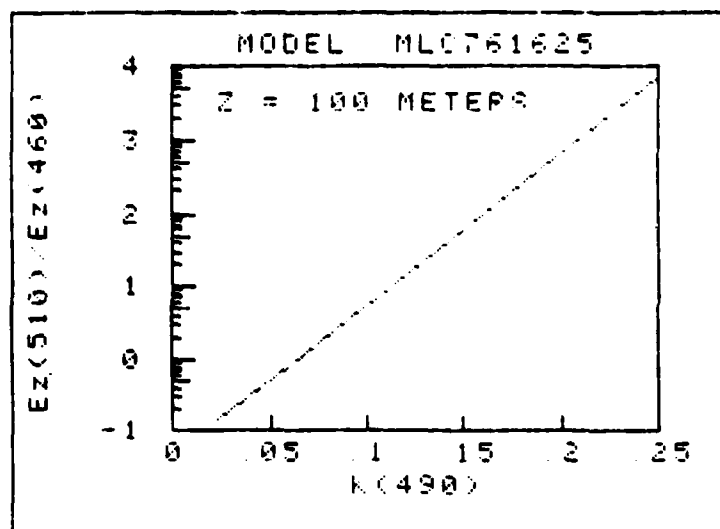
MODEL: MLC761625

WAVELENGTHS: 460 AND 510 nm

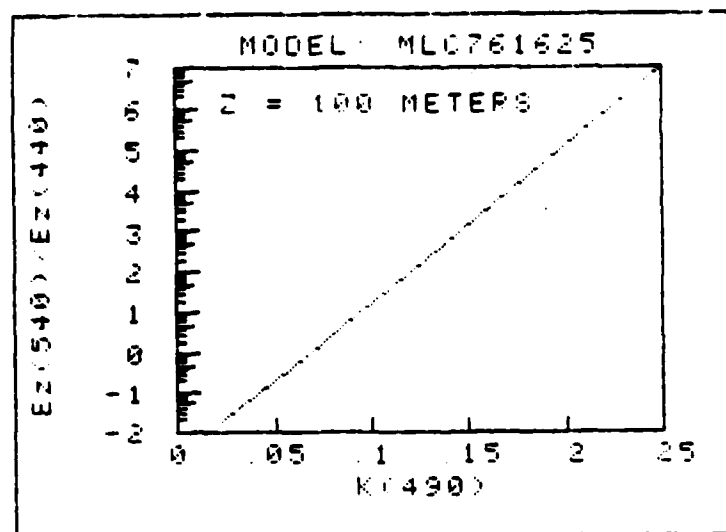DEPTH (Z) = 100 METERS

BANDPASS: 10 nm $\tau a(490) = .01$

Q = .477

IF $\Delta K(490) = .001$ THEN $\Delta R = 1.043$

K(490)	K(460)	K(510)
0.0224	0.0176	0.0368
0.0400	0.0406	0.0515
0.0600	0.0657	0.0681
0.0800	0.0929	0.0847
0.1000	0.1190	0.1013
0.1200	0.1452	0.1180
0.1400	0.1713	0.1346
0.1600	0.1975	0.1512
0.1800	0.2237	0.1678
0.2000	0.2498	0.1844
0.2200	0.2760	0.2011
0.2400	0.3021	0.2177
0.2600	0.3283	0.2343

K(490)	Ez(460)	Ez(510)
0.0224	3.09E+001	4.23E+000
0.0400	3.09E+000	9.81E-001
0.0600	2.26E-001	1.86E-001
0.0800	1.66E-002	3.53E-002
0.1000	1.21E-003	6.70E-003
0.1200	8.85E-005	1.27E-003
0.1400	6.48E-006	2.41E-004
0.1600	4.74E-007	4.58E-005
0.1800	3.46E-008	8.69E-006
0.2000	2.53E-009	1.65E-006
0.2200	1.85E-010	3.13E-007
0.2400	1.35E-011	5.94E-008
0.2600	9.91E-013	1.13E-008

Fig. 7. Same as Fig. 6 except wavelengths are $\lambda_1=460$ and $\lambda_2=510$nm ($\Delta\lambda=50$nm).

MODEL: MLC761625

WAVELENGTHS: 440 AND 540 nm

DEPTH (Z) = 100 METERS

BANDPASS: 10 nm   τa(490) = .01

Q =   982

IF ΔK(490)=.001 THEN ΔR=1.092

K(490)	K(440)	K(540)
0.0224	0.0177	0.0577
0.0400	0.0444	0.0689
0.0600	0.0748	0.0816
0.0800	0.1051	0.0943
0.1000	0.1355	0.1070
0.1200	0.1658	0.1197
0.1400	0.1961	0.1324
0.1600	0.2265	0.1451
0.1800	0.2568	0.1578
0.2000	0.2872	0.1705
0.2200	0.3175	0.1832
0.2400	0.3478	0.1959
0.2600	0.3782	0.2086

K(490)	Ez(440)	Ez(540)
0.0224	2.71E+001	4.99E-001
0.0400	1.87E+000	1.63E-001
0.0600	9.02E-002	4.58E-002
0.0800	4.34E-003	1.29E-002
0.1000	2.09E-004	3.61E-003
0.1200	1.01E-005	1.01E-003
0.1400	4.84E-007	2.85E-004
0.1600	2.33E-008	8.00E-005
0.1800	1.12E-009	2.25E-005
0.2000	5.40E-011	6.31E-006
0.2200	2.60E-012	1.77E-006
0.2400	1.25E-013	4.98E-007
0.2600	6.02E-015	1.40E-007

Fig. 8. Same as Fig's. 6 & 7 except wavelengths are λ_1=440 and λ_2=540nm. ($\Delta\lambda$ = 100nm).

```
MODEL: MLC761625

WAVELENGTHS: 460 AND 510 nm

K(490) =  .067 1/M

K(460 0)=0.0759  K(510 0)=0.0739

BANDPASS: 10 nm  T(490) = .01

UNITS FOR Ez: uW/cm²nm


DEPTH  Ez(460)   Ez(510)   RATIO

    0  1.8E+002  1.7E+002  9.5E-001
   20  3.9E+001  3.3E+001  9.8E-001
   40  8.5E+000  8.7E+000  1.0E+000
   60  1.9E+000  2.0E+000  1.1E+000
   80  4.1E-001  4.5E-001  1.1E+000
  100  8.9E-002  1.0E-001  1.2E+000
  120  2.0E-002  2.3E-002  1.2E+000
  140  4.3E-003  5.4E-003  1.2E+000
  160  9.4E-004  1.2E-003  1.3E+000
  180  2.1E-004  2.8E-004  1.3E+000
  200  4.5E-005  6.3E-005  1.4E+000
```
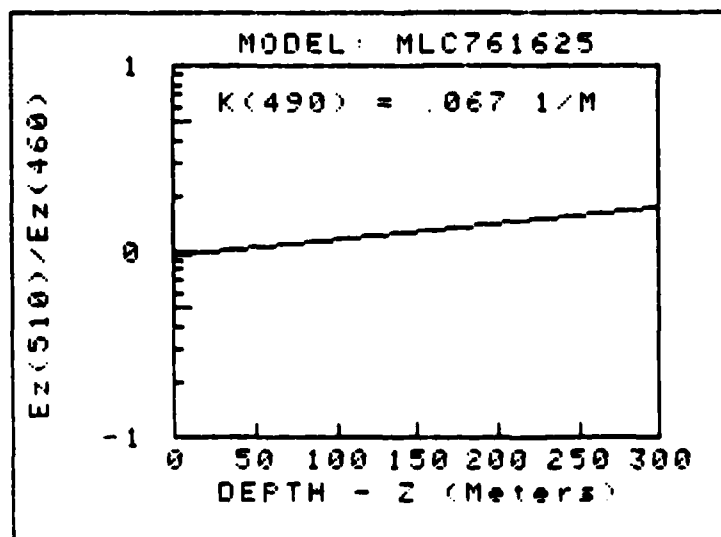

Fig. 9. Sensitivity to changes in depth with wavelengths λ_1=460 and λ_2=510nm. Water type K(490)=0.067.

-23-

```
MODEL  MLC761625

WAVELENGTHS  460 AND 510 nm

K(490) =   038 1/M

K(460.0)=0.0380  K(510.0)=0.0498

BANDPASS  10 nm  r(490) =  01

UNITS FOR Ez  uW/cm²nm


DEPTH Ez(460)  Ez(510)   RATIO

    0   1.8E+002 1 7E+002 9.5E-001
   20   3 3E+001 6.2E+001 7.5E-001
   40   3.9E+001 2.3E+001 5.9E-001
   60   1.8E+001 8.4E+000 4.6E-001
   80   8.5E+000 3.1E+000 3.7E-001
  100   4.0E+000 1.1E+000 2.9E-001
  120   1.9E+000 4.2E-001 2.3E-001
  140   8.7E-001 1.6E-001 1.8E-001
  160   4.1E-001 5.8E-002 1 4E-001
  180   1.9E-001 2.1E-002 1.1E-001
  200   8.9E-002 7.9E-003 8.8E-002
```
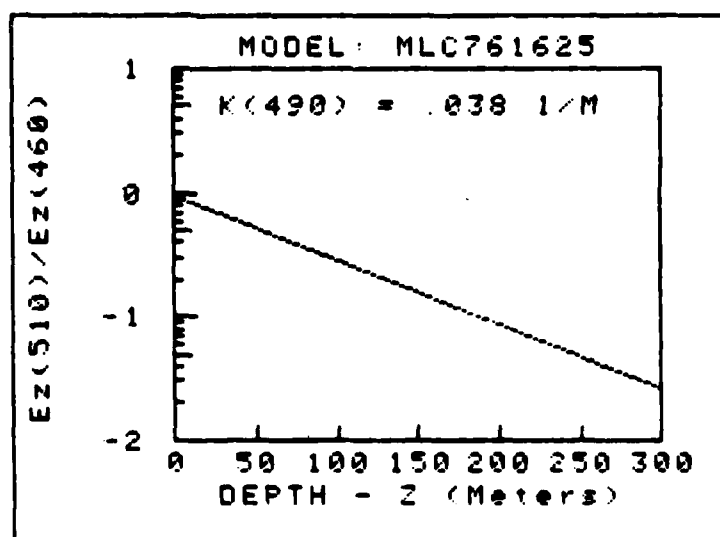

Fig. 10. Same as Fig. 9 except K(490)=0.038.

```
MODEL  MLC761625

WAVELENGTHS  460 AND 510 nm

K(490) = .115 1/M

K(460.0)=0.1386   K(510.0)=0.1138

BANDPASS: 10 nm   τa(490) = .01

UNITS FOR Ez: μW/cm²nm


DEPTH Ez(460)  Ez(510)  RATIO

    0  1.8E+002 1.7E+002 9.4E-001
   20  1.1E+001 1.7E+001 1.6E+000
   40  7.0E-001 1.8E+000 2.5E+000
   60  4.4E-002 1.8E-001 4.2E+000
   80  2.7E-003 1.9E-002 6.9E+000
  100  1.7E-004 1.9E-003 1.1E+001
  120  1.1E-005 2.0E-004 1.9E+001
  140  6.6E-007 2.0E-005 3.1E+001
  160  4.2E-008 2.1E-006 5.0E+001
  180  2.6E-009 2.1E-007 8.3E+001
  200  1.6E-010 2.2E-008 1.4E+002
```
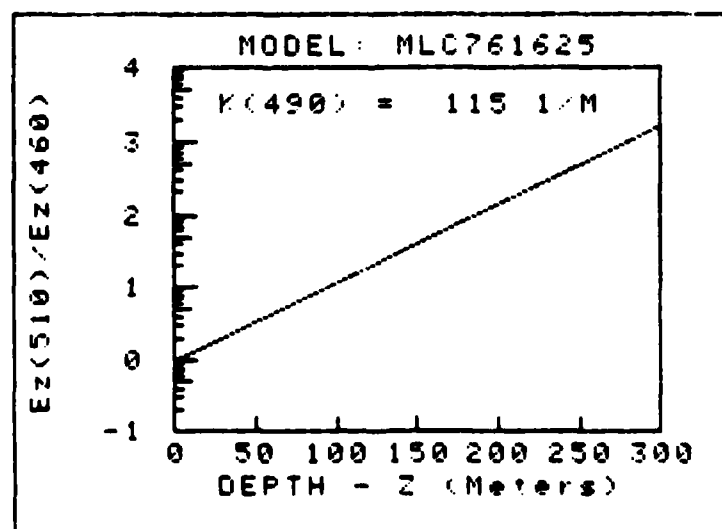

Fig. 11. Same as Fig's. 9 & 10 except K(490)=0.115.

-25-
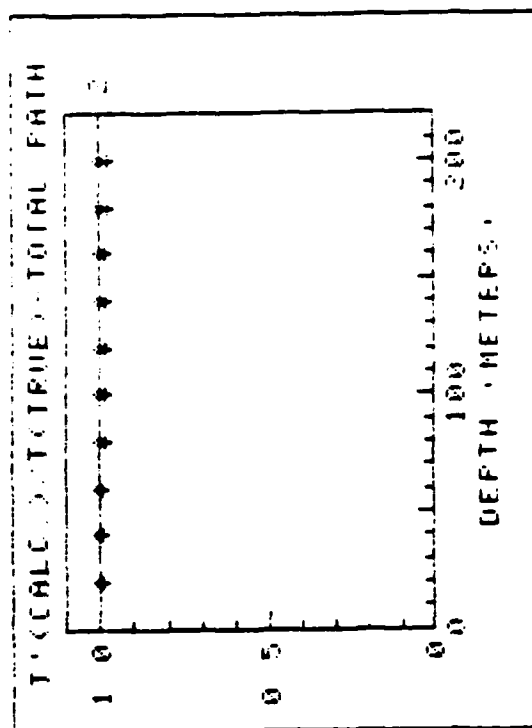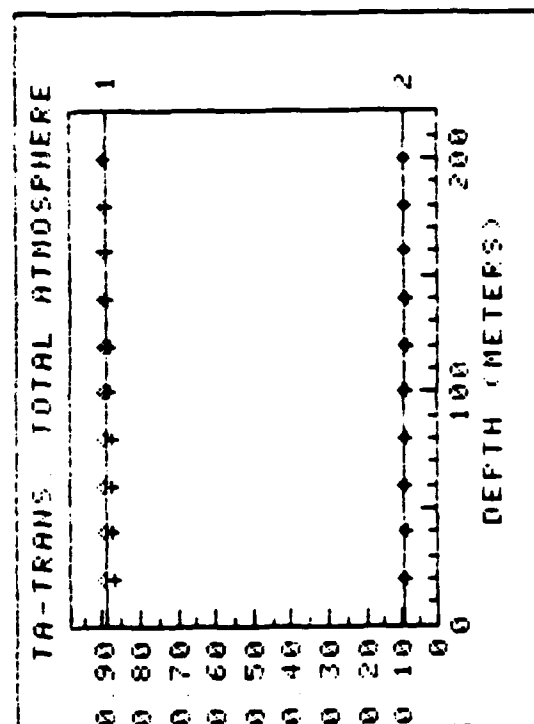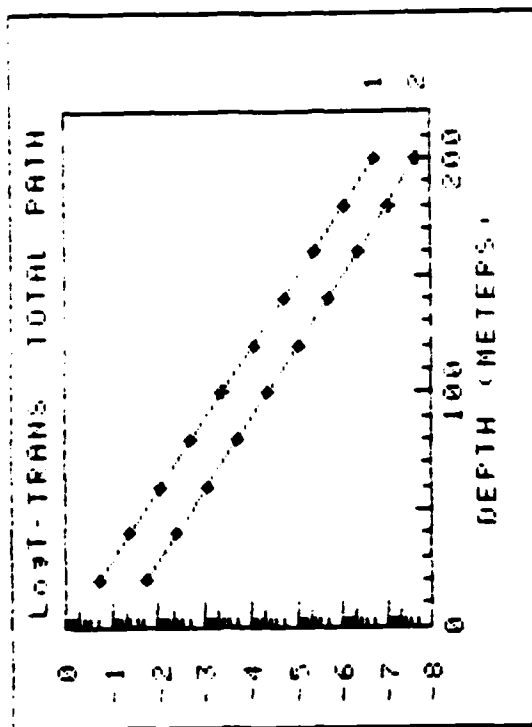
Fig. 12. Sensitivity to wavelength error. $K(490)=0.067$, $\theta_3 = 30°$. Curve labled "1" for haze, $\tau_a=0.10$, $\lambda=1.00$. Curve labeled "2" for overcast $\tau_a=10-20$, $\lambda=0.0$. Results shown for $\lambda=459$nm and unit air mass. Measurement wavelengths $\lambda_1=420$, $\lambda_2=490$nm. Error +2nm in λ_2.
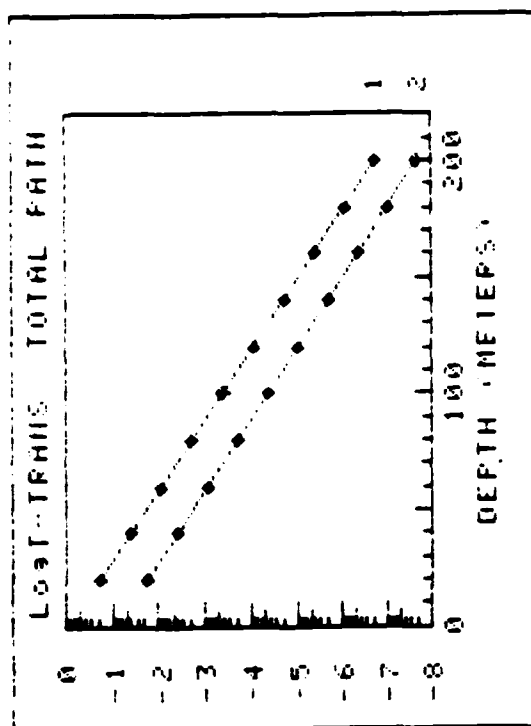
Fig. 13. Same as Fig. 12 except error is -2nm in λ_2.

MODEL MLCTG1625
SOLAR ZENITH ANG -- 30 Deg.
ATMOSPHERE TYPE (Ta at 450nm)
 1 HAZE - Ta=0.100 a=1.00
 2 OVERCAST- Ta=10-20 a=0.00
BANDPASS: 10nm
WAVELENGTHS 460 AND 510 nm

ERROR FACTOR(S):
λ1 +0 nm λ2 +2 nm

FROM RESULTS AT 510.0nm

λ=459.0nm Eo=203.61µW/(CM²·nm)
K(459.0)=0.076 YR=0.200
K(490.0)=0.067 YOZ=0.003

LOG(TRANS) TOTAL PATH

DEPTH (METERS)

T'(CALC)/T(TRUE) TOTAL PATH

DEPTH (METERS)

TA-TRANS TOTAL ATMOSPHERE
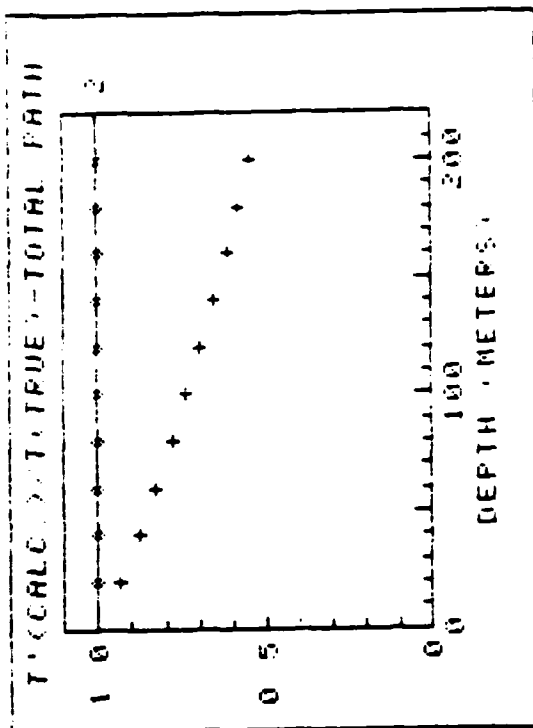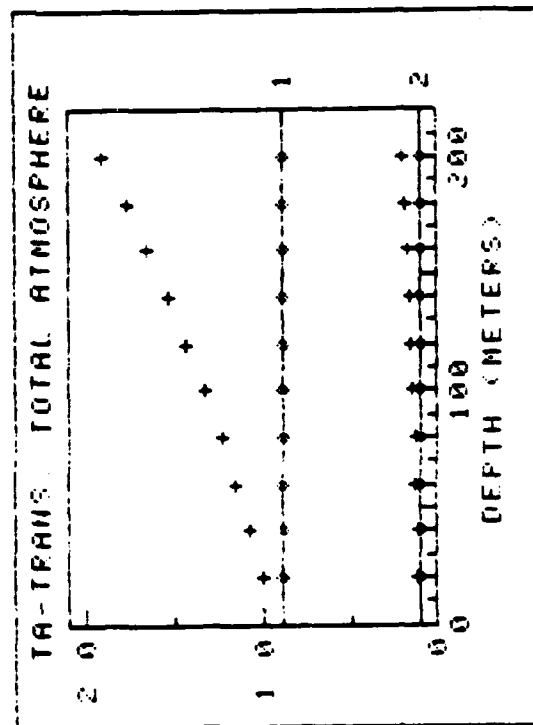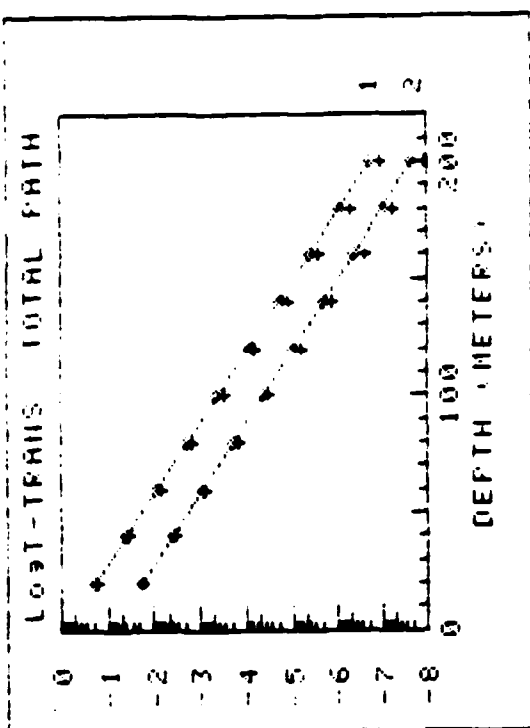
DEPTH (METERS)

Fig. 14. Same as Fig. 12 except $\lambda_1=460$, $\lambda_2=510$. Error is +2nm in λ_2.

-28-

MODEL MLC761625
SOLAR ZENITH ANG -- 30 Deg
ATMOSPHERE TYPE (τa at 490nm)
 1 HAZE   - τa=0 100 α=1.00
 2 OVERCAST- τa=10-20 α=0.00
BANDPASS: 10nm
WAVELENGTHS: 460 AND 510 nm

ERROR FACTOR(S):
λ1 +0 nm λ2 -2 nm

FROM RESULTS AT 510.0nm

λ=459.0nm Eo=203 61μW/(CM2·nm)
K(459.0)=0.076   τR=0.200
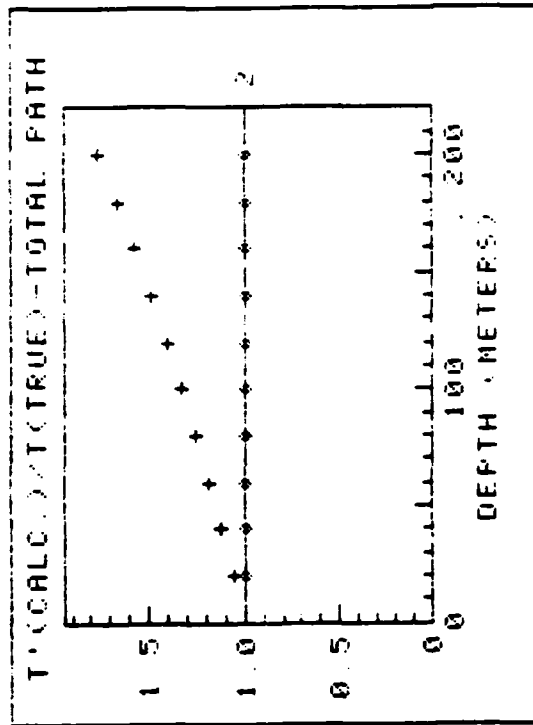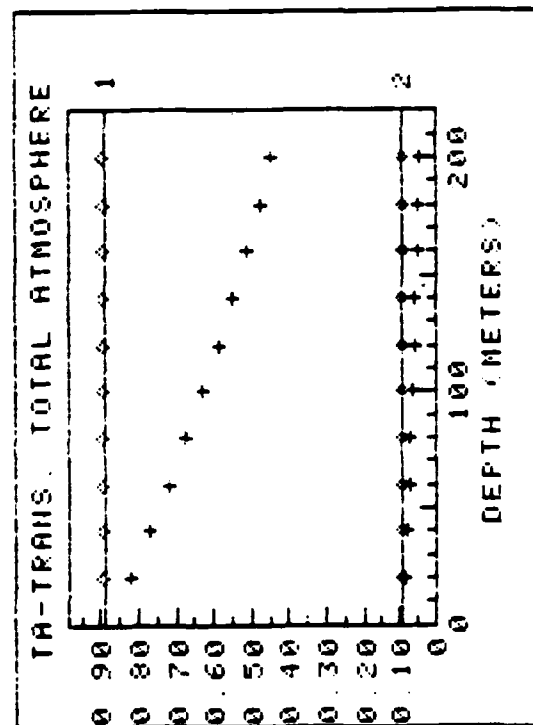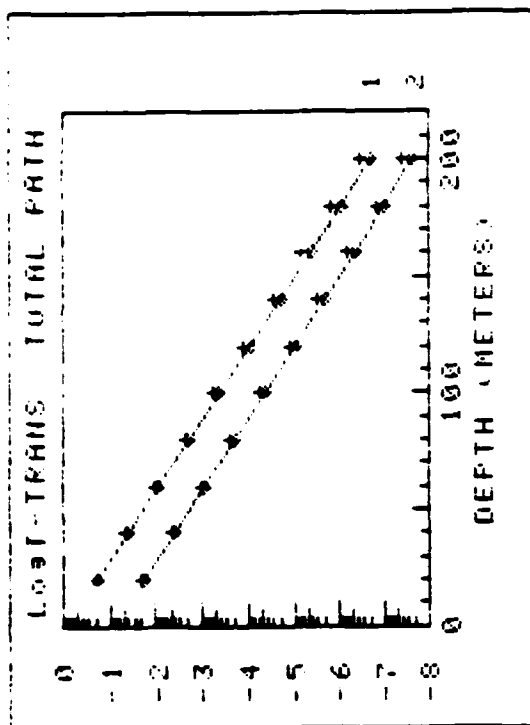K(490.0)=0.067   τOZ=0.003

Fig. 15. Same as Fig. 14 except error is −2nm in λ_2.

-29-

MODEL: MLO761635
SOLAR ZENITH ANG   -- 30 Deg
ATMOSPHERE TYPE (τa at 490nm):
  1 HAZE   - τa=0.100 α=1.00
  2 OVERCAST - τa=10-20 α=0.00
BANDPASS: 10nm
WAVELENGTHS: 420 AND 550 nm

ERROR FACTOR(%):
  λ1 +0 nm λ2 +2 nm

  FROM RESULTS AT 550.0nm

λ=459.0nm Eo=203.61μW/(CM2*nm)
  K(459.0)=0.315   τR =0.200
  K(490.0)=0.248   τOZ=0.003

LOG(T-TRANS), TOTAL PATH
DEPTH (METERS)

TA-TRANS, TOTAL ATMOSPHERE
DEPTH (METERS)

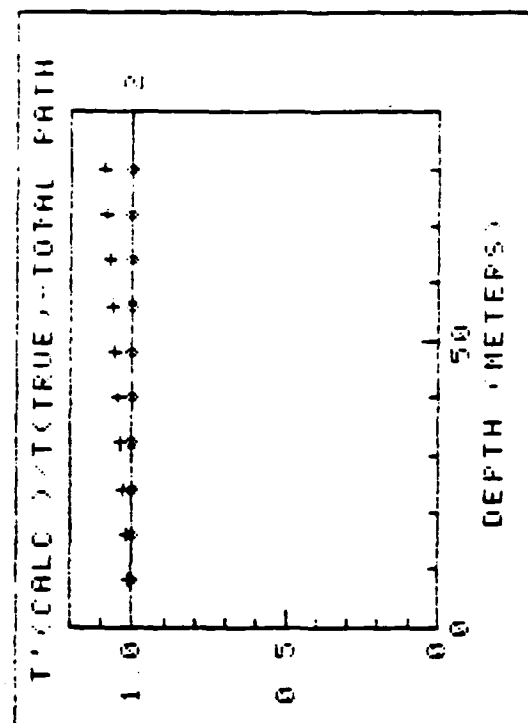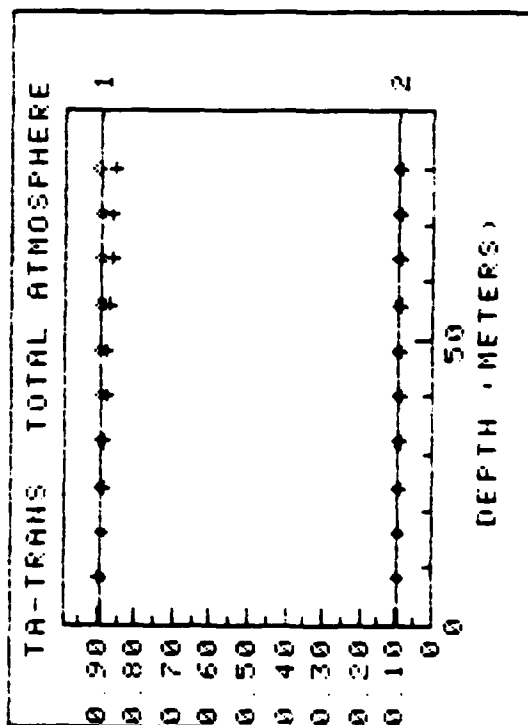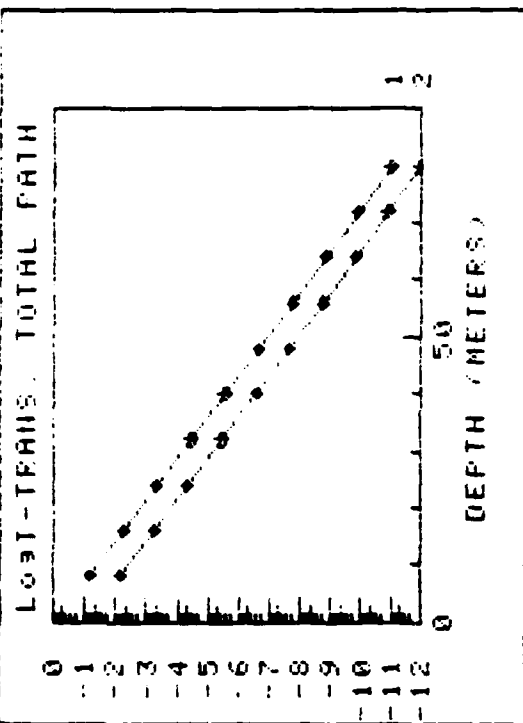T'(CALC)/T(TRUE), TOTAL PATH
DEPTH (METERS)

Fig. 16. Same as Fig. 12 except K(490)=0.248, λ_1=420, λ_2=550. Error is +2nm in λ_2.

-30-

MODEL: MLC781625
SOLAR ZENITH ANG -- 30 Deg.
ATMOSPHERE TYPE (τa at 490nm)
  1 HAZE   - τa=0.100 α=1.00
  2 OVERCAST- τa=10-20 α=0.00
BANDPASS: 10nm
WAVELENGTHS: 420 AND 550 nm

ERROR FACTOR(S):
λ1 +0 nm λ2 -2 nm

   FROM RESULTS AT 550.0nm

λ=459.0nm Eo=203.61μW/(CM²×nm)
K(459.0)=0.315   rR =0.200
K(490.0)=0.248   rOZ=0.003

Log T-TRANS TOTAL PATH

DEPTH (METERS)

T'(CALC)/T(TRUE)-TOTAL PATH

DEPTH (METERS)

TA-TRANS, TOTAL ATMOSPHERE

DEPTH (METERS)

Fig. 17. Same as Fig. 16 except error is −2nm in λ₂.

-31-

Log T-TRANS. TOTAL PATH

DEPTH (METERS)

T'(CALC.)/T(TRUE)-TOTAL PATH

DEPTH (METERS)

TA-TRANS. TOTAL ATMOSPHERE

DEPTH (METERS)

MODEL: ML07616SS
SOLAR ZENITH ANG --- 30 Deg.
ATMOSPHERE TYPE (τa at 490nm).
  1 HAZE -   τs=0.100 α=1.00
  2 OVERCAST- τs=10-20 α=0.00
BANDPASS: 10nm
WAVELENGTHS: 527 AND 577 nm

ERROR FACTOR(S):
  λ1 +0 nm λ2 +2 nm

FROM RESULTS AT 577.0nm

λ=459.0nm   Eo=203.61μW/(CM2*nm)
  K(459.0)=0.315   τR =0.200   τOZ=0.003
  K(490.0)=0.248

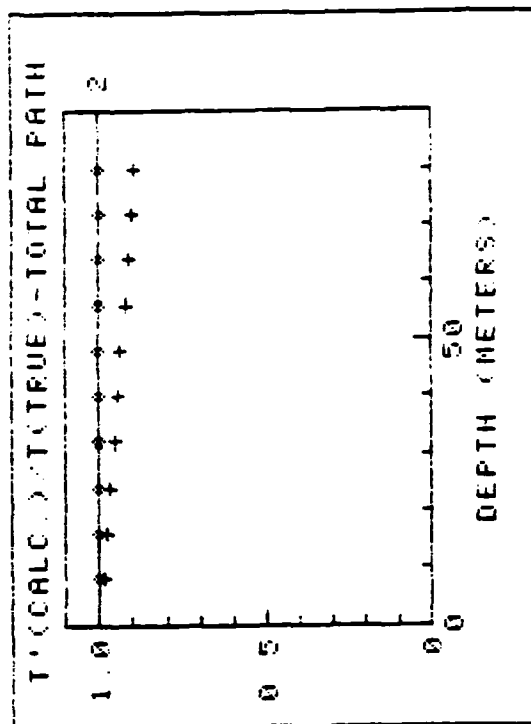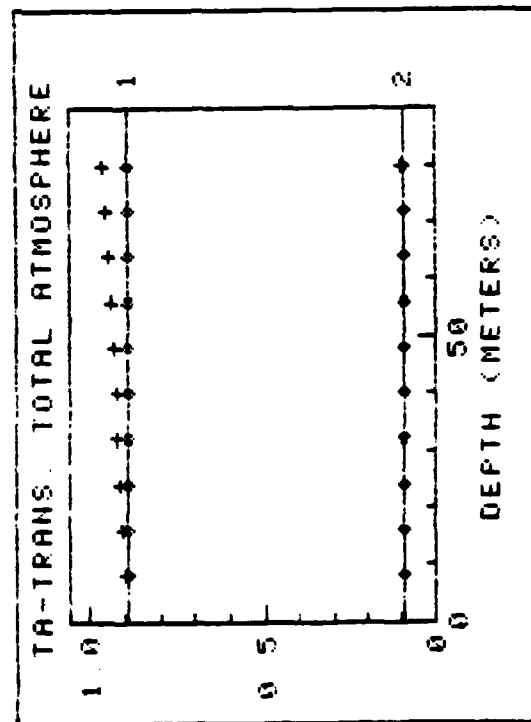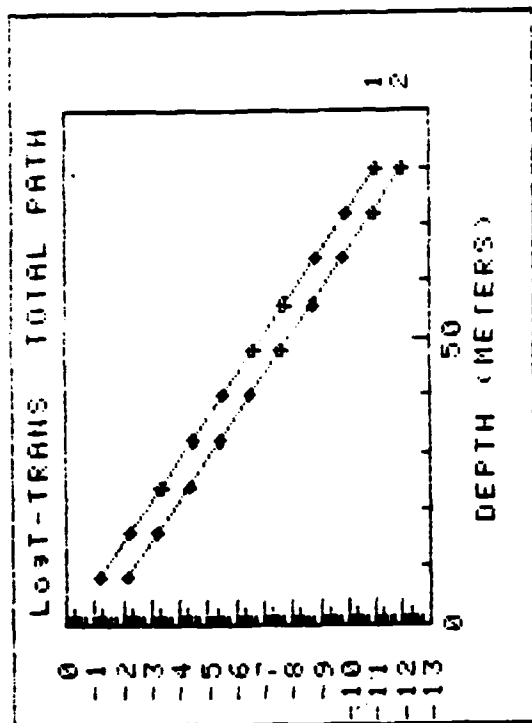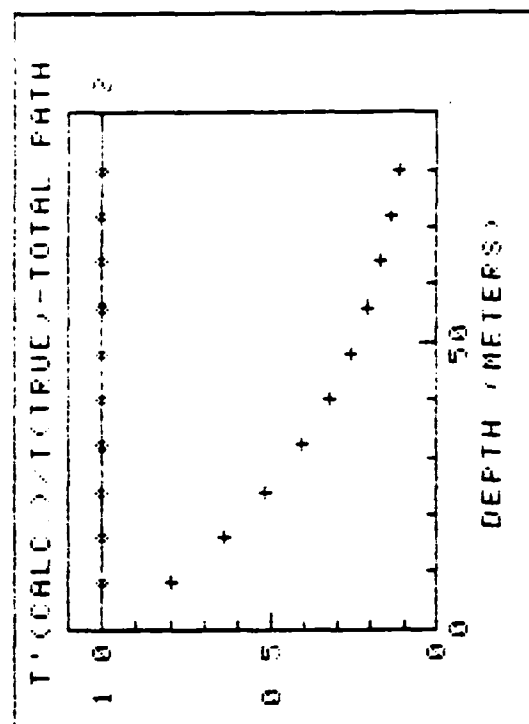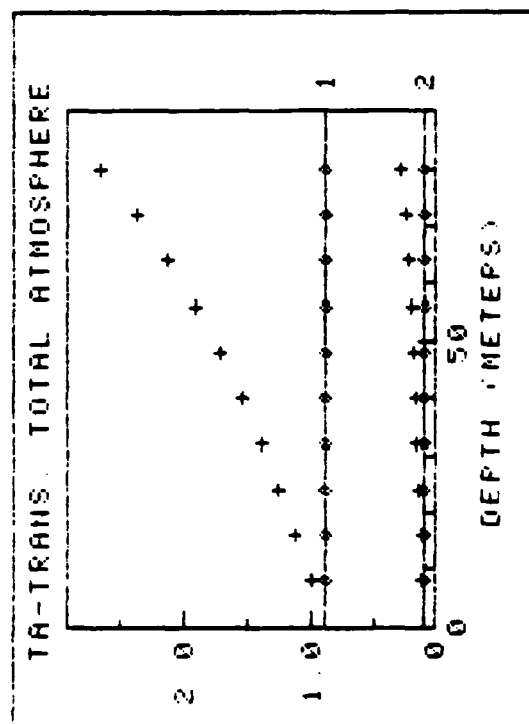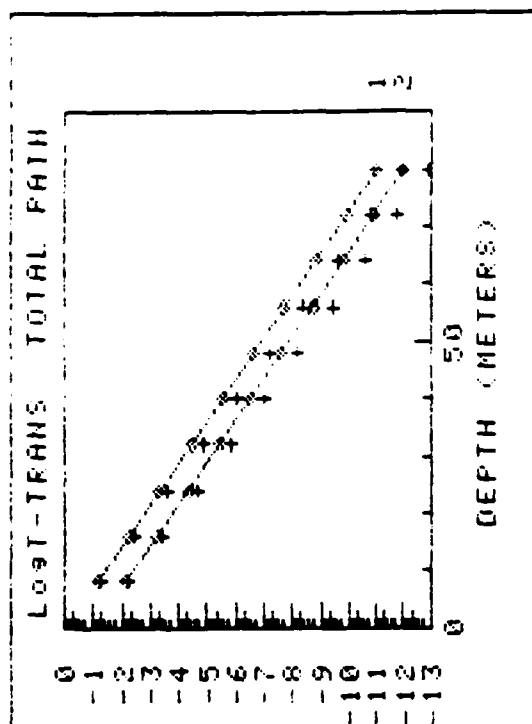Fig. 18. Same as Fig. 16 except λ_1=527nm, λ_2=577nm. Error is +2nm in λ_2.

-32-
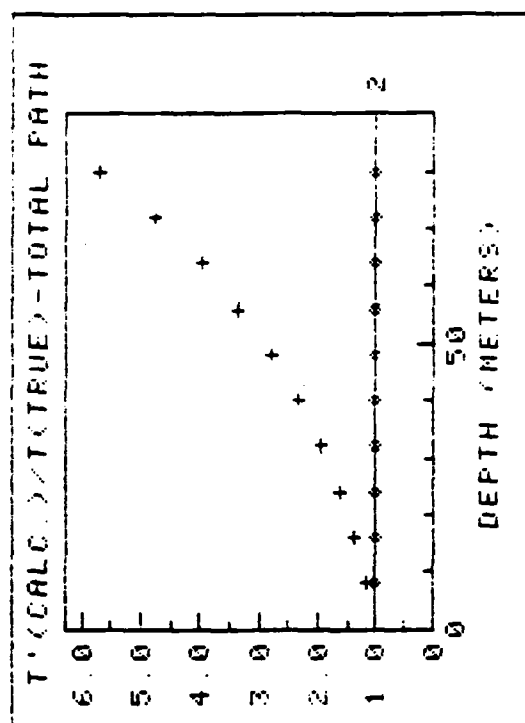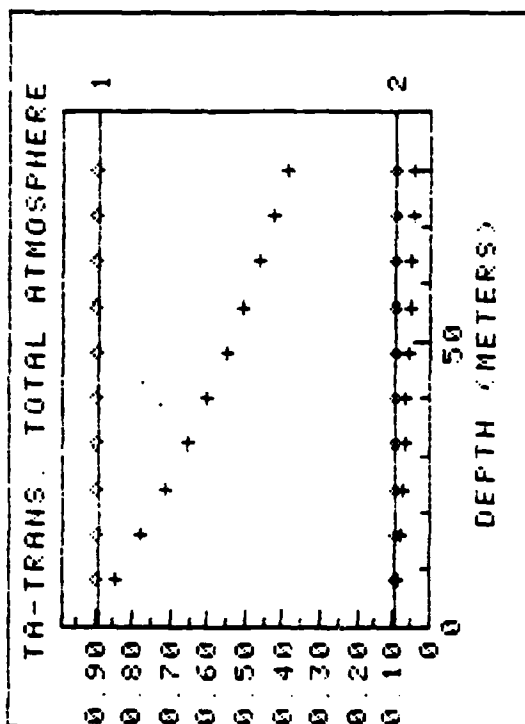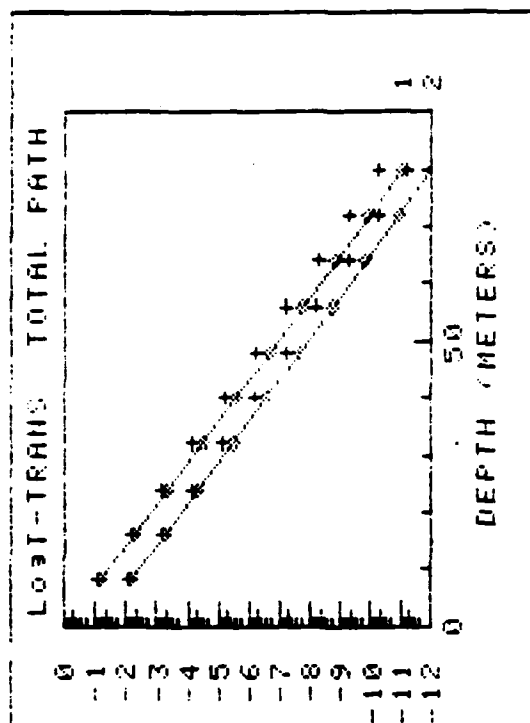
Fig. 19. Same as Fig. 18 except error is –2nm in λ_2.

MODEL MLC761625
SOLAR ZENITH ANG. -- 30 Deg.
ATMOSPHERE TYPE (τa at 490nm):
 1 HAZE - τs=0.100 α=1.00
 2 OVERCAST- τs=10-20 α=0.00
BANDPASS: 10nm
WAVELENGTHS: 420 AND 470 nm

ERROR FACTOR(S):
 0.95*Ez1 1.00*Ez2

FROM RESULTS AT 470.0nm

λ=459.0nm Eo=203.61μW/(CM2*nm)
 K(459.0)=0.017 τR =0.200
 K(490.0)=0.022 τOZ=0.003
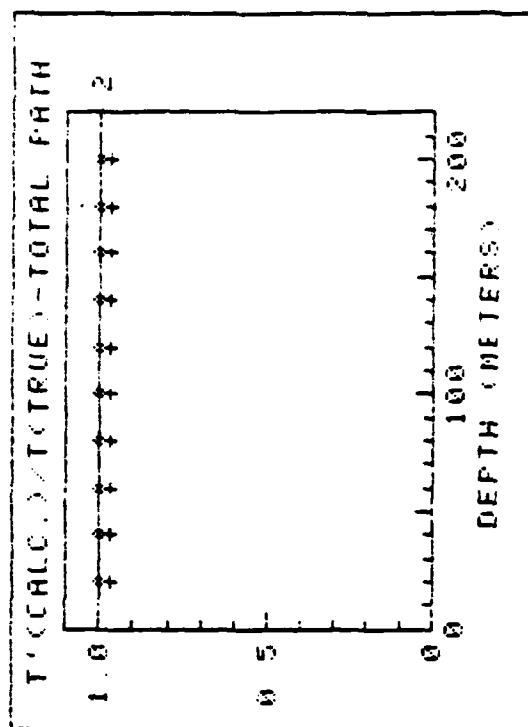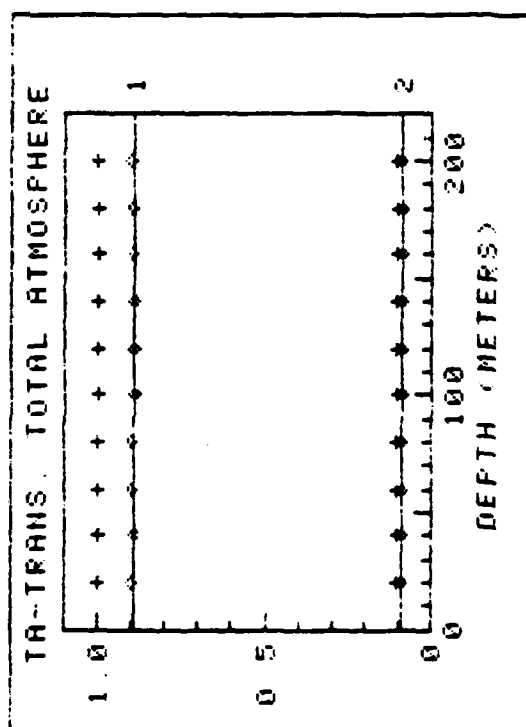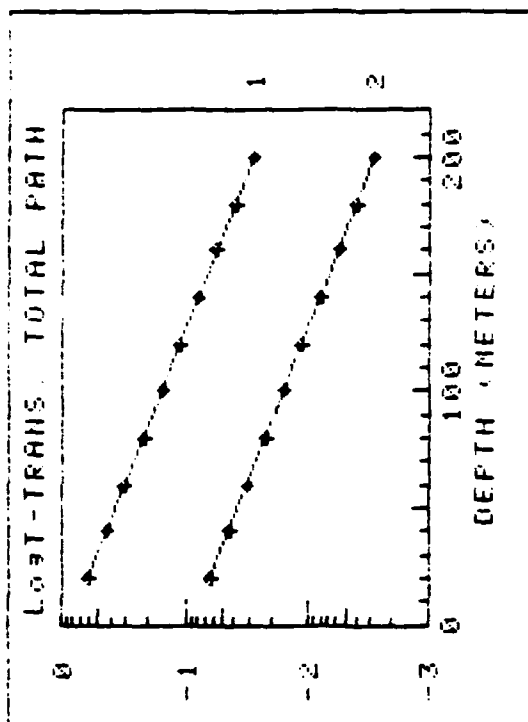
Fig. 20. Sensitivity to Radiometric error, K(490)=0.022m^{-1}, λ_1=420, λ_2=470nm. Error is -5% in $E_z(\lambda_1)$. Other conditions as in Fig. 12.

LOG T-TRANS TOTAL PATH

DEPTH (METERS)

T'(CALC)/T(TRUE)-TOTAL PATH

DEPTH (METERS)

MODEL MLC761635
SOLAR ZENITH ANG   -- 30 Dea
ATMOSPHERE TYPE (ts at 496nm)
 1 HAZE   - ra=0.100 α=1.00
 2 OVERCAST- ts=10-20 α=0.00
BANDPASS: 10nm
WAVELENGTHS: 420 AND 530 nm

ERROR FACTOR(S):
 0.95*Ez1 1.00*Ez2

FROM RESULTS AT 530.0nm

λ=459.0nm Eo=203.61μW/(CM2*nm)
K(459.0)=0.017   rR =0.200
K(490.0)=0.022   rOZ=0.003

TA-TRANS TOTAL ATMOSPHERE

DEPTH (METERS)

Fig. 21. Same as Fig. 20 except λ_1=420, λ_2=530nm.

MODEL MLS(61635
SOLAR ZENITH ANG -- 30 De3
ATMOSPHERE TYPE (τs at 490nm)
  1 HAZE   -   τs=0.100   α=1.00
  2 OVERCAST-   τs=10-20   α=0.00
BANDPASS: 10nm
WAVELENGTHS: 420 AND 470 nm

ERROR FACTOR(3/4)
  0.954Ez1 1.00×Ez2

FROM RESULTS AT 470.0nm
λ=459.0nm   Eo=203.61µW/(CM²×nm)
  K(459.0)=0.153   τR=0.200
  K(490.0)=0.125   τOZ=0.003

LoG(-TRANS) TOTAL PATH

DEPTH (METERS)

1
2

T(CALC)/T(TRUE) TOTAL PATH

DEPTH (METERS)

2

TA-TRANS TOTAL ATMOSPHERE

DEPTH (METERS)

1

2

Fig. 22. Same as Fig. 20 except K(490)=0.125.

Fig. 23. Same as Fig. 22 except $\lambda_1=420$, $\lambda_2=530$nm.
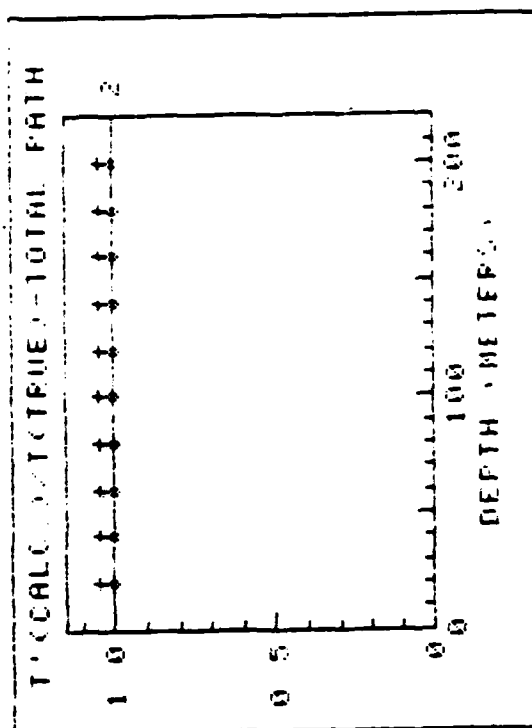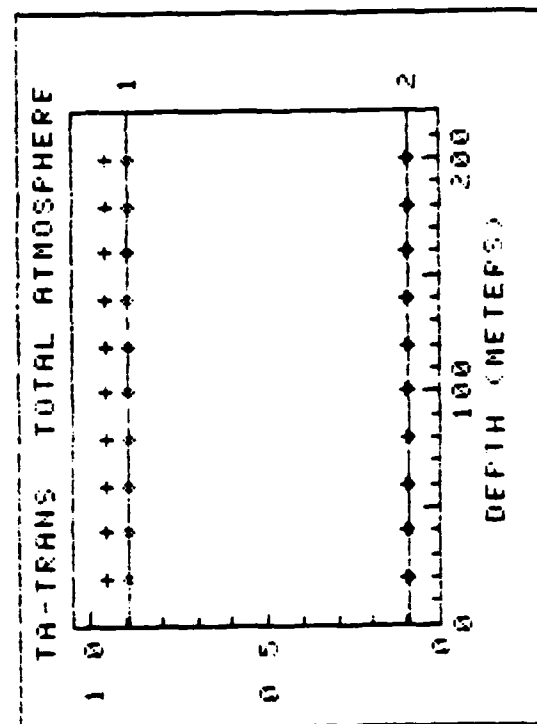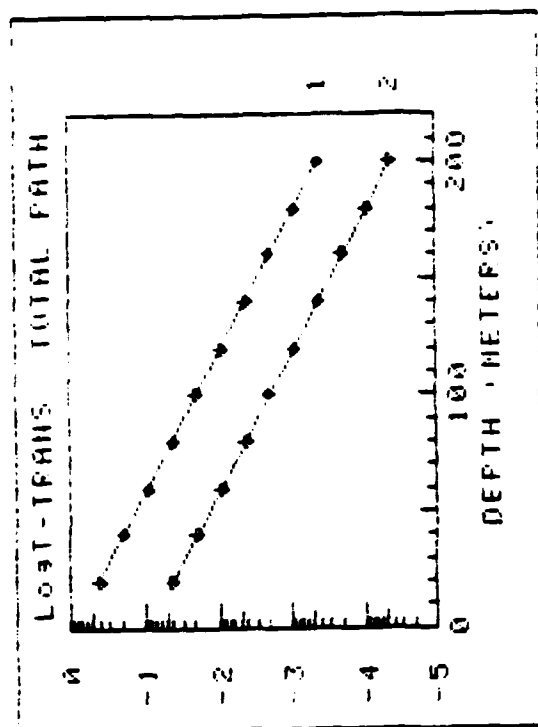
Fig. 24. Sensitivity to errors in depth of u/w sensor. $K(490)=0.038m^{-1}$, $\lambda_1=420$, $\lambda_2=530$. Error is 1 meter offset in 2. Other conditions as in Fig. 12.

MODEL: ALT616...
SOLAR ZENITH ANG. -- 30 Deg.
ATMOSPHERE TYPE (τs at 490nm)
  1 HAZE   - τs=0.100 α=1.00
  2 OVERCAST- τs=10-20 α=0.00
BANDPASS: 10nm
WAVELENGTHS: 420 AND 530 nm

ERROR FACTOR(S)
  1.00*(Z+1) Z=DEPTH(Meters)

    FROM RESULTS AT 420.0nm

λ=459.0nm Eo=203.61µW/(CM²*nm)
  K(459.0)=0.318   rR =0.200
  K(490.0)=0.250   rOZ=0.003
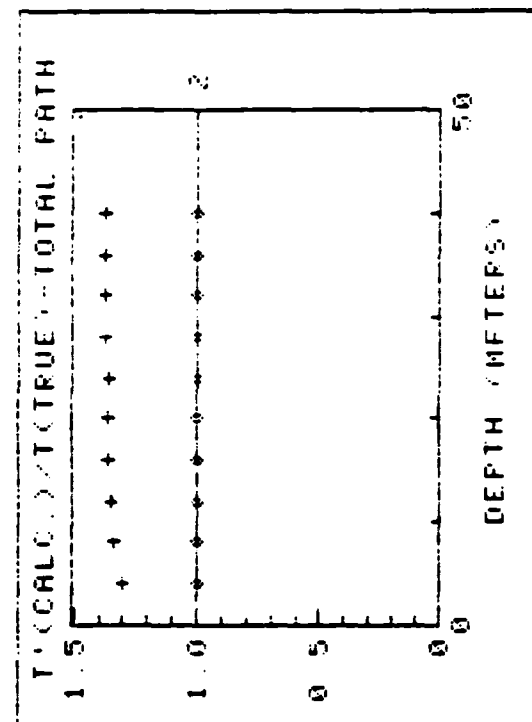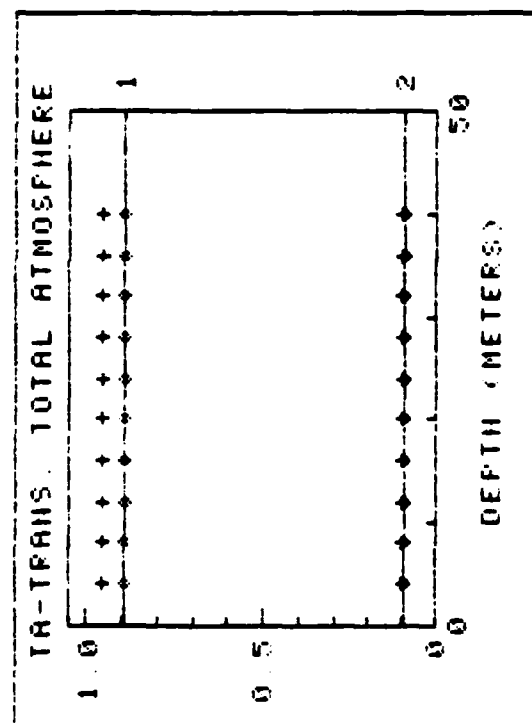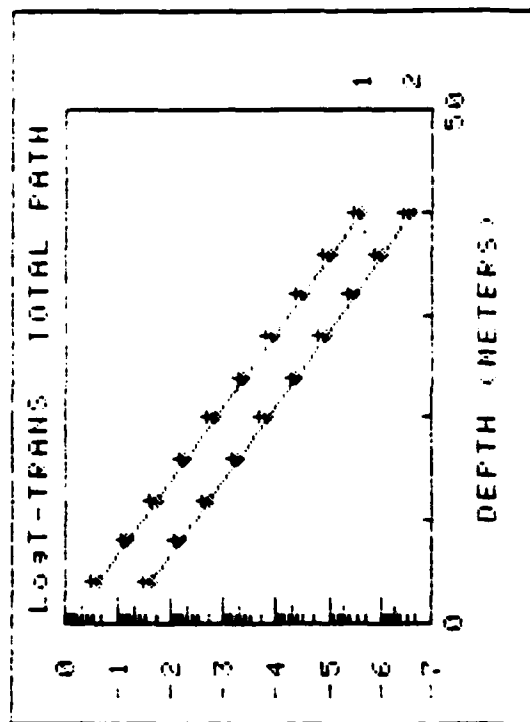
Fig. 25. Same as Fig. 24 except K(490)=0.250m⁻¹.

-39-

MODEL MLC761625
SOLAR ZENITH ANG. -- 30 Deg.
ATMOSPHERE TYPE (τa at 450nm)
  1 HAZE   - τa=0.100 α=1.00
  2 OVERCAST- τa=10-20 α=0.00
BANDPASS: 10nm
WAVELENGTHS: 420 AND 530 nm

ERROR FACTOR(S):
  1.01%(Z +0) Z=DEPTH(Meters)

  FROM RESULTS AT 420.0nm

λ=459.0nm Eo=203.61µW/(CM²*nm)
  K(459.0)=0.038   τR =0.200
  K(490.0)=0.038   τOZ=0.003
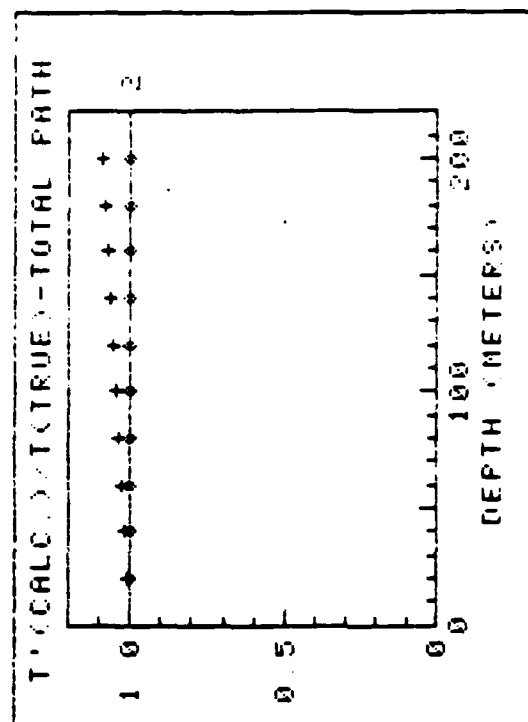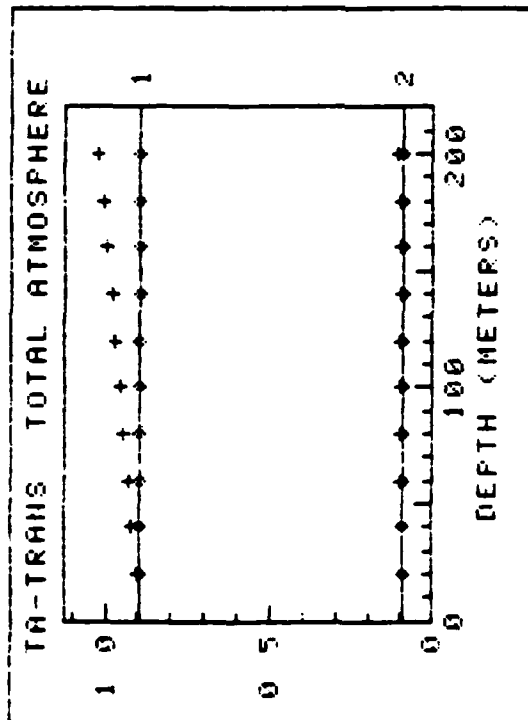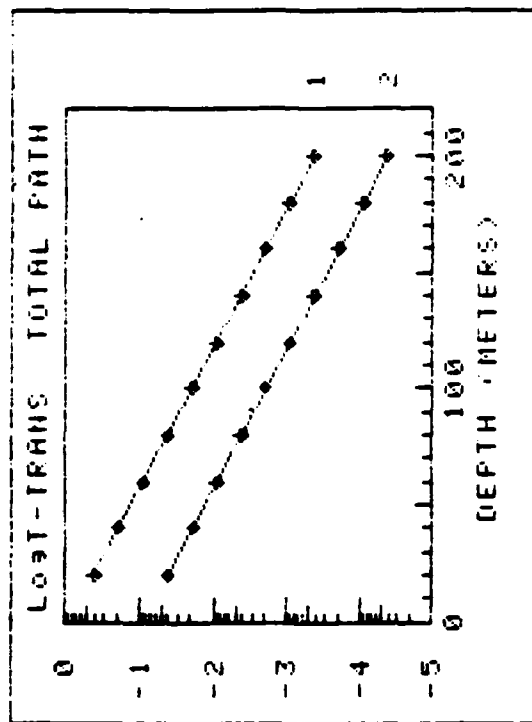
Fig. 26. Same as Fig. 24 except 1% error in Z.

-40-

MODEL: MLOT618?5
SOLAR ZENITH ANG. -- 30 Deg
ATMOSPHERE TYPE (τa at 490nm):
1 HAZE   - τa=0.100 α=1.00
2 OVERCAST- τa=10-20 α=0.00
BANDPASS: 10nm
WAVELENGTHS: 420 AND 530 nm

ERROR FACTOR(3):
1.01*(2.+0) Z=DEPTH(Meters)

FROM RESULTS AT 420.0nm

λ=459.0nm Eo=203.61μW/(CM²·nm)
K(459.0)=0.318   τR =0.200
K(490.0)=0.250   τO2=0.003
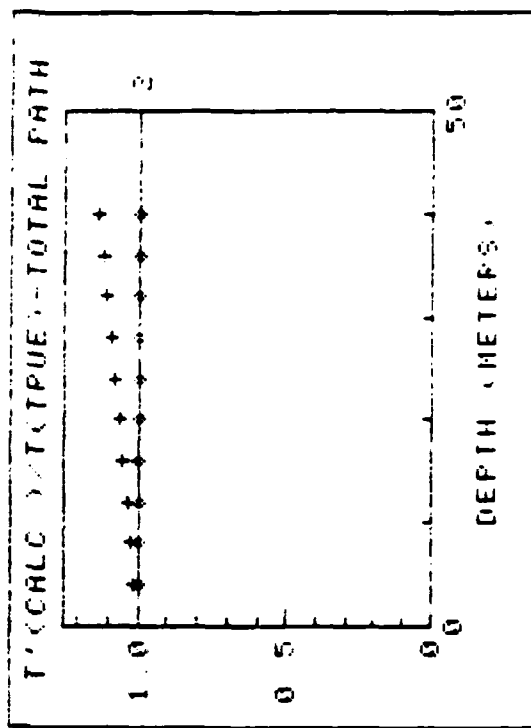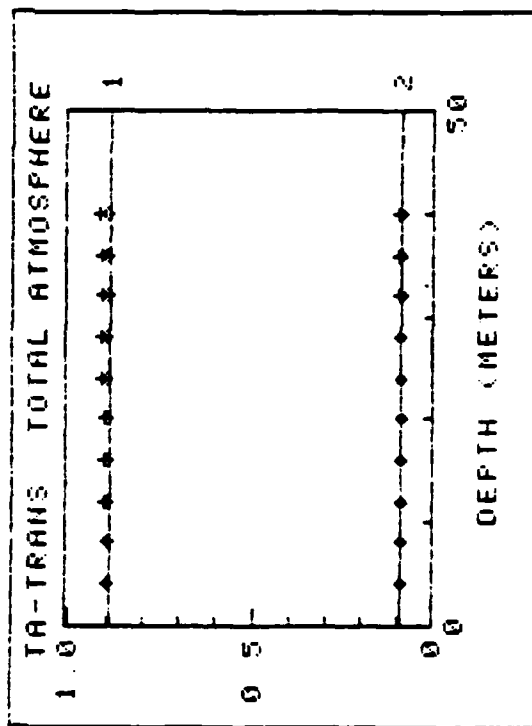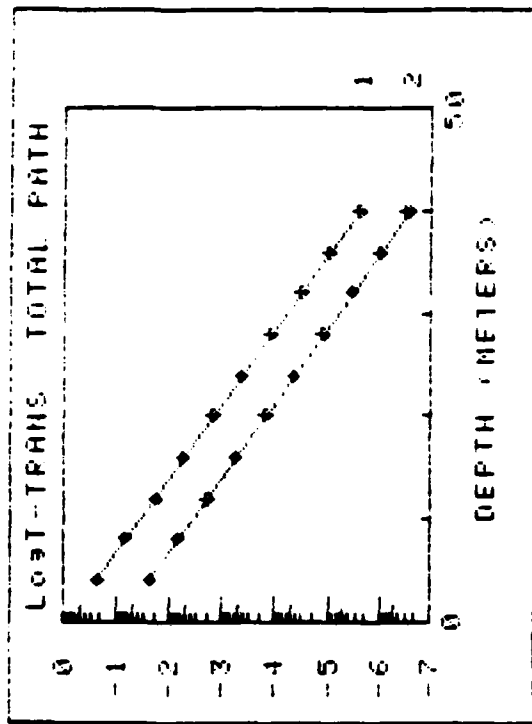
Fig. 27. Same as Fig. 26 except K(490)=0.250m⁻¹.

-41-

Fig. 28. Sensitivity to error in solar zenith angle. K(490)=0.038, λ_1=420, λ_2=530nm, θ_s=30°. Error: 5° offset in θ_s.

Fig. 29. Same as Fig. 28 except $\theta_s=60°$.

MODEL MLC7616.25
SOLAR ZENITH ANG   -- 30 Deg
ATMOSPHERE TYPE (ra at 490nm)
  1 HAZE   -   ra=0.100 σ=1.00
  2 OVERCAST- ra=10-20 α=0.00
BANDPASS: 10nm
WAVELENGTHS: 420 AND 470 nm

ERROR FACTOR(S):
  1.05*Eo1 1.00*Eo2

    FROM RESULTS AT 470.0nm

λ=459.0nm   Eo=203.61μW/(CM2*nm)
  K(459.0)=0.017   rR =0.200
  K(490.0)=0.022   rOZ=0.003

Fig. 30. Sensitivity to errors in solar spectral irradiance. $K(490)=0.022m^{-1}$, $\lambda_1=420$, $\lambda_2=470nm$. Error: 5% in $E_o(\lambda_1)$. Other conditions same as in Fig. 12.

44

MODEL MLC7616-3?
SOLAR ZENITH ANG -- 30 De3
ATMOSPHERE TYPE (τa at 490nm)
1 HAZE - τa=0.100 α=1.00
2 OVERCAST- τa=10-20 α=0.00
BANDPASS: 10nm
WAVELENGTHS: 420 AND 470 nm

ERROR FACTOR(S):
1.05%Eo1 1.00%Eo2

FROM RESULTS AT 470.0nm

λ=459.0nm Eo=203.61μW/(CM2*nm)
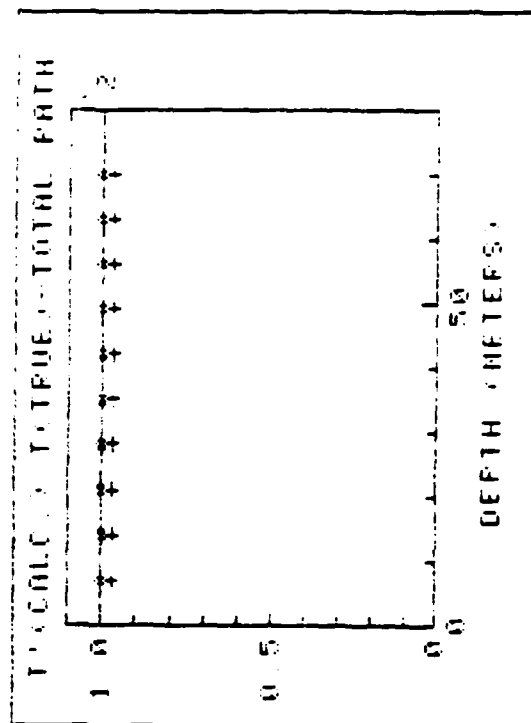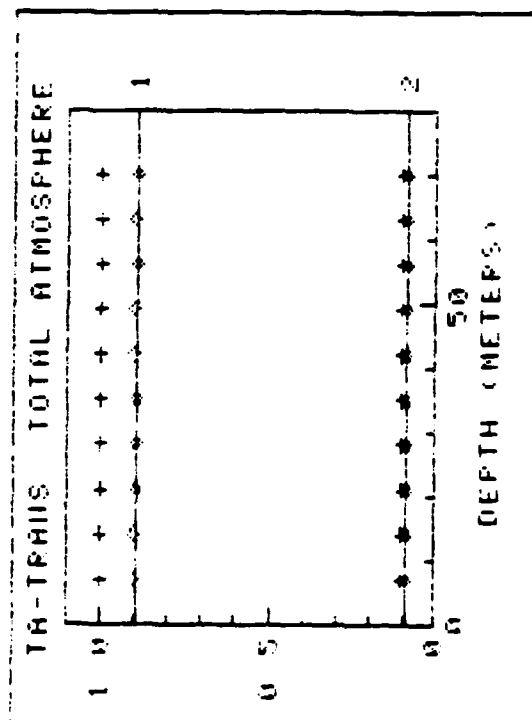K(459.0)=0.153 rR=0.200
K(496.0)=0.125 rOz=0.003
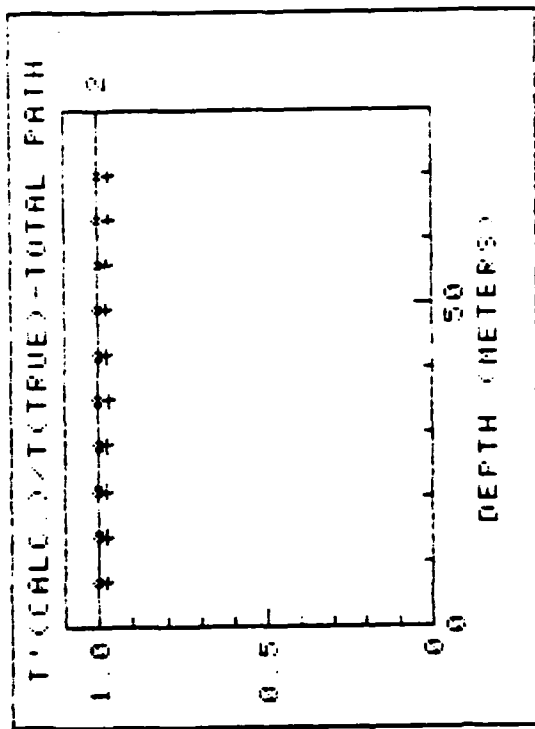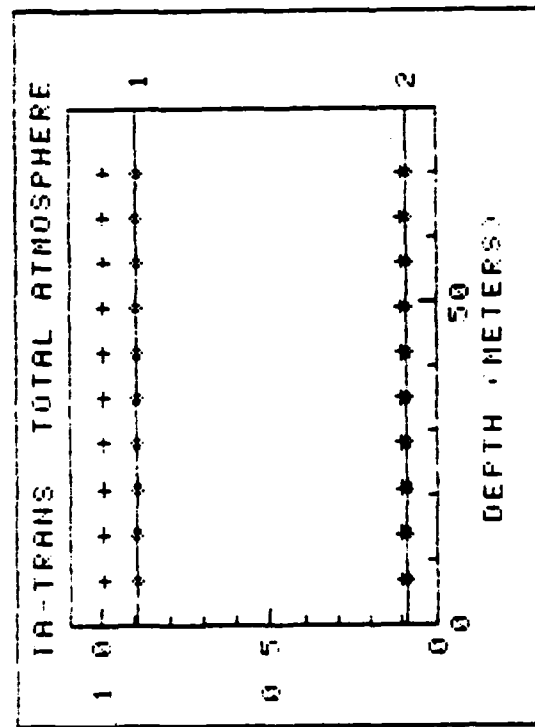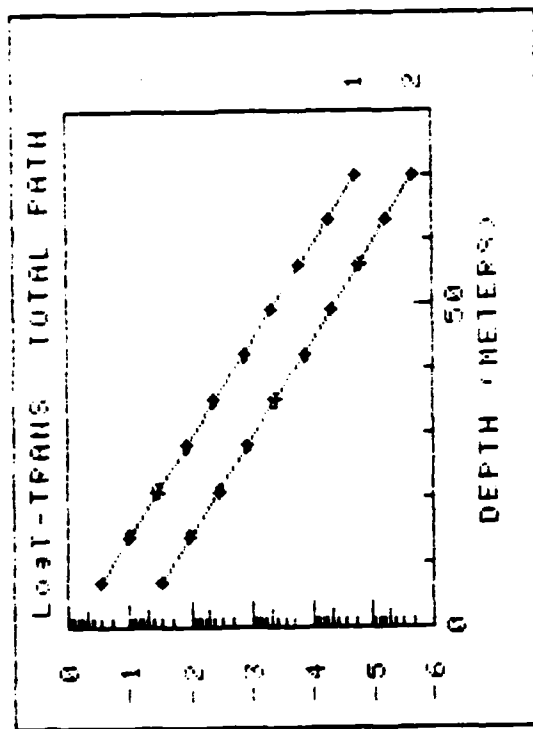
Fig. 31. Same as Fig. 30 except $K(490)=0125m^{-1}$.

MODEL MLC261625
SOLAR ZENITH ANG -- 30 Deg
ATMOSPHERE TYPE (Ta at 490nm)
1 HAZE - Ts=0.100 α=1.00
2 OVERCAST- Ta=10-20 α=0.00
BANDPASS: 10nm
WAVELENGTHS: 420 AND 530 nm

ERROR FACTOR(S):
1.05%E01 1.00%E02

FROM RESULTS AT 530.0nm

λ=459.0nm Eo=203.61μW/(CM²*nm)
K(459.0)=0.017 τR=0.200
K(490.0)=0.022 τOZ=0.003
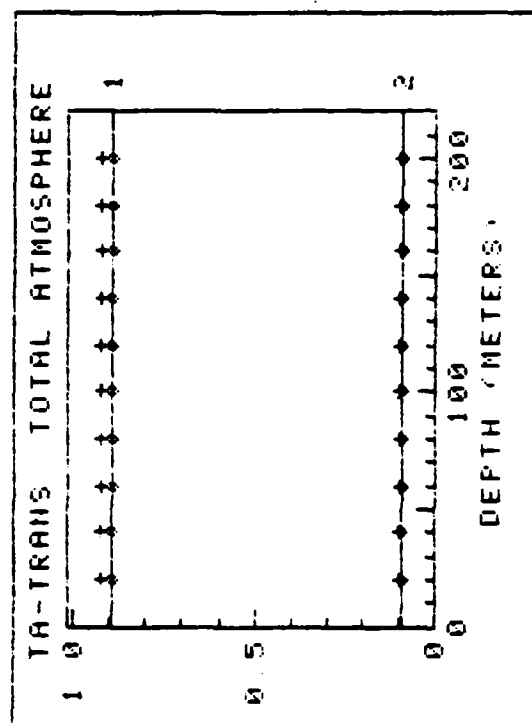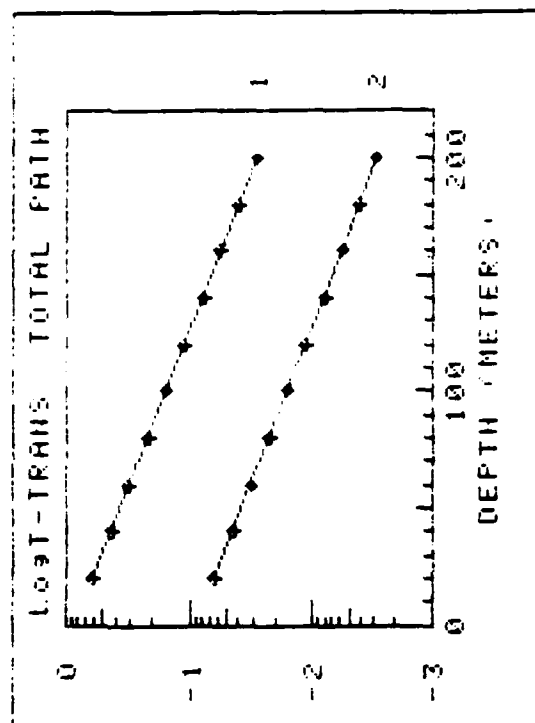
Fig. 32. Same as Fig. 30 except $\lambda_1=420$, $\lambda_2=530$.
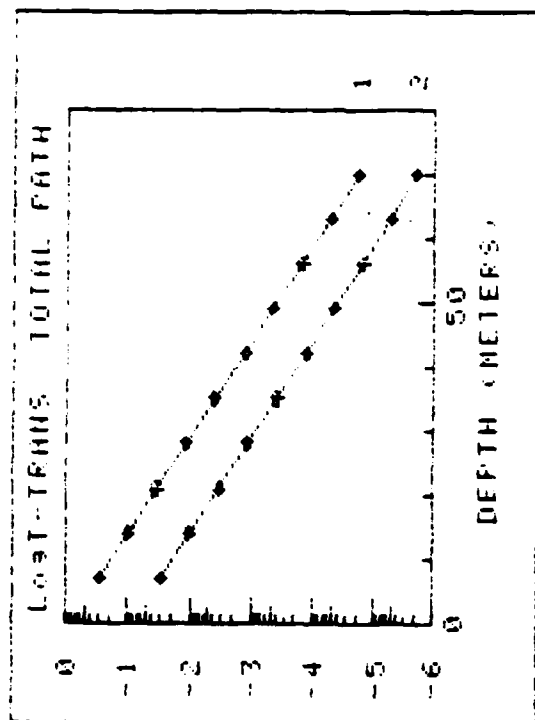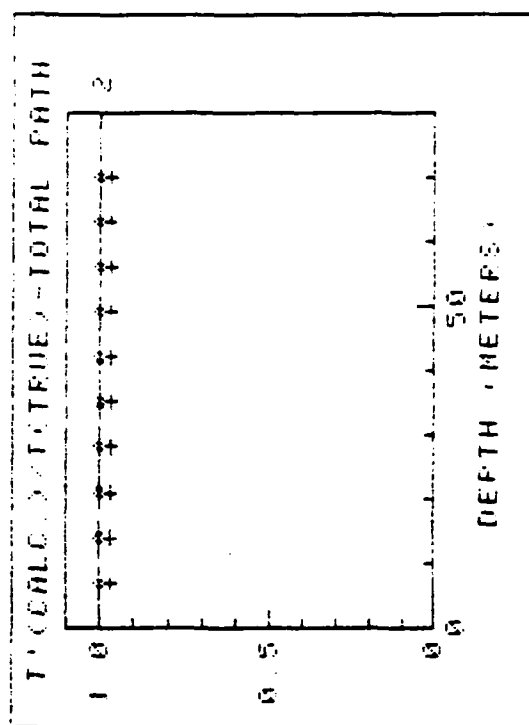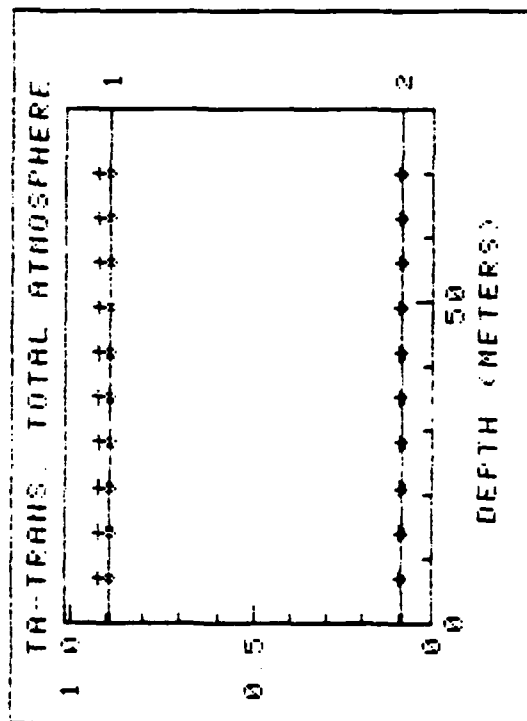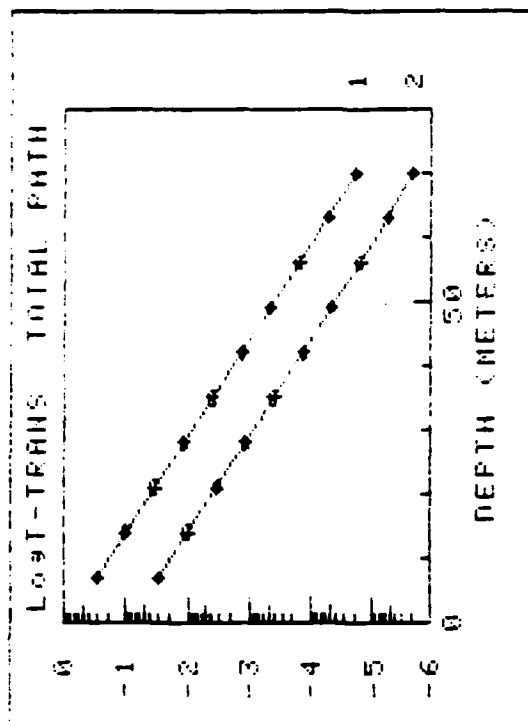
Fig. 33. Same as Fig. 32 except K(490)=0125m^{-1}.

-47-

MODEL: MLC761625
SOLAR ZENITH ANG   -- 30 Deg
ATMOSPHERE TYPE (ta at 490nm)
  1 HAZE   -   Ta=0.100   a=1.00
  2 OVERCAST-   Ta=10-20   a=0.00
BANDPASS: 10nm
WAVELENGTHS: 420 AND 530 nm

ERROR FACTOR(S):
  λ1 +2 nm λ2 +0 nm

       FROM RESULTS AT 530.0nm

λ=459.0nm   Eo=203.61µW/(CM2·nm)
    K(459.0)=0.076   TR =0.200
    K(490.0)=0.067   TO2=0.003

(a)

(b)

Fig. 34. Sensitivity of K determination to errors in wavelength, K(490)=0.067m⁻¹, λ₁=420, λ₂=530nm. Error: +2nm in λ₁ (a) Haze (τₐ=0.1, α=1.0), (b) Overcast (τₐ=10-20, α=0). Other conditions as in Fig. 12.

-48-

MODEL: MLC761625
SOLAR ZENITH ANG. -- 30 Deg.
ATMOSPHERE TYPE (τs at 490nm):
  1 HAZE   -   τs=0.100   α=1.00
  2 OVERCAST- τs=10-20   α=0.00
BANDPASS: 10nm
WAVELENGTHS: 420 AND 530 nm

ERROR FACTOR(S):
  λ1 +2 nm λ2 +0 nm

FROM RESULTS AT 530.0nm

λ=459.0nm   Eo=203.61μW/(CM2*nm)
  K(459.0)=0.038   τR=0.200
  K(490.0)=0.038   τOZ=0.003

(a)
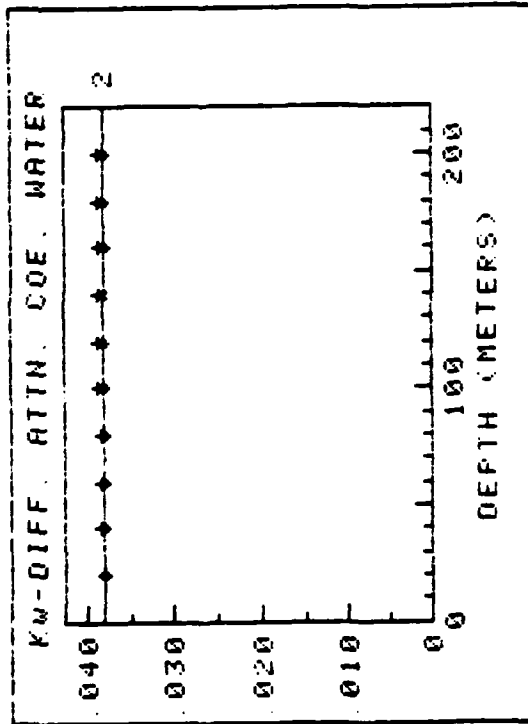
MODEL: MLC761625
SOLAR ZENITH ANG. -- 30 Deg.
ATMOSPHERE TYPE (τs at 490nm):
  1 HAZE   -   τs=0.100   α=1.00
  2 OVERCAST- τs=10-20   α=0.00
BANDPASS: 10nm
WAVELENGTHS: 420 AND 530 nm

ERROR FACTOR(S):
  λ1 +2 nm λ2 +0 nm

FROM RESULTS AT 530.0nm

λ=459.0nm   Eo=203.61μW/(CM2*nm)
  K(459.0)=0.188   τR=0.200
  K(490.0)=0.152   τOZ=0.003

(b)

Fig. 35. Same as Fig. 34 except: (a) $K(490)=0.038 m^{-1}$, (b) $K(490)=0.152 m^{-1}$.

MODEL: MLC761635
SOLAR ZENITH ANG. -- 30 Deg.
ATMOSPHERE TYPE (τa at 490nm):
  1 HAZE   -   τa=0.100   α=1.00
  2 OVERCAST- τa=10-20   α=0.00
BANDPASS: 10nm
WAVELENGTHS: 420 AND 530 nm

ERROR FACTOR(S):
  0.95*Ez1 1.00*Ez2

FROM RESULTS AT 530.0nm

λ=459.0nm   Eo=203.61μW/(CM2*nm)
  K(459.0)=0.188   τR =0.200
  K(490.0)=0.152   τOZ=0.003

(b)

MODEL: MLC761635
SOLAR ZENITH ANG. -- 30 Deg.
ATMOSPHERE TYPE (τa at 490nm):
  1 HAZE   -   τa=0.100   α=1.00
  2 OVERCAST- τa=10-20   α=0.00
BANDPASS: 10nm
WAVELENGTHS: 420 AND 530 nm

ERROR FACTOR(S):
  0.95*Ez1 1.00*Ez2

FROM RESULTS AT 530.0nm

λ=459.0nm   Eo=203.61μW/(CM2*nm)
  K(459.0)=0.038   τR =0.200
  K(490.0)=0.038   τOZ=0.003

(a)
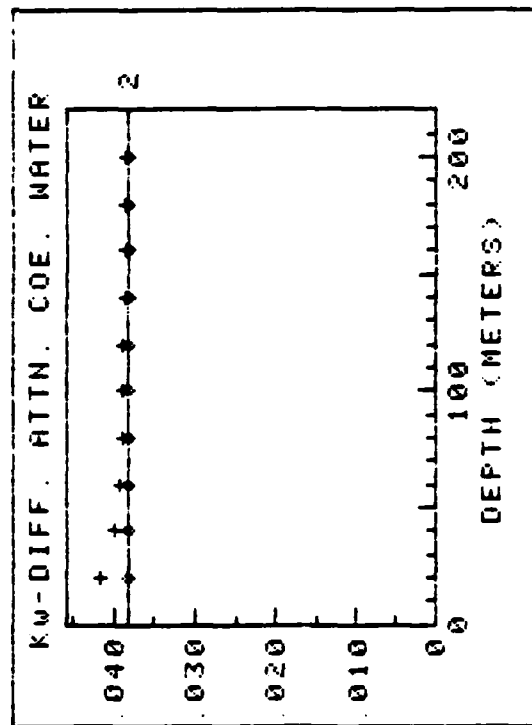
Fig. 36. Sensitivity of K determination to radiometric error. λ_1=420, λ_2=530nm. Error: −5% in $E_z(\lambda_1)$. (a) K(490)=0.038m^{-1}. (b) K(490)=0.152m^{-1}. Other conditions as in Fig. 12.

MODEL: MLC761625
SOLAR ZENITH ANG. -- 30 Deg.
ATMOSPHERE TYPE (Ta at 490nm):
  1 HAZE   - Ta=0.100 α=1.00
  2 OVERCAST- Ta=10-20 α=0.00
BANDPASS: 10nm
WAVELENGTHS: 420 AND 530 nm

ERROR FACTOR(S):
  1.00*(Z+1) Z=DEPTH(Meters)

FROM RESULTS AT 530.0nm

λ=459.0nm Eo=203.61µW/(CM²*nm)
K(459.0)=0.038   TR =0.200
K(490.0)=0.038   TOZ=0.003

MODEL: MLC761625
SOLAR ZENITH ANG. -- 30 Deg.
ATMOSPHERE TYPE (Ta at 490nm):
  1 HAZE   - Ta=0.100 α=1.00
  2 OVERCAST- Ta=10-20 α=0.00
BANDPASS: 10nm
WAVELENGTHS: 420 AND 530 nm

ERROR FACTOR(S):
  1.00*(Z+1) Z=DEPTH(Meters)

FROM RESULTS AT 530.0nm

λ=459.0nm Eo=203.61µW/(CM²*nm)
K(459.0)=0.188   TR =0.200
K(490.0)=0.152   TOZ=0.003

(a)

(b)

Fig. 37. Sensitivity of K determination depth of u/w sensor. λ_1=420, λ_2=530. Error: 1 meter offset in Z, (a) K=0.038m^{-1}, (b) K=0.152m^{-1}. Other conditions as in Fig. 12.

-51-
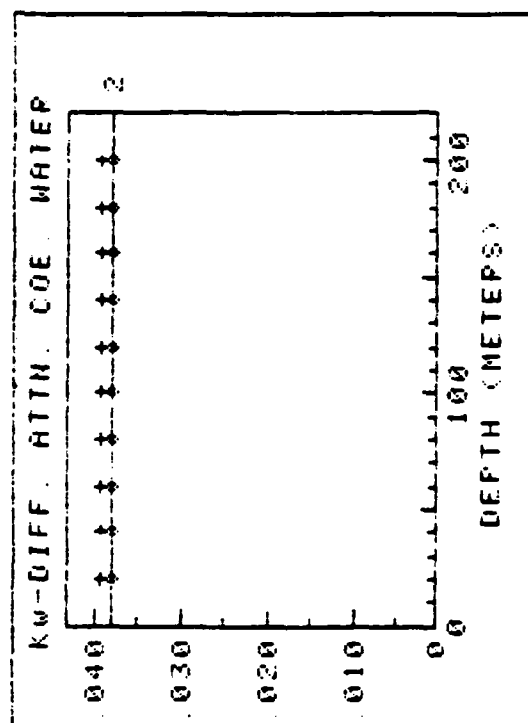
Fig. 38. Same as Fig. 37 except +5% error in Z.

-52-

MODEL MLC7616535
SOLAR ZENITH ANG. -- 30 Deg
ATMOSPHERE TYPE (ts at 490nm):
  1 HAZE   -   ts=0.100 α=1.00
  2 OVERCAST- ts=10-20   o=0.00
BANDPASS: 10nm
WAVELENGTHS: 420 AND 530 nm

ERROR FACTOR(S):
  SUN ANGLE: 0s +5 Deg.

FROM RESULTS AT 530.0nm

λ=459.0nm   Eo=203.61µW/(CM²*nm)
    K(459.0)=0.038 .   tR =0.200
    K(490.0)=0.038   tOZ=0.063

(a)

MODEL MLC7616535
SOLAR ZENITH ANG. -- 30 Deg
ATMOSPHERE TYPE (ts at 490nm):
  1 HAZE   -   ts=0.100 o=1.00
  2 OVERCAST- ts=10-20   o=0.00
BANDPASS: 10nm
WAVELENGTHS: 420 AND 530 nm
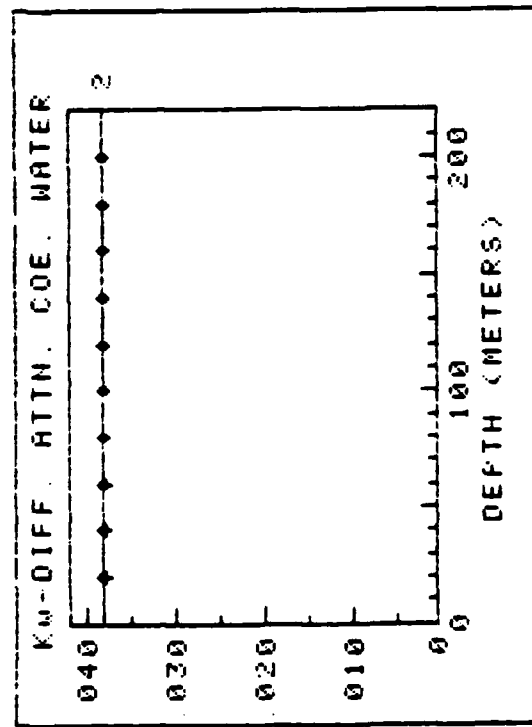
ERROR FACTOR(S):
  SUN ANGLE: 0s +5 Deg.

FROM RESULTS AT 530.0nm

λ=459.0nm   Eo=203.61µW/(CM²*nm)
    K(459.0)=0.188   tR =0.200
    K(490.0)=0.152   tOZ=0.063

(b)

Fig. 39. Sensitivity of K determination to error in solar zenith angle. θ_s=30°, error: 5° offset in θ_s. (a) K(490)=0.038m^{-1}, (b) K(490)=0.152m^{-1}. Other conditions as in Fig. 12.

MODEL MLC761625
SOLAR ZENITH ANG. -- 60 Deg
ATMOSPHERE TYPE (τa at 490nm):
  1 HAZE   - τa=0.100 α=1.00
  2 OVERCAST- τa=10-20 α=0.00
BANDPASS: 10nm
WAVELENGTHS: 420 AND 530 nm

ERROR FACTOR(S):
  SUN ANGLE: θs +5 Deg

  FROM RESULTS AT 530.0nm

λ=459.0nm   Ec=203.61µW/(CM²*nm)
  K(459.0)=0.033   τR =0.200
  K(490.0)=0.038   τOZ=0.003

(a)
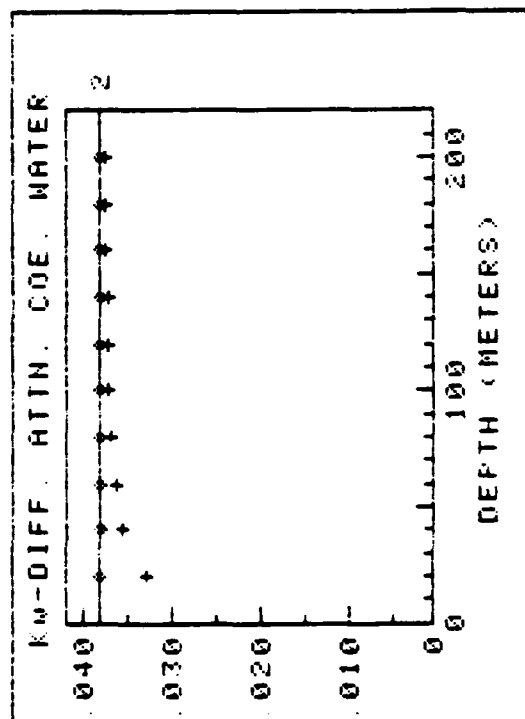
MODEL MLC761625
SOLAR ZENITH ANG. -- 60 Deg
ATMOSPHERE TYPE (τa at 490nm):
  1 HAZE   - τa=0.100 α=1.00
  2 OVERCAST- τa=10-20 α=0.00
BANDPASS: 10nm
WAVELENGTHS: 420 AND 530 nm

ERROR FACTOR(S):
  SUN ANGLE: θs +5 Deg

  FROM RESULTS AT 530.0nm

λ=459.0nm   Ec=203.61µW/(CM²*nm)
  K(459.0)=0.188   τR =0.200
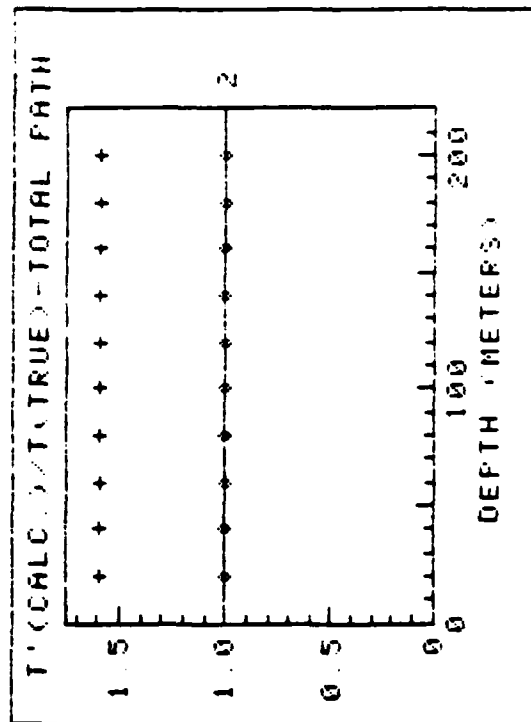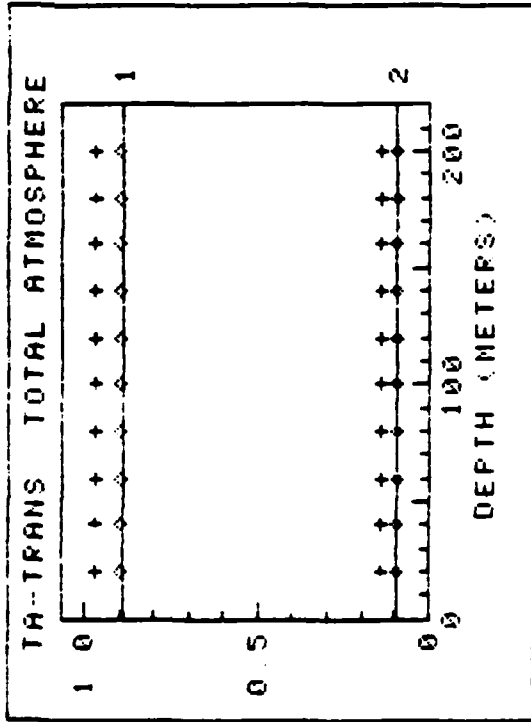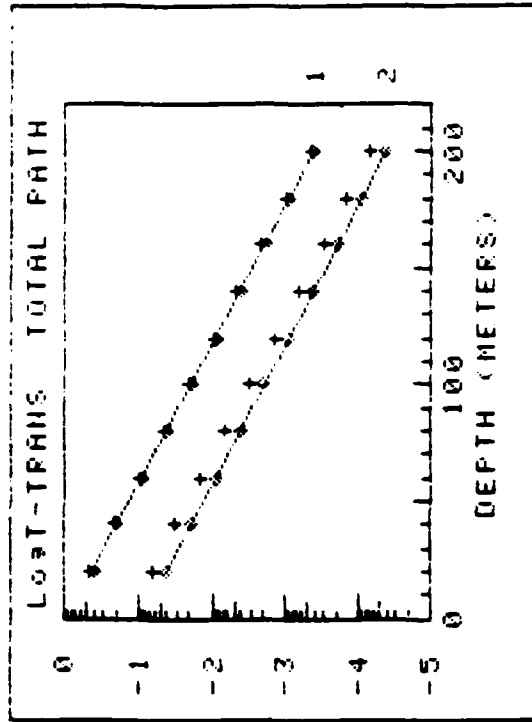 K(490.0)=0.152   τOZ=0.003

(b)

Fig. 40. Same as Fig. 39 except θ_s=60°.

-54-

MODEL MLC7616-35
SOLAR ZENITH ANG   -- 30 Deg.
ATMOSPHERE TYPE (τa at 490nm)
  1 HAZE   -   τa=0.100 α=1.00
  2 OVERCAST- τa=10-20 α=0.00
BANDPASS: 10nm
WAVELENGTHS: 420 AND 530 nm

ERROR FACTOR(S):
  0.95*Eo1 1.00*Eo2

FROM RESULTS AT 530.0nm

λ=459.0nm   Eo=203.61µW/(CM2*nm)
K(459.0)=0.038   τR =0.200
K(490.0)=0.038   τOZ=0.003

(a)
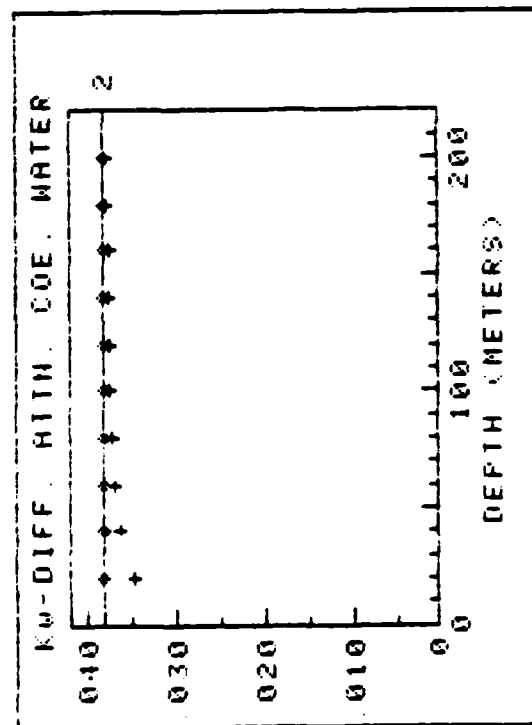
MODEL MLC7616-35
SOLAR ZENITH ANG   -- 30 Deg.
ATMOSPHERE TYPE (τa at 490nm)
  1 HAZE   -   τa=0.100 α=1.00
  2 OVERCAST- τa=10-20 α=0.00
BANDPASS: 10nm
WAVELENGTHS: 420 AND 530 nm

ERROR FACTOR(S):
  0.95*Eo1 1.00*Eo2

FROM RESULTS AT 530.0nm

λ=459.0nm   Eo=203.61µW/(CM2*nm)
K(459.0)=0.188   τR =0.200
K(490.0)=0.152   τOZ=0.003

(b)

Fig. 41. Sensitivity of K determinations to errors in solar spectral irradiance. λ_1=420, λ_2=530. Error: -5% in $E_o(\lambda_1)$. (a) K(490)=0.038m^{-1}, (b) K(490)=0.152m^{-1}. Other conditions as in Fig. 12.

-55-

Appendix I   14 February 1983

EN-001-83t

TECHNICAL MEMORANDUM

SUBJECT: Determination of the Optical Properties of the Atmosphere above
          the Ocean's Surface from Spectral Measurements of the Natural
          Light made below the Surface.

1.0   INTRODUCTION

This brief study was made in response to the question: From optical
measurements made at an arbritary depth (z) in the open oceans, can the
optical character of the atmosphere existing at the time of the measurement(s)
be determined? That is, can we conceive of a technique which, using the
ambient light at some depth in the ocean, will provide information from which
we can determine the type of atmosphere (clear, hazy, overcast, etc.) existing
overhead? It is assumed that the depth (z), at which the measurement is made,
and the zenith angle of the sun (θs) (i.e. time of day and latitude etc.) are
known.

2.0   CONCEPT

Prior work indicates that there exists an apparent spectral relation-
ship between the diffuse attenuation coefficient, $K(\lambda)$, and the various "types"
of natural waters found in the open oceans. The attenuation, $K(\lambda)$, varies with
wavelength and its spectral form is quite different for clear water than for
more turbid water. If this relationship is consistent and known for the
waters of interest, then by making measurements of the ambient spectral
irradiance at depth we should be able to determine the attenuation characteris-
tics of the water column. Assuming we can determine the diffuse attenuation
of the water above the instrument and that the instrument measures the absolute
downwelling irradiance, the downwelling irradiance at the surface can be com-
puted. From the irradiance at the surface the attenuation through the atmos-
phere can be found using established values of the solar irradiance outside
the atmosphere.

3.0   TWO WAVELENGTH MODEL

A two wavelength model is used to illustrate the procedure. The
wavelengths (λ) used, λ = 490 nm and λ = 520 nm, were chosen to take advan-
tage of a fairly large body of data which has been processed by the Visibility
Laboratory to yield the spectral relationship of the diffuse attenuation co-
efficient $K(\lambda)$ at these specific wavelengths. These may not be the optimum
wavelengths, but they serve well to illustrate the mechanism of the concept.

3.1   K(λ) Relationships

A study at the Visibility Laboratory[1] has developed the
following relationships:

$$K(490) = 0.0883 \left[\frac{Lss(443)}{Lss(550)} \right]^{-1.491} + 0.022 \tag{1}$$

$$K(520) = 0.0663 \left[\frac{Lss(443)}{Lss(550)} \right]^{-1.398} + 0.044 \tag{2}$$

Where $Lss(\lambda)$ is the subsurface upwelling radiance at
wavelength λ.

From this it follows that

$$K(520) = 0.0663 \left[11.325 \times K(490) - 0.2492 \right]^{0.9376} + 0.044 \tag{3}$$

3.2   Propagation of the Light Downward
Let:

T_A = the transmittance through the atmosphere

T_S = the transmittance through the water surface

(1) Ref. R.W. Austin; Remote Sensing of the Diffuse Attenuation Coefficient of
Ocean Water, Visibility Laboratory, 29th Symposium of the AGARD Electromagnetic
Wave Propagation Panel; Monterey, Calif., April 1981.

T_W = the transmittance through the water to depth z

μo = Cosine of Solar zenith angle

All transmittances are for diffuse light.

Then the irradiance at depth z is

$$E_{z(\lambda)} = \mu o \cdot T_A(\lambda) \cdot T_S(\lambda) \cdot T_W(\lambda) \cdot E_o(\lambda) \quad \text{where} \tag{4}$$

E_o = the solar irradiance outside the atmosphere.

$$T_A(\lambda) = e^{-\frac{1}{\mu o} \left[\tau_R(\lambda) + \tau_o(\lambda) + \tau_a(\lambda) \right]} \tag{5}$$

Where τ_R, τ_o and τ_a are the optical depths of the atmosphere for unit air mass for Rayleigh (air molecules), for ozone, and for the aerosol, respectively. The values for $\tau_R(\lambda)$ and $\tau_o(\lambda)$ are fairly well known and are essentially fixed, appearing to vary slightly with season and latitude. The aerosol component has a wavelength dependency which appears to follow a power law so that

$$\tau(\lambda_1) = \left(\frac{\lambda_1}{\lambda_2} \right)^{-\alpha} \cdot \tau(\lambda_2) . \tag{6}$$

The exponent, α, is known as the Angstrom exponent and is commonly taken to be in the range of 1.1 -1.4 for fairly clear atmospheres and it will, we believe, be around zero for very heavy (fog, overcast) aerosols.

$$T_S = 0.98 \tag{7}$$

$$T_W = e^{-K(\lambda) \cdot z} \tag{8}$$

And we get

$$E_z(\lambda) = \mu o \cdot (0.98) \cdot e^{-\frac{1}{\mu o} \left(\tau_R(\lambda) + \tau_o(\lambda) + \tau_a(\lambda) \right)} \cdot e^{-K(\lambda) \cdot z} \cdot E_o \tag{9}$$

- 4 -

3.3 Solving the problem

The above (section 3.2) is used only to calculate the irradiance $E(\lambda)$, which would arrive at depth z for various types of atmospheric conditions and sea water, to use for inputs in solving the problem. At this juncture we are at depth z with an instrument which measures $E_z(\lambda)$ at two wavelengths 490 and 520 nm. From these two measurements we wish to determine the type of atmosphere overhead.

Let λ_1 be the first wavelength, $\left(\lambda_1 = 490 \text{ nm}\right)$ and λ_2 be the second $\left(\lambda_2 = 520 \text{ nm}\right)$. From (9) we can get the ratio

$$\frac{E_z(1)}{E_z(2)} = e^{-\frac{1}{\mu o}\left(\tau_R(1) - \tau_R(2) + \tau_0(1) - \tau_0(2)\right)} \cdot e^{-\frac{1}{\mu o}\left(\tau_a(1)-\tau_a(2)\right)}$$

$$\cdot e^{-\left|K(1)-K(2)\right| \cdot z}. \tag{10}$$

$\tau_R(\lambda)$ and $\tau_0(\lambda)$ are very nearly constant so let

$$C_1 = e^{-\frac{1}{\mu o}\left(\tau_R(1) - \tau_R(2) + \tau_0(1) - \tau_0(2)\right)} \tag{11}$$

$\tau_a(1)$ and $\tau_a(2)$, the optical thickness due to aerosols and clouds, are unknowns which we are seeking to establish. However, since λ_1 and λ_2 are close together and the Angstrom exponent in Eq. (6) is small (<1.4) we assume that they are equal and then

$$e^{-\frac{1}{\mu o}\left(\tau_a(1)-\tau_a(2)\right)} \approx 1.0 .^*$$

thus

$$\frac{E_z(1)}{E_z(2)} \approx C_1 \cdot e^{-\left|K(1)-K(2)\right| \cdot z}$$

* See section 4 for a discussion of the magnitude of error caused by this assumption.

$$K(1)-K(2) = -\frac{1}{z} \ln \frac{1}{C_1} \cdot \frac{E_z(1)}{E_z(2)}$$

$$K(2)-K(1) = \frac{1}{z} \ln C_1 \cdot \frac{E_z(2)}{E_z(1)} \tag{12}$$

Substituting Eq. (3) into (12) we get

$$K'(2)-0.0663 \left[(11.325) \cdot K'(1)-0.2492\right]^{0.9376} -0.044$$

$$= \frac{1}{z} \ln C_1 \cdot \frac{E_z(2)}{E_z(1)} \tag{13}$$

Where $K'(1)$ is a calculated value as opposed to $K(1)$ the "true" value.

From Eq. (13) by successive approximation $K'(1)$ can be calculated and if desired $K(1)$ can be calculated using (3).

The irradiance at the surface can now be estimated using $K'(\lambda)$, i.e.,

$$E'_S(\lambda) = \frac{1}{0.98} \cdot e^{K'(\lambda) \cdot z} \cdot E_z(\lambda).$$

The calculated atmospheric transmittance is then

$$T'_A(\lambda) = \frac{1}{\mu o} \cdot \frac{E'_S(\lambda)}{E_o(\lambda)}$$

and since

$$T_A(\lambda) = e^{-\frac{1}{\mu o} \left(\tau_R(\lambda) + \tau_o(\lambda) + \tau_a(\lambda)\right)}$$

then

$$\tau_a(\lambda) = -\mu o \cdot \ln T'_A(\lambda) - \tau_R(\lambda) - \tau_o(\lambda)$$

$$= -\mu o \cdot \ln \frac{1}{\mu o} \frac{E'_S(\lambda)}{E_o(\lambda)} - \tau_R(\lambda) - \tau_o(\lambda)$$

$$\tau_a'(\lambda) = -\mu o \cdot \ln \frac{1}{0.98 \cdot \mu o} \cdot e^{K'(\lambda) \cdot z} \cdot \frac{E_z(\lambda)}{E_o(\lambda)} - \tau_R(\lambda) - \tau_o(\lambda)$$

$$\boxed{\tau_a'(\lambda) = -\mu o \cdot \left[K'(\lambda) \cdot z + \ln \frac{1}{0.98 \cdot \mu o} \cdot \frac{E_z(\lambda)}{E_o(\lambda)} \right] - \tau_R(\lambda) - \tau_o(\lambda)} \tag{14}$$

The magnitude of $\tau_a'(\lambda)$ is an indicator of the aerosol density. For example:

$\tau_a'(\lambda) \gtrsim .1$ Clear → fairly clear

     $\approx .5$ Haze - light overcast

     > 1 Overcast → heavy overcast

4.0 COMMENTS

4.1 The duffuse attenuation coefficents, $K(\lambda)$, are the mean or "effective" values over the total water column above depth z. The models used for K(490) and K(520) were developed using data roughly over one attenuation length $\left(z = \Gamma / K(\lambda) \right)$ from the surface downward. It has been assumed that these relationships hold for the mean $K(\lambda)$ over greater depths (1 → 200 meters). This needs to be verified.

4.2 The solution determines the optical thickness normalized to one air mass but from conditions mainly in the direction of the sun not directly overhead.

4.3 Assuming a non-spectrally dependent aerosol in going from (10) to (12)(Section 3.3)results in an error, at this point, of approximately 1% for Hi sun and clear air; 2% for Hi sun and heavy overcast. The worst case would be with a low sun and hazy sky where the error (at this point) for a sun zenith angle of 80° would be approximately 10%. A choice other than zero might be slightly better here. Also, an itterative process could be used where the "α" exponent is estimated from the τ_a found and the computations repeated, etc.

4.4 Errors of ± 5% in the measurement of the irradiances $E_{z(1)}$ and $E_{z(2)}$ do not seriously degrade the ability to estimate the type of atmosphere present.

4.5 The precision with which the attenuation coefficients $K(\lambda)$ are determined is increased with increased path length (z). On the other hand over long path lengths the effect of error in $K(\lambda)$ becomes more detrimental to the final results. These two things are somewhat compensating.

4.6 The place where this model is weakest is probably in the $K(\lambda)$ relationships used. Although it is based on a fairly large body of data (88 points for $\lambda = 490$ and $\lambda = 520$) the precision and variability of the data base, as is always the case with this type of in-situ measurement, is not as good as we would like. We are left with questions. Will this $K(\lambda)$ model or some variation of it work adequately over the distances contemplated and how well will it work when used under actual in-situ conditions. These and other questions are best, and perhaps can only, be answered by field work in the ocean.

4.7 The wavelengths used here are not necessarily the optimum wavelengths. In choosing wavelengths we wish to work with those which will provide the best determination of the attenuation of the water so that our extrapolation back to the surface is most accurate. We must also not forget the approximation made in Section 3.3 which becomes less significant with less separation between the wavelengths used.

4.8 Examples of the two wavelengths scheme have been worked up for a variety of input conditions. The spectral irradiances at depths z, i.e. $E_z(\lambda_1)$ and $E_z(\lambda_2)$, were computed using Eq. (10) for the set of assumed input parameters (i.e. all water, atmospheric and geometric variables are known and the underwater irradiances computed. Using the values of $E_z(\lambda_1)$ and $E_z(\lambda_2)$ that were computed above and a knowledge

of depth beneath the surface, time, date, latitude, and longitude, appropriate values of μ_0, $\tau_R(\lambda_1)$, $\tau_R(\lambda_2)$, $\tau_0(\lambda_1)$, and $\tau_0(\lambda_2)$ may be determined, and from Eq. (11), $K'(\lambda_1)$, the estimate of the diffuse attenuation coefficient at λ_1 may be determined. $K'(\lambda_1)$ may then be inserted in Eq. (14) to obtain an estimate of the aerosol optical thickness $\tau_a'(\lambda)$. With only two wavelengths, hence two equations, it is not possible to solve completely for K, τ_a, and α, the three unknown variables in the complete radiative transfer equation. Hence the necessity to assume $\tau_a(\lambda_2) \approx \tau_a(\lambda_1)$, i.e. that the Angstrom exponent, α, is sufficiently small and $\frac{\lambda_1}{\lambda_2}$ is sufficiently close to 1 that $\left(\frac{\lambda_1}{\lambda_2}\right)^{-\alpha} \to 1$. This assumption is not correct in the general case and in order to obtain a solution when $\tau_a(\lambda_1) \neq \tau_a(\lambda_2)$ we must resort to measurements at a third wavelength for which we must obtain a relationship similar to that of Eqs. (1) and (2). We would then have three equations of the form of Eq. (9) and three unknowns and could solve for $\tau_a(\lambda_1)$ the optical thickness of the aerosol component of the atmosphere at the wavelength of interest with $K(\lambda)$ and α as byproducts.

T. J. Petzold

ATMOSPHERE

$$E_0(\lambda)$$

$$T_A(\lambda) = e^{-\frac{1}{\mu_0}\left(\tau_R(\lambda) + \tau_0(\lambda) + \tau_G(\lambda)\right)}$$

$$\mu_0 = \cos\theta_s$$

$$\theta_s$$

$$E_S = \mu_0 \times T_A(\lambda) \times E_0(\lambda)$$

$$T_S$$

$$E_z(\lambda) = T_S \times T_W \times E_S$$

$$T_S = .98$$

$$T_W = e^{-K(\lambda) \times z}$$

$$z$$

$$E_z(\lambda)$$
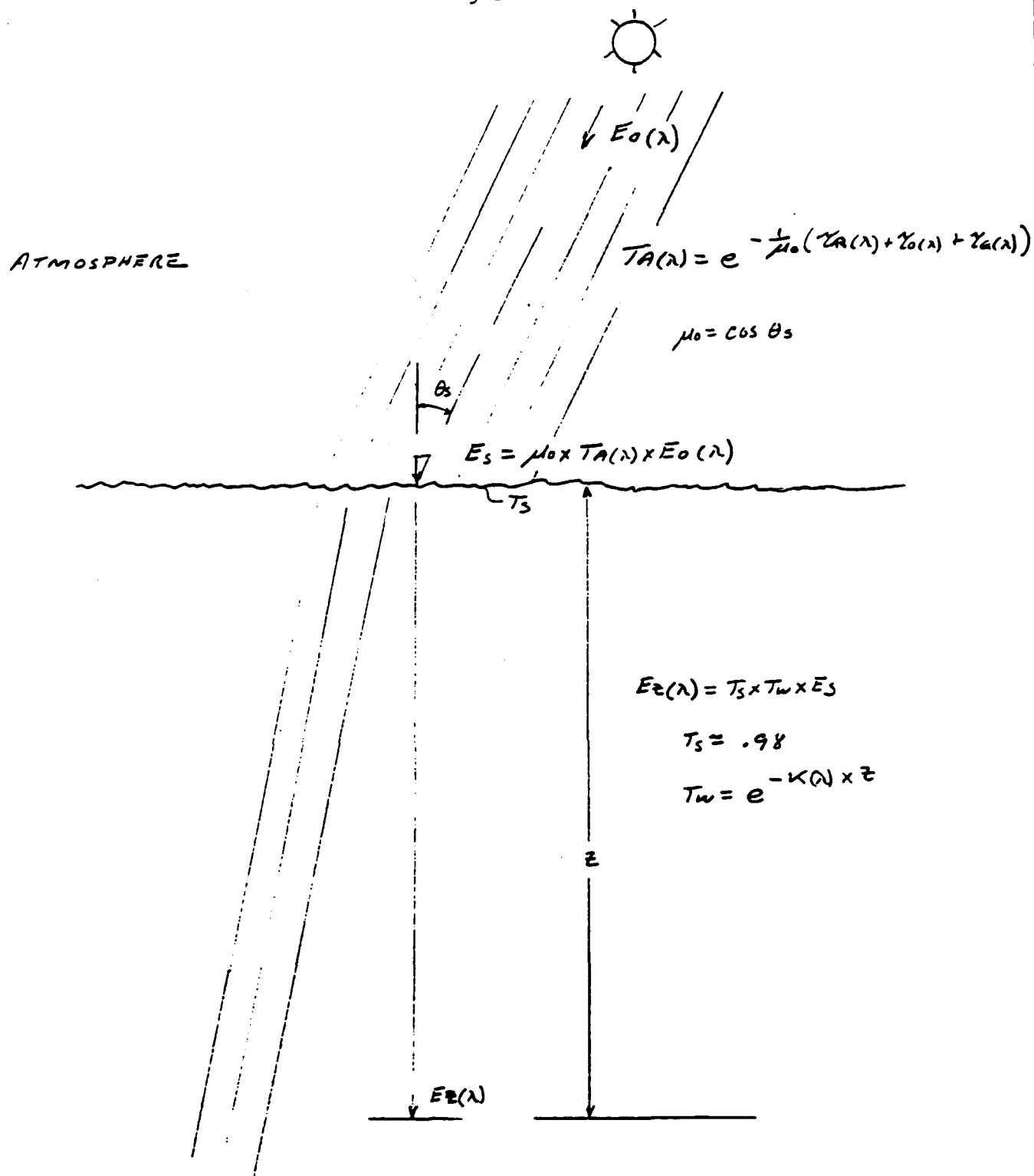
$$E_z(\lambda) = 0.98 \times \mu_0 \times e^{-\frac{1}{\mu_0}\left(\tau_R(\lambda) + \tau_0(\lambda) + \tau_G(\lambda)\right)} \times e^{-K(\lambda) \times z}$$

Figure 1

A Reprint from the

PROCEEDINGS

Of SPIE-The International Society for Optical Engineering

Volume 489

Ocean Optics VII

June 25-28, 1984
Monterey, California

Spectral dependence of the diffuse attenuation coefficient of light in ocean waters

R. W Austin, T. J. Petzold
Visibility Laboratory, Scripps Institution of Oceanography
University of California, San Diego, La Jolla, California 92093

SPECTRAL DEPENDENCE OF THE DIFFUSE ATTENUATION
COEFFICIENT OF LIGHT IN OCEAN WATERS

R. W. Austin and T. J. Petzold

Visibility Laboratory
Scripps Institution of Oceanography
University of California, San Diego
La Jolla, California 92093

Abstract

A study of the spectral nature of the diffuse attenuation coefficient of light, $K(\lambda)$, for various types of oceanic waters has been performed. These attenuation spectra were computed from downwelling spectral irradiance data, $E_d(\lambda)$, obtained by U.S., French and Japanese investigators, working in widely separated oceanic regions and using different measuring techniques and equipment. Attenuation properties were calculated over the spectral region from 365 to 700 nm and for depths from near-surface to in excess of 100 meters.

Examining the $K(\lambda)$ data, we find strong, simple, and useful relationships exist between the value of K at some selected reference wavelength, λ_o, and the value of K at some other wavelength such that $K(\lambda) = M(\lambda)[K(\lambda_o) - K_w(\lambda_o)] + K_w(\lambda)$, where K_w is the attenuation coefficient for pure sea water. For oceanic waters (for example, Jerlov types I through III) the relationships are linear. These relationships appear to be useful throughout the entire spectral range examined and are particularly good between 420 and say 580 nm.

The significance of the existence of such relationships is that they allow the inference of the spectral attenuation coefficient at all wavelengths from the attenuation value at a single wavelength, and provide analytical expressions for modeling the spectral nature of the attenuation in ocean and clear coastal water.

Introduction

The need for information with respect to the optical properties of ocean water greatly exceeds its availability. For example, little data exists on the spectral diffuse attenuation coefficient of sea water, if one insists on data based on *in situ* measurements. If we examine such attenuation spectra, however, we find that they behave in a well ordered and regular fashion over most of the spectrum, particularly if we restrict our attention to the open ocean where the water may be classified as Jerlov Types I through III (Jerlov 1976). The concept of the Jerlov water types itself is based on a specification of attenuation spectra. For many applications the Jerlov classification may, in fact, provide an adequate description of the spectral nature of the water attenuation.

We have reexamined the problem using new spectral data as obtained by a variety of investigators, working in various geographical regions, using different types of equipment and varied methods. The results which we have obtained are similar in many respects to those presented by Jerlov but show some important differences in detail. The method of presentation of the results allows the user to estimate attenuation spectra for ocean water knowing only the value of the diffuse attenuation coefficient, K, at a single wavelength. Thus, the value of K at any wavelength that may be available for a particular water may be used to:

(a) estimate the value of K at any other wavelength of interest,

(b) estimate the complete spectral characteristics of the diffuse attenuation coefficient for the water, or

(c) determine the Jerlov water type.

Discussion

It is helpful conceptually to partition the diffuse attenuation coefficient into components associated with known constituent components of the water. For example, subtracting K_w, the K associated with pure sea water, leaves the contribution to K resulting from all material suspended and dissolved in the water, denoted here as K'. Thus if $K(\lambda)$ is the total diffuse attenuation coefficient at wavelength λ, then

$$K'(\lambda) = K(\lambda) - K_w(\lambda) . \tag{1}$$

$K(\lambda)$ may be further subdivided into contributions from components due to say, (a) the presence of phytoplankton and the detrital material that is associated with it; (b) to the absorption of dissolved yellow substance which is found in varying concentrations in ocean water; and (c) to the suspended particulates which do not co-vary with phytoplankton or its related pigment concentrations.

Smith and Baker (1978), for example, used a model wherein K' was composed of two components, *i.e.* one proportional to concentration of chlorophyll-like pigments and the other, $K_x(\lambda)$, "... a variable representing the average contribution to spectral attenuation not directly attributable to chlorophyll-like pigments". They successfully reproduced the general shape of measured spectral attenuation spectra using empirically derived values of $K_w(\lambda)$, $K_x(\lambda)$ and the specific spectral attenuation coefficient for chlorophyll, $k_c(\lambda)$, together with a knowledge of the pigment concentrations.

If one attempts to model the attenuation $K'(\lambda)$ using varying amounts of two or three component spectra, each dependent on a concentration, then one must know the value of $K'(\lambda)$ at a minimum of two or three wavelengths in order to solve for the various concentrations and specify the complete $K(\lambda)$ spectrum. Such a technique has the potential advantage that the concentrations of these constituents may be determined provided that a unique set of specific attenuation spectra has been determined. We have elected in this study, however, to attempt to determine a single spectral component $K'(\lambda)$ which when added to $K_w(\lambda)$, the spectral attenuation of pure sea water, will provide the complete diffuse attenuation coefficient specification of the water, $K(\lambda)$.

The Data Base

Downwelling spectral irradiance data from various sources were first examined for general suitability, spectral range, and availability of contemporaneous data at other depths. Irradiance data from 148 stations each having measurements at from 2 to 12 depths were interpolated to provide values of irradiance, $E_d(\lambda)$, at uniform 5 nm steps. Various pairs of these spectra at each station were then used to compute the $K(\lambda)$ for the selected depth interval using the relationship,

$$K(\lambda) = -\frac{1}{z_2 - z_1} \ln \frac{E_d(\lambda, z_2)}{E_d(\lambda, z_1)} \tag{2}$$

These $K(\lambda)$ spectra were then examined for artifacts such as might be attributable to changes in environmental conditions during the acquisition of the irradiance data, ship shadows, etc., and a selection made of the spectra to be used as a data base. No more than one spectra was selected from a station[*]. The value of K at 490 nm was used as a classification index for the spectra. No data were used if the $K(490)$ value exceeded $0.25(m^{-1})$. This limit excluded relatively few stations in areas such as enclosed bays and in coastal areas of very high productivity or regions of high terrigenous input. Those excluded data do not affect the generality of the results for applications to the open ocean and many coastal regions. For the special cases where $K(490)$ exceeds $0.25(m^{-1})$ the shapes of the spectra are more disparate and there is real merit to using a multicomponent model as suggested above to obtain a better fit to the data and to obtain a measure of the concentration of the several constituents of the water[**].

Table 1 lists the sources of the data used in the present study. The three groups of investigators that acquired the irradiance spectra were Smith and his colleagues at the Visibility Laboratory of the Scripps Institution of Oceanography; Morel and his colleagues at the Laboratoire de Physique et Chemie, Villefranche-sur-Mer; and Okami, Kishino and Sugihara at the Physical Oceanography Laboratory of the Institute of Physical and Chemical Research in Japan. The geographical regions include open ocean, upwelling areas, coastal waters and marginal seas. The irradiance spectra were obtained at depths from 1 to 118 meters. The K's were calculated using irradiance data separated in depth by from 5 to 78 meters. Because the absorption of water becomes particularly significant at the longer wavelengths, the spectral range varied with the depth of the deeper of the two irradiance spectra used to calculate $K(\lambda)$. The values of the classification index, $K(490)$, varied from a very clear $0.025 m^{-1}$ in the Sargasso Sea to a turbid 0.245 near the mouth of the Mississippi River. A total of 76 $K(\lambda)$ spectra were selected for the data base from the 148 stations examined.

Diffuse attenuation coefficient of pure sea water

The process of isolating the attenuation effects of the material suspended or dissolved in the sea water required a knowledge of the attenuation due to the base sea water to which these materials were added. Excellent reviews of the knowledge of the attenuation properties of clear natural waters have been provided by Morel (1974) and by Smith and Baker (1981). Briefly K_w for pure water may be approximated by the sum of the absorption coefficient, a_w, and the backscattering coefficient b'_{sw}. In "pure" sea water the scattering would be molecular or "Rayleigh" with a phase function having equal forward and backward lobes. The backscattering coefficient was thus assumed to be one half the total scattering coefficient and $K_w(\lambda)$, therefor, determined as

$$K_w(\lambda) = a_w + \frac{1}{2} b_{sw}. \tag{3}$$

Using $a_w(\lambda)$ as given by Morel and Prieur (1977) and values for $b_{sw}(\lambda)$, the sea water scattering coefficient, presented by Morel (1974), we have arrived at the $K_w(\lambda)$ values listed in Table 2 in the column labeled "Morel". These values have been smoothed and interpolated to provide estimates of $K_w(\lambda)$ every 5 nm (only 10 nm intervals are presented in the table). The entries differ by a small amount from those given by Smith and Baker in their Table 1 (usually less than one unit in the third decimal place) due to procedural differences.

Because subsequent processing of the data was to be performed by a computer, it was deemed desirable to find an analytic fit to the $K_w(\lambda)$ curve. As can be seen in Fig. 1(a), the curve does not lend itself to fitting with a single function.

---

[*] On the S C O R DISCOVERER expedition Morel and Smith both measured spectral irradiance using different equipment and methods. Of the 17 stations selected from Morel's work and the 7 stations selected from Smith's, 5 were the same. For three of those, different depth intervals were used; on one station the 58 meter depth interval selected from Smith's work included the 30 meter interval of Morel's; on the fifth station the same interval was selected.

[**] A multicomponent model has been tried with excellent success using constituent spectra for absorption from Morel and Prieur (1977) Using these functions and values of $K(\lambda)$ at 3 properly chosen wavelengths, a wide range of shapes of the measured $K(\lambda)$ spectra could be reproduced and relative amounts of the concentrations of chlorophyll-like pigments, yellow substance and "other material" could be determined

Table 1. Data base for K(λ) study

	YEAR	EXPEDITION (or vessel)	LOCATION	(a) NO STATIONS USED	(b) DEPTHS (m)	(c) WAVELENGTH RANGE (nm)	(d) K(490) RANGE (m⁻¹)	REFERENCE
1	1967	OLIVER	Gulf Stream	1	5-15	385-690	0.039	Tyler & Smith (1970)
2	1968	FRESNEL I & II	Gulf of California I Tres Marias	6	3-20	365-695	0.049-0.158	Tyler & Smith (1970)
3	1970	DISCOVERER (Morel)	Caribbean, Sargasso Sea	17	5-57	400-590	0.025-0.119	Tyler (1973)
4	1970	DISCOVERER (Smith)	Gulf of Panama, E Equatorial Pac	7	6-87	365-660	0.029-0.073	Tyler (1973)
5	1971	HARMATTAN	Central E Atlantic	12	2-118	400-610	0.038-0.144	Morel & Caloumenos (1971)
6	1974	CINECA 5/ CHARCOT	Upwelling off Mauritania	15	4-40	400-685	0.109-0.228	Morel & Prieur (1976)
7	1974	SEIYO-MARU	Sagami Bay, Japan	3	5-30	420-460	0.030-0.098	Okami, et al (1978)
8	1976	TANSEI-MARU	Sagami Bay, Japan	3	5-20	420-670	0.090-0.227	Okami, et al (1978)
9	1976	SHINYO-MARU	Sea of Japan	3	5-20	420-680	0.028-0.058	Okami, et al (1978)
10	1977	RESEARCHER	Gulf of Mexico	2	1-11	390-690	0.206-0.245	VisLab (unpublished)
11	1978	GYRE	Gulf of Mexico	1	1-11	380-685	0.094	VisLab (unpublished)
12	1979	NEW HORIZON	California Bight	6	1-13	375-700	0.043-0.227	VisLab (unpublished)

(a) Number of stations selected. 76 stations selected from total of 148 in the data base.

(b) Range of depths for the $E_d(\lambda)$ spectral pairs used from each expedition. First number is the minimun z_1, second is the maximum z_2.

(c) Range of wavelengths for the $E_d(\lambda)$ spectral pairs used from each expedition. First number is the smallest of all minimum wavelengths, second is the largest of the maximum wavelengths.

(d) Range of K values at 490 nm for the set of $K(\lambda)$ spectra selected for each expedition

Table 2.

		Diffuse Attenuation Coefficient of Pure Sea Water, K_w											
λ	Model	Morel	Ratio	Diff.	λ	Model	Morel	Ratio	Diff.	λ	Model	Morel	Ratio	Diff.
350	0.0510	0.0513	0.9934	−0.0003	470	0.0179	0.0182	0.9848	−0.0003	590	0.1578	0.1577	1.0003	+0.0001
360	0.0405	0.0403	1.0052	+0.0002	480	0.0193	0.0195	0.9896	−0.0002	600	0.2409	0.2457	0.9803	−0.0049
370	0.0331	0.0328	1.0078	+0.0003	490	0.0224	0.0216	1.0373	+0.0008	610	0.2892	0.2906	0.9952	−0.0014
380	0.0278	0.0277	1.0040	+0.0001	500	0.0280	0.0275	1.0181	+0.0005	620	0.3124	0.3106	1.0056	+0.0018
390	0.0242	0.0242	0.9989	−0.0000	510	0.0369	0.0373	0.9880	−0.0004	630	0.3196	0.3206	0.9969	−0.0010
400	0.0217	0.0218	0.9948	−0.0001	520	0.0498	0.0492	1.0114	+0.0006	640	0.3290	0.3305	0.9954	−0.0015
410	0.0200	0.0204	0.9812	−0.0004	530	0.0526	0.0521	1.0096	+0.0005	650	0.3559	0.3505	1.0155	+0.0054
420	0.0189	0.0191	0.9903	−0.0002	540	0.0577	0.0571	1.0108	+0.0006	660	0.4105	0.4105	0.9999	−0.0000
430	0.0182	0.0178	1.0226	+0.0004	550	0.0640	0.0650	0.9851	−0.0010	670	0.4278	0.4304	0.9939	−0.0026
440	0.0178	0.0175	1.0145	+0.0003	560	0.0723	0.0719	1.0053	+0.0004	680	0.4521	0.4504	1.0038	+0.0017
450	0.0176	0.0173	1.0145	+0.0003	570	0.0842	0.0808	1.0427	+0.0034	690	0.5116	0.5004	1.0224	+0.0112
460	0.0176	0.0176	0.9977	−0.0000	580	0.1065	0.1088	0.9784	−0.0024	700	0.6514	0.6504	1.0015	+0.0010

Mean · 1.0002   0.0000

Std Dev · 0.0130   0.0022

Col 1 λ · wavelength in nanometers

Col 2 Model · least squares fit of values from "Morel" (column 3) to parabolic functions (see text)

Col 3 Morel · values of K_w as determined from Eq. (3) using a_w from Morel and Prieur (1977) and b_{sw} from Morel (1974)

Col 4 Ratio · column 2 divided by column 3

Col 5 Diff · column 2 minus column 3

It was subdivided into 5 wavelength intervals: (1) 350 to 445 nm, (2) 445 to 520 nm, (3) 520 to 590 nm, (4) 590 to 660 nm and (5) 660 to 700 nm, and best least square fits obtained to parabolic functions. The values obtained from the model are listed in Table 2 in the "model" column. The model reproduces the values derived from Morel's work with a standard deviation of 0.013 as determined from the ratios of the Model to the Morel values (4th columns in Table 2) and the standard deviation of the differences (columns 5) was 0.0022. Figures 1(b-f) show the values plotted (+) and the analytic fits obtained (solid line) for each of the 5 spectral regions.
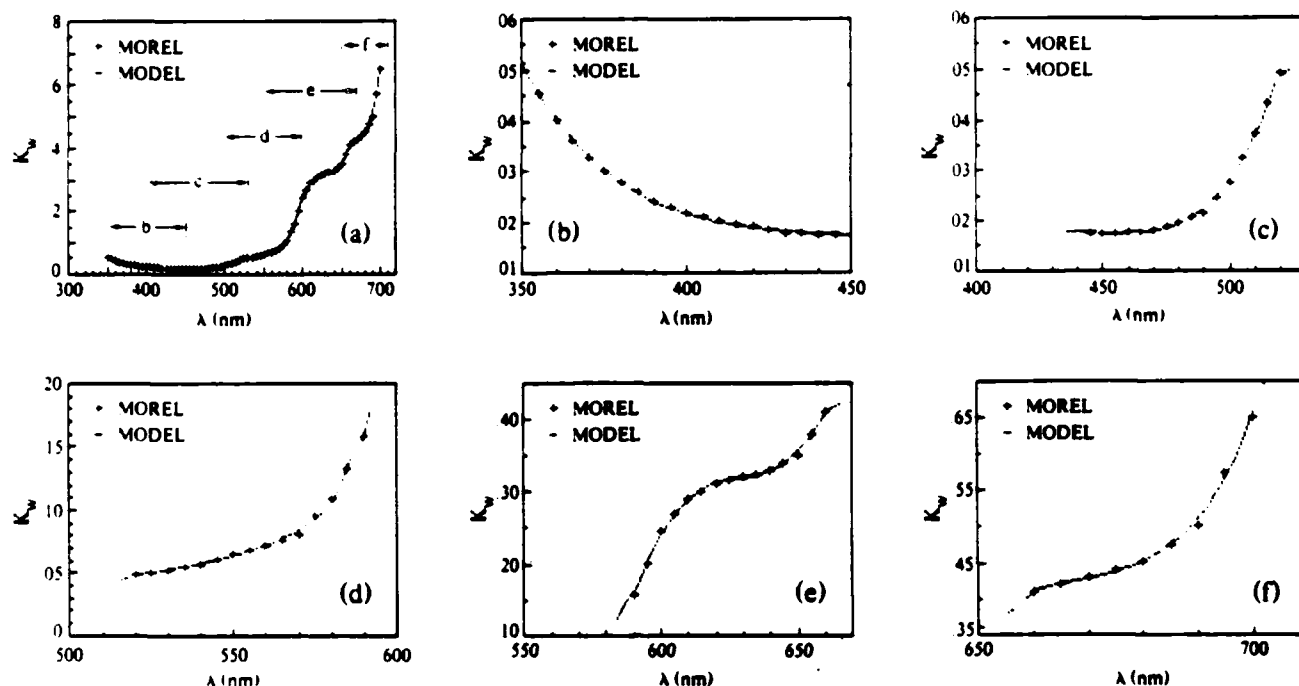
Fig. 1. Comparison of values of K_w as determined by means of Eq. (3) (points marked +) and the fitted functions or "Model" (shown as the continuous line). Panels b-f show the 5 subregions that were individually fitted to the points using a least squares technique.

Data Analysis

If one plots all the available $K(\lambda)$ values at each of the 68 wavelengths from 365 to 700 nm against the corresponding values of the classification index, $K(490)$, one finds that these scatter diagrams provide strong evidence that there is a linear relationship between the two variables up to some maximum value of $K(490)$. Figure 2, for example, shows such scatter plots for wavelengths of 400, 440, 520 and 560 nm. We have noticed that for the shorter wavelengths there is a tendency for the data to depart from linearity at the larger values of $K(490)$. As a result we have used only data where $K(490) < 0.160$ for fitting purposes when working at wavelengths below 580 nm. No significant lessening of linearity was found for longer wavelengths when all $K(490) < 0.250$ were included.

The linear equation is of the form

$$K(\lambda) = I(\lambda) + M(\lambda) \, K(490) \tag{4}$$

and since $K_w(\lambda)$ is a special case of $K(\lambda)$, i.e., the lower limit, we see that we can determine a set of values for $K_w(\lambda)$ from a knowledge of the slopes, $M(\lambda)$, the intercepts, $I(\lambda)$, and a value of K_w at some reference wavelength, say $K_w(490)$. This technique has been tried and provides values very close to those shown in Table 2. We have chosen to use in our analysis, however, the $K_w(\lambda)$ values in the columns labeled "Model" (Col. 2) in Table 2. The slopes that were calculated for each of the 68 wavelengths were based on fitting, by least squares technique, a linear equation of the form,

$$K(\lambda) = M(\lambda) \, [K(490) - K_w(490)] + K_w(\lambda) \tag{5}$$
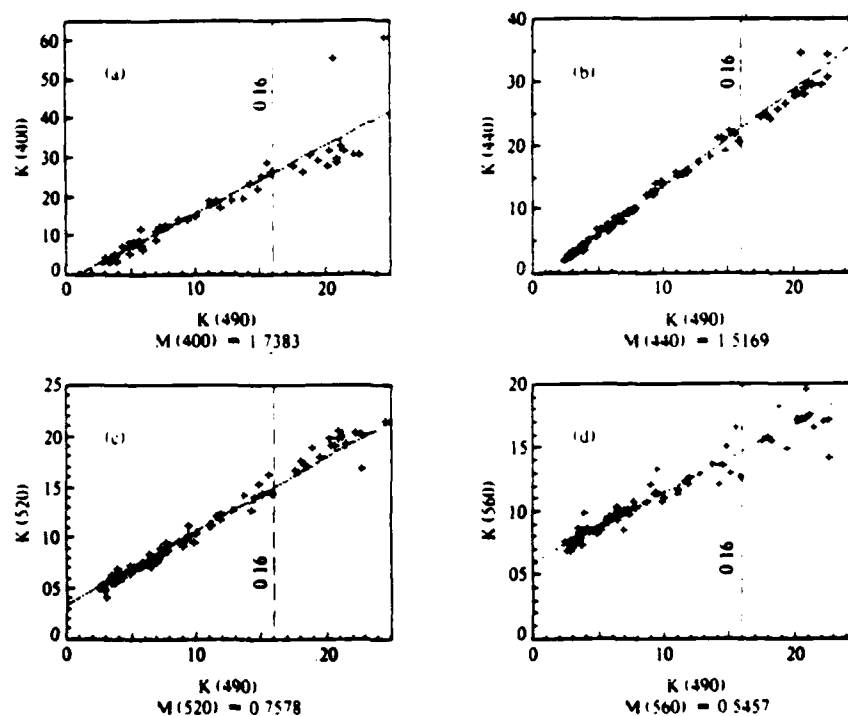
Fig. 2. Examples of scatter plots of $K(\lambda)$ vs $K(490)$, for wavelengths shown are 400, 440, 520 and 560 nm.

to the data in the scatter plots. By using the tabulated values of $K_w(\lambda)$ as the intercept in the linear equation, we have in essence assumed that the $K_w(\lambda)$ values are correct. The effect of this was to decrease the excellence of the fit slightly over that which would be obtained had we used the data to determine the values of K_w. At most wavelengths the effect was trivial. Those few wavelengths where the effect seemed noticeable were at the extremes of the wavelength range where the environmental and instrumental problems associated with field measurements were greater and the number of samples was small or, in a few instances, at wavelengths where the data was "noisier" than usual.

Figure 3 is a plot of the values of the slopes, $M(\lambda)$, at each of the 68 wavelengths as determined by the procedure described above. A piecewise least squares fit was made to these data providing analytic relationships that could be used for further computational analysis. Figures 3(b) to 3(d) show the details of the three spectral sections; (1) 365-420 nm, (2) 420-620 nm, and (3) 625 to 700 nm. Both the data and the mathematical fit to these data are shown. The fitting process not only facilitates the use of the model by the computer but also provides additional smoothing to the overall data set, essentially enlarging its size on a local basis thereby providing better estimates of the slope than can be obtained from a regression at single wavelength. Table 3 lists the values of the slopes as determined from the individual fits to the $K'(\lambda)$ vs $K'(490)$ plots (Col.3, headed "Data") and the values determined from the fitted mathematical functions (Col.2, headed "Model"). The fourth column in each panel is the ratio of the value from column 2 divided by column 3 and provides a measure of the relative agreement between the model and the data used to construct the model. The fifth column is the difference between the model and the data and is thus a measure of the absolute agreement. Slopes were calculated for every 5 nm. The table lists values at 10 nm intervals.

Applications

A major application of the tables is the estimation of $K(\lambda)$ at a wavelength other than that for which data may be available. For example, if the value of $K(490)$ is known then Eq. (5) may be used directly to compute $K(\lambda)$. Values for $M(\lambda)$ and $K_w(\lambda)$ are provided in Table 4 at every 5 nm from 350 to 700 nm. (The values of $M(\lambda)$ for 350, 355, and 360 nm contained in the table were estimated by extrapolation using the fitted mathematical function and should be used with caution.)

Similarly, if the known K is at any wavelength, λ_1, then the unknown K at wavelength λ_2 is,

$$K(\lambda_2) = \frac{M(\lambda_2)}{M(\lambda_1)} \left[K(\lambda_1) - K_w(\lambda_1) \right] + K_w(\lambda_2) . \tag{6}$$
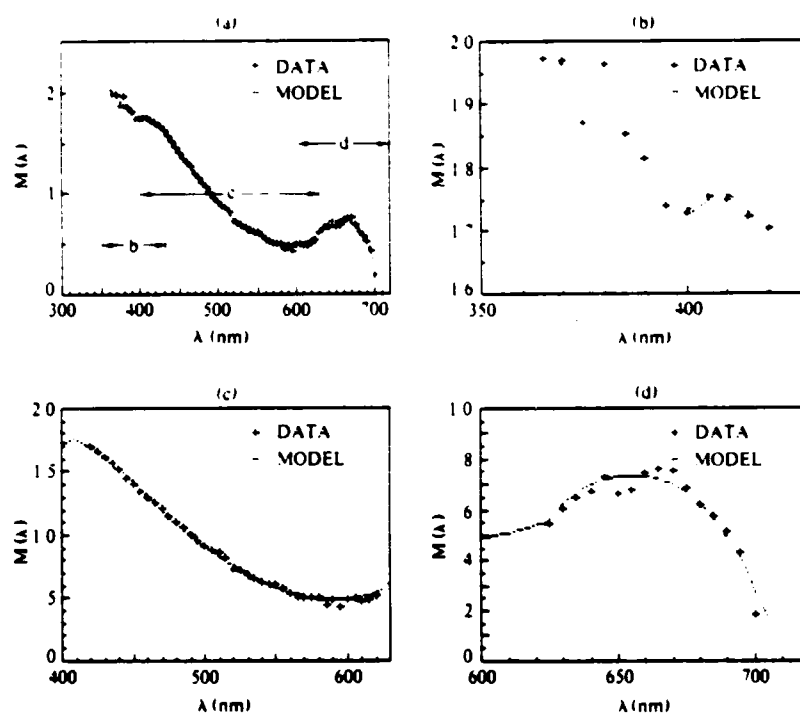
Fig. 3. Slopes $M(\lambda)$, as determined from individual scatter plots of $K(\lambda)$ vs $K(490)$ shown as ($+$). Solid lines show the piecewise fits of the parabolic expressions to the three sections of the spectrum.

Table 3. Slopes of $K'(\lambda)$ versus $K'(490)$

							SLOPE $M(\lambda)$							
λ	Model	Data	Ratio	Diff	λ	Model	Data	Ratio	Diff	λ	Model	Data	Ratio	Diff
350	.	.	.	.	470	1.1982	1.2013	0.9974	-0031	590	0.4840	0.4884	0.9909	-0045
360	.	.	.	.	480	1.0955	1.1005	0.9955	-0050	600	0.4903	0.4970	0.9865	-0067
370	1.9610	1.9708	0.9950	-0098	490	1.0000	1.0000	1.0000	+0000	610	0.5090	0.4822	1.0556	+0268
380	1.8772	1.9653	0.9552	-0881	500	0.9118	0.9129	0.9988	-0011	620	0.5380	0.5260	1.0228	+0120
390	1.8009	1.8158	0.9918	-0149	510	0.8310	0.8571	0.9695	-0261	630	0.6231	0.6061	1.0280	+0170
400	1.7383	1.7292	1.0053	+0091	520	0.7578	0.7253	1.0448	+0325	640	0.7001	0.6677	1.0486	+0325
410	1.7591	1.7487	1.0060	+0104	530	0.6924	0.6814	1.0160	+0109	650	0.7300	0.6638	1.0996	+0661
420	1.6974	1.7044	0.9959	-0070	540	0.6350	0.6271	1.0126	+0079	660	0.7301	0.7464	0.9782	-0163
430	1.6108	1.6175	0.9959	-0067	550	0.5860	0.6032	0.9714	-0172	670	0.7008	0.7537	0.9299	-0528
440	1.5169	1.5169	1.0000	+0000	560	0.5457	0.5395	1.0114	+0062	680	0.6245	0.6214	1.0050	+0031
450	1.4158	1.3981	1.0127	+0177	570	0.5146	0.5011	1.0270	+0135	690	0.4901	0.5121	0.9571	-0220
460	1.3077	1.2969	1.0084	+0108	580	0.4935	0.5078	0.9718	-0143	700	0.2891	0.1868	1.5476	+1023

Col 1 λ - wavelength in nanometers

Col 2 Model - least squares fit of slopes in column 3 (Data) to parabolic functions of wavelength (see text)

Col 3 Data - slopes determined from linear least squares fit of scatter plots of $K(\lambda)$ vs $K(490)$

Col 4 Ratio - column 2 divided by column 3

Col 5 Diff - column 2 minus column 3

Table 4. Values of the slope function $M(\lambda)$
and $K_w(\lambda)$ for use in Eqs. 5 and 6

λ (nm)	M (λ)	K_w (λ)	λ (nm)	M (λ)	K_w (λ)	λ (nm)	M (λ)	K_w (λ)
350	2.1442	0.0510	470	1.1982	0.0179	590	0.4840	0.1578
355	2.0968	0.0453	475	1.1460	0.0184	595	0.4853	0.2043
360	2.0504	0.0405	480	1.0955	0.0193	600	0.4903	0.2409
365	2.0051	0.0365	485	1.0469	0.0206	605	0.4983	0.2688
370	1.9610	0.0331	490	1.0000	0.0224	610	0.5090	0.2892
375	1.9183	0.0302	495	0.9550	0.0248	615	0.5223	0.3040
380	1.8772	0.0278	500	0.9118	0.0280	620	0.5380	0.3124
385	1.8379	0.0258	505	0.8704	0.0320	625	0.5659	0.3174
390	1.8009	0.0242	510	0.8310	0.0369	630	0.6231	0.3196
395	1.7671	0.0228	515	0.7934	0.0428	635	0.6683	0.3227
400	1.7383	0.0217	520	0.7578	0.0498	640	0.7001	0.3290
405	1.7463	0.0208	525	0.7241	0.0504	645	0.7201	0.3397
410	1.7591	0.0200	530	0.6924	0.0526	650	0.7300	0.3559
415	1.7312	0.0194	535	0.6627	0.0550	655	0.7323	0.3789
420	1.6974	0.0189	540	0.6350	0.0577	660	0.7301	0.4105
425	1.6550	0.0185	545	0.6094	0.0607	665	0.7205	0.4208
430	1.6108	0.0182	550	0.5860	0.0640	670	0.7008	0.4278
435	1.5648	0.0180	555	0.5647	0.0678	675	0.6693	0.4372
440	1.5169	0.0178	560	0.5457	0.0723	680	0.6245	0.4521
445	1.4673	0.0176	565	0.5289	0.0776	685	0.5651	0.4755
450	1.4158	0.0176	570	0.5146	0.0842	690	0.4901	0.5116
455	1.3627	0.0175	575	0.5027	0.0931	695	0.3984	0.5671
460	1.3077	0.0176	580	0.4935	0.1065	700	0.2891	0.6514
445	1.2521	0.0177	585	0.4871	0.1341			

Values for $M(\lambda)$ and $K_w(\lambda)$ should be interpolated when precise wavelengths are defined. Equation (5) or (6) and Table 4 are all that are needed to estimate entire $K(\lambda)$ spectra if the known value of K indicates the water to be oceanic or moderately clear coastal water, for example Jerlov Type I through III oceanic or Type 1 coastal, or if $K(490) < 0.16\ m^{-1}$.

Figure 4(a) is a plot of the model $K(\lambda)$ versus wavelength with $K(490)$ as a parameter. In Fig. 4(b) $K'(\lambda)$, i.e. $K(\lambda) - K_w(\lambda)$, is plotted for the same $K(490)$ values. In Table 5 values of $K(\lambda)$ are listed for each 10 nm from 350 to 700 nm, inclusive, for a variety of values of the water classification index, $K(490)$, from 0.03 to 0.18 m^{-1}. Figure 4 and Table 5 comprise a summary of the results of the model.
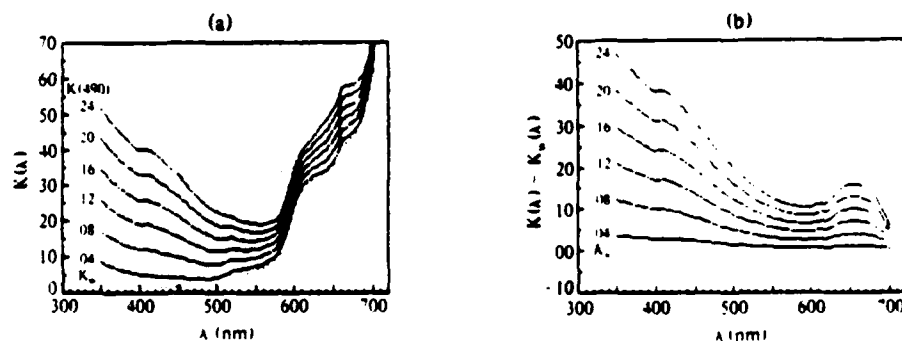
Figure 4. Plots of the water model with values of K(490) as a parameter. Bottom curve K(490) = 0.022 is $K_w(\lambda)$

Figure 5 shows plots of the model superimposed on $K(\lambda)$ values calculated from the measured downwelling irradiance spectra at 5 of the stations used in the original data base. The $K(490)$ values range from 0.033 for Fig. 5(a) to 0.116 for Fig. 5(e). The comparison between the model and the measured data provides examples of the manner in which the model represents the data from which it was formed. Figure 6 provides another measure of the degree of the fit between the model and the data. Figure 6(a) shows the standard deviation of the ratio of the K values calculated from the model to those obtained from the measured irradiances. Figure 6(b) shows the standard deviation of the differences between the two. Figure 7 presents the number of points used at each of the 68 wavelengths between 365 and 700 in the original data set.

Table 5. Values of $K(\lambda)$ for selected $K(490)$, the water classification index.

Wavelength (nm)	K_w m^{-1}	$K(\lambda)$ m^{-1}											
350	0.0510	0.0672	0.0887	0.1101	0.1316	0.1530	0.1745	0.1959	0.2173	0.2602	0.3031	0.3460	0.3889
360	0.0405	0.0561	0.0766	0.0971	0.1176	0.1381	0.1586	0.1791	0.1996	0.2406	0.2816	0.3226	0.3636
370	0.0331	0.0480	0.0676	0.0872	0.1068	0.1264	0.1460	0.1656	0.1852	0.2244	0.2637	0.3029	0.3421
380	0.0278	0.0421	0.0608	0.0796	0.0984	0.1172	0.1359	0.1547	0.1735	0.2110	0.2486	0.2861	0.3236
390	0.0242	0.0379	0.0559	0.0739	0.0919	0.1099	0.1279	0.1459	0.1639	0.1999	0.2360	0.2720	0.3080
400	0.0217	0.0349	0.0523	0.0697	0.0870	0.1044	0.1218	0.1392	0.1566	0.1913	0.2261	0.2609	0.2956
410	0.0200	0.0334	0.0510	0.0686	0.0861	0.1037	0.1213	0.1389	0.1565	0.1917	0.2269	0.2621	0.2972
420	0.0189	0.0318	0.0488	0.0658	0.0827	0.0997	0.1167	0.1336	0.1506	0.1846	0.2185	0.2525	0.2864
430	0.0182	0.0304	0.0465	0.0627	0.0788	0.0949	0.1110	0.1271	0.1432	0.1754	0.2076	0.2398	0.2721
440	0.0178	0.0293	0.0444	0.0596	0.0748	0.0899	0.1051	0.1203	0.1355	0.1658	0.1961	0.2265	0.2568
450	0.0176	0.0283	0.0425	0.0566	0.0708	0.0849	0.0991	0.1133	0.1274	0.1557	0.1840	0.2124	0.2407
460	0.0176	0.0275	0.0406	0.0536	0.0667	0.0798	0.0929	0.1060	0.1190	0.1452	0.1713	0.1975	0.2236
470	0.0179	0.0270	0.0390	0.0510	0.0630	0.0749	0.0869	0.0989	0.1109	0.1349	0.1588	0.1828	0.2067
480	0.0193	0.0276	0.0386	0.0495	0.0605	0.0714	0.0824	0.0933	0.1043	0.1262	0.1481	0.1700	0.1919
490	0.0224	0.0300	0.0400	0.0500	0.0600	0.0700	0.0800	0.0900	0.1000	0.1200	0.1400	0.1600	0.1800
500	0.0280	0.0349	0.0440	0.0532	0.0623	0.0714	0.0805	0.0896	0.0987	0.1170	0.1352	0.1535	0.1717
510	0.0369	0.0432	0.0515	0.0598	0.0681	0.0764	0.0847	0.0930	0.1013	0.1180	0.1346	0.1512	0.1678
520	0.0498	0.0555	0.0631	0.0707	0.0783	0.0858	0.0934	0.1010	0.1086	0.1237	0.1389	0.1540	0.1692
530	0.0526	0.0579	0.0648	0.0717	0.0786	0.0856	0.0925	0.0994	0.1063	0.1202	0.1340	0.1479	0.1617
540	0.0577	0.0625	0.0689	0.0752	0.0816	0.0879	0.0943	0.1006	0.1070	0.1197	0.1324	0.1451	0.1578
550	0.0640	0.0685	0.0743	0.0802	0.0861	0.0919	0.0978	0.1036	0.1095	0.1212	0.1329	0.1447	0.1564
560	0.0723	0.0764	0.0819	0.0873	0.0928	0.0983	0.1037	0.1092	0.1146	0.1255	0.1364	0.1474	0.1583
570	0.0842	0.0882	0.0933	0.0984	0.1036	0.1087	0.1139	0.1190	0.1242	0.1345	0.1448	0.1551	0.1653
580	0.1084	0.1102	0.1151	0.1201	0.1250	0.1299	0.1349	0.1398	0.1447	0.1546	0.1645	0.1744	0.1842
590	0.1578	0.1614	0.1663	0.1711	0.1759	0.1808	0.1856	0.1905	0.1953	0.2050	0.2147	0.2243	0.2340
600	0.2408	0.2446	0.2495	0.2544	0.2593	0.2642	0.2691	0.2740	0.2789	0.2887	0.2985	0.3083	0.3181
610	0.2892	0.2931	0.2982	0.3033	0.3083	0.3134	0.3185	0.3236	0.3287	0.3389	0.3491	0.3592	0.3694
620	0.3123	0.3164	0.3218	0.3272	0.3326	0.3379	0.3433	0.3487	0.3541	0.3648	0.3756	0.3864	0.3971
630	0.3196	0.3243	0.3306	0.3368	0.3430	0.3493	0.3555	0.3617	0.3680	0.3804	0.3929	0.4053	0.4178
640	0.3290	0.3343	0.3413	0.3483	0.3553	0.3623	0.3693	0.3763	0.3833	0.3973	0.4113	0.4253	0.4393
650	0.3559	0.3615	0.3688	0.3761	0.3834	0.3907	0.3980	0.4053	0.4126	0.4272	0.4418	0.4564	0.4710
660	0.4105	0.4160	0.4233	0.4306	0.4379	0.4452	0.4525	0.4598	0.4671	0.4817	0.4963	0.5109	0.5255
670	0.4278	0.4331	0.4401	0.4471	0.4541	0.4611	0.4681	0.4751	0.4821	0.4962	0.5102	0.5242	0.5382
680	0.4521	0.4569	0.4631	0.4693	0.4756	0.4818	0.4881	0.4943	0.5006	0.5131	0.5256	0.5380	0.5505
690	0.5116	0.5154	0.5203	0.5252	0.5301	0.5350	0.5399	0.5448	0.5497	0.5595	0.5693	0.5791	0.5889
700	0.6513	0.6535	0.6564	0.6593	0.6622	0.6651	0.6680	0.6709	0.6738	0.6796	0.6853	0.6911	0.6969

Discoverer Sta. 18 Exp. 2 Morel
K (490) = 0.033, Depth: 15-46m (a)

Shinyo-Maru Sta. 4 Okami, *et al*
K (490) = 0.058, Depth: 10-19.6m (b)

Discoverer Sta. 9 Smith
K (490) = 0.073, Depth: 10.5-20.1m (c)

New Horizon Sta. 9 Smith
K (490) = 0.076, Depth: 5.2-12.4m (d)

Fresnel, Gulf of California, Smith
K (490) = 0.116, Depth: 6-16m (e)

Fig. 5. Examples of $K(\lambda)$ spectra as determined from irradiance data at 5 selected locations (+). Solid curve is plot of model using $K(490)$ values determined from data.
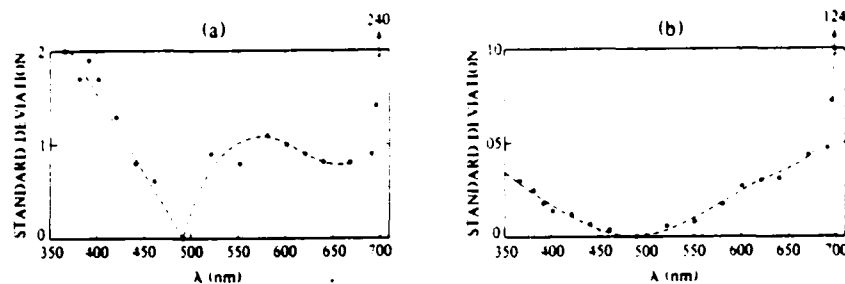
Fig. 6. Approximate standard deviations of comparisons between model and measured data at each of the 68 wavelengths examined between 365 and 700nm. (a) Standard deviation of the ratio $K_c(\lambda)/K_m(\lambda)$ where K_c is the value calculated from the model and K_m is the value determined from measured $E_d(\lambda, z)$. (b) Standard deviation of the differences $K_c(\lambda) - K_m(\lambda)$.
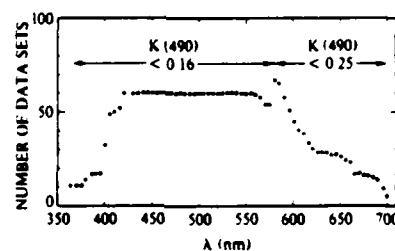

Fig. 7. Number of $K_m(\lambda)$ samples used at each wavelength to form the data base for the model

Comparison with Jerlov water types

It is interesting to compare our results with those presented by Jerlov (1976). The Jerlov water types were designed to be used as a general means of classification the upper, usually well mixed, 10 meters of the ocean. The oceanic water types I, IA, IB, II, and III have a minimum $K(\lambda)$ at about 475 nm as may be seen from Jerlov's Table XXVII and Fig. 70. Using 475 nm as a reference wavelength we have plotted $K(\lambda)$ vs $K(475)$ using our model and the values of $K(475)$ from Jerlov's Table XXVII. Figure 8 is a plot of $K(\lambda)$ from 350 to 600nm showing the manner in which the attenuation changes for the 5 Jerlov oceanic water types. We observe that our model shows the minimum attenuation shifting to longer wavelengths as the water turbidity increases which is consistent with most observations. We also call attention to the fact that some of the attenuation values for Type I oceanic water as given by Jerlov are less than the values we suggest for $K_w(\lambda)$. In fact, at some wavelengths the values given by Jerlov for K are less than the values of absorption alone published by Morel and Prieur (1977). We recommend, therefore, that the values of $K(\lambda)$ as published by Jerlov be replaced by those in Table 6. The values for Type I water given in the table are those of pure sea water, K_w. The other tabulated values were computed using our model and the values for $K(475)$ given by Jerlov in his Table XXVII. The form of Table 6 allows direct comparison with Jerlov's table. Figure 9 presents a comparison between the $K(\lambda)$ values at the wavelength in Jerlov's table and our model for oceanic water types IA, II and III. The disagreement between the two is generally greater in the blue. This would be consistent with our finding less evidence of yellow substance in the data which we used as a basis for our model than Jerlov had in the data upon which he based his work.
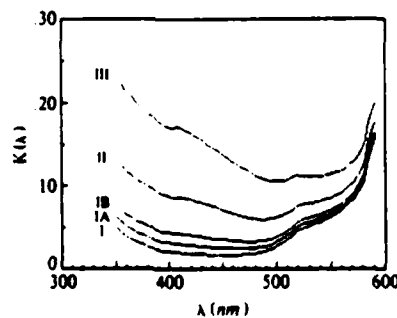

Fig. 8. Spectral diffuse attenuation coefficients for Jerlov water types I-III.

Table 6. Downward irradiance attenuation coefficients $K(\lambda)$ for Jerlov water type

Water Type	WAVELENGTH (nm)														
	350	375	400	425	450	475	500	525	550	575	600	625	650	675	700
I	0.0510	0.0302	0.0217	0.0185	0.0176	0.0184	0.0280	0.0504	0.0640	0.0931	0.2408	0.3174	0.3559	0.4372	0.6513
IA	0.0632	0.0412	0.0316	0.0280	0.0257	0.0250	0.0332	0.0545	0.0674	0.0960	0.2437	0.3206	0.3601	0.4410	0.6530
IB	0.0782	0.0546	0.0438	0.0395	0.0355	0.0330	0.0396	0.0596	0.0715	0.0995	0.2471	0.3245	0.3652	0.4457	0.6550
II	0.1325	0.1031	0.0878	0.0814	0.0714	0.0620	0.0627	0.0779	0.0863	0.1122	0.2595	0.3389	0.3837	0.4626	0.6623
III	0.2335	0.1935	0.1697	0.1594	0.1381	0.1160	0.1056	0.1120	0.1139	0.1359	0.2826	0.3655	0.4181	0.4942	0.6760
1	0.3345	0.2839	0.2516	0.2374	0.2048	0.1700	0.1486	0.1461	0.1415	0.1596	0.3057	0.3922	0.4525	0.5257	0.6896

Values of $K(\lambda)$ in body of Table have units, m^{-1} Compare with Table XXVII Jerlov(1976)
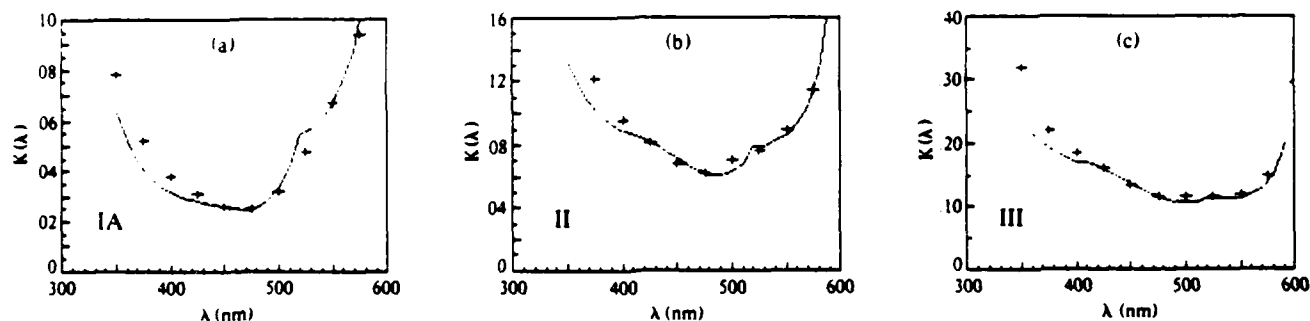

Fig. 9. Comparison between Jerlov oceanic Types IA, II and III with the present model when $K(475)$ set equal to Jerlov's tabulated values.

Figure 10 is a plot of $K(\lambda)$ *versus* $K(475)$ for each 25 nm from 350 to 700 nm. This plot is directly comparable to Figure 70 in Jerlov (1976). The slopes associated with each of the lines in the plot were taken from the present model and are listed in the figure.

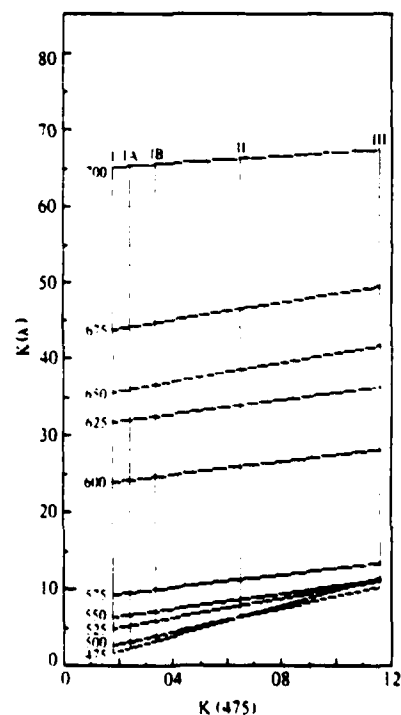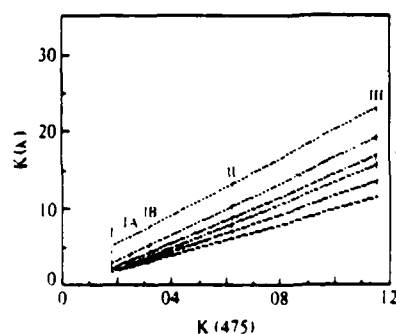| λ (nm)	Slope (M)
350	1.871
375	1.674
400	1.517
425	1.444
450	1.236
475	1.000
500	0.796
525	0.632
550	0.511
575	0.439
600	0.428
625	0.494
650	0.637
675	0.584
700	0.252

Fig. 10. Irradiance attenuation coefficient, $K(\lambda)$, as a function of $K(475)$. Vertical lines drawn at $K(475)$ corresponding to Jerlov oceanic water types. (Compare with Jerlov 1976 Fig. 70)

Summary

The spectral characteristics of the diffuse attenuation coefficient of oceanic water behave in an orderly , predictable, fashion. The complete spectra may be predicted knowing the value of the diffuse attenuation coefficient at a single wavelength through the use of a model based on the analysis of many such spectra. Regressions of the attenuation coefficient at any wavelength from 365 to 700 nm against the corresponding value of the coefficient at a second reference wavelength show a linear relationship between the two variables (Eq. (4), Fig. 2(a-d)). From the slopes and intercepts of linear equations fitted to these regressions the value of the attenuation of pure sea water, $K_w(\lambda)$ may be inferred. Such values were found to be very close to the values obtained using Eq. (3) with the spectral absorption and scattering values published by Morel and Prieur (1977) and Morel (1974). Using these latter values for $K_w(\lambda)$ and Eq. (5), new slopes, $M(\lambda)$, were calculated which with $K_w(\lambda)$ form the basis for the model of spectral diffuse attenuation coefficient. Table 5 lists the values of K_w and M at 5 nm intervals from 350 to 700 nm. These values may be used in Eqs. (5) or (6) to provide estimates of $K(\lambda)$ at any wavelength, given the value of K at a second, reference wavelength. Table 5 lists values of $K(\lambda)$ calculated as described using selected values of $K(490)$ from 0.03 to $0.18\,m^{-1}$ as a water classification index.

Jerlov water types may be redefined using the model presented here. Table 6 presents values of the diffuse attenuation coefficient at the same wavelengths as published by Jerlov for oceanic Types I, IA, IB, II, III and coastal Type 1. The tabulated values at 475 nm are the same as those used by Jerlov.

An alternative to the use of Jerlov water types would be the use of a classification index such as the value of K at a selected reference wavelength (e.g. our $K(490)$). This has the advantage that the value of the index provides a quantitative indication of the water clarity (i.e. attenuation coefficient) and allows the user to classify the water by selecting any range of values of the classification index that may be appropriate to the particular application.

We observe that the spectral nature of the attenuation coefficient did not appear to be dependent on the geographical location of the water investigated nor on the depth of the observation in the water column providing the classification index, $K(490)$ was less than approximately $0.16\,m^{-1}$. We believe, therefore, that the model can be considered as generally applicable for water at the surface or at depth as long as $K(490) < 0.16\,m^{-1}$.

References

Jerlov, N.G. (1976), "Marine Optics," in *Elsevier Oceanography Series*, vol. 14, Elsevier Scientific Publishing Co., Amsterdam, Oxford, New York.

Morel, A. and L. Caloumenos (1971), "Mesures D'enclairements Sous Marins Flux De Photons Et Analyse Spectrale," *Centre De Recherches Oceanographiques*, Report No.11, La Darse - 06230 Villefranche-sur-Mer, De Villegranche-Sur-Mer, France.

Morel, A. (1974), "Properties of Pure Water and Pure Sea Water," in *Optical Aspects of Oceanography*, eds. N.G. Jerlov and B. Steemann Nielsen, pp. 1-24, Academic Press, New York, N.Y.

Morel, A. and L. Prieur (1976), "Irradiation Journaliere En Surface Et Measure Des Eclairements Sous Marins: Flux De Photons Et Analyse Spectrale," Resultats De La Campagne Cineca 5 - J. Charcot - Capricorne 7403, Report No.10, Serie: Resultats des Campagnes a la Mer, Groupe MEDIPROD, Centre National Pour L'Exploitation Des Oceans (CNEXO).

Morel, A. and L. Prieur (1977), "Analysis of Variations in Ocean Color," Limnol. Oceanogr., 22 (4), pp. 709-722.

Okami, N., M. Kishino, and S. Sugihara (1978), "Measurements of Spectral Irradiance in the Seas Around the Japanese Islands," Technical Report No. 2, The Physical Oceanography Laboratory of the Institue of Physical and Chemical Research, Tokyo, Japan.

Smith, R.C. and K.S. Baker (1978), "Optical Classification of Natural Waters," Limnol. and Oceanogr., 23, pp. 260-267. Also issued as University of California, San Diego, Scripps Institution of Oceanography, Visibility Laboratory, SIO Ref. 77-4.

Smith, R.C. and K.S. Baker (1981), "Optical Properties of the Clearest Natural Waters (200-800nm)," Appl. Opt., 20, pp. 177-184.

Tyler, J.E. and R.C. Smith (1970), in *Measurement of Spectral Irradiance Underwater*, pp. xii - 103, Gordon and Breach, New York, London, Paris.

Tyler, J.E. (1973), "Data Report of the Discoverer Expedition," SIO Ref. 73-16, pp. 1-1000, University of California, San Diego, Scripps Institution of Oceanography, Visibility Laboratory.

Acknowledgment

END

Feb.

1988

DTIC